

ESCOLA
POLITÉCNICA
DA USP

PMR 3301

Simulação de Processos no Estado Sólido

Izabel Machado

machadoi@usp.br

Mechatronics and Mechanical Systems Engineering Department – Escola Politécnica – University of São Paulo

<http://lattes.cnpq.br/6705415923436933>

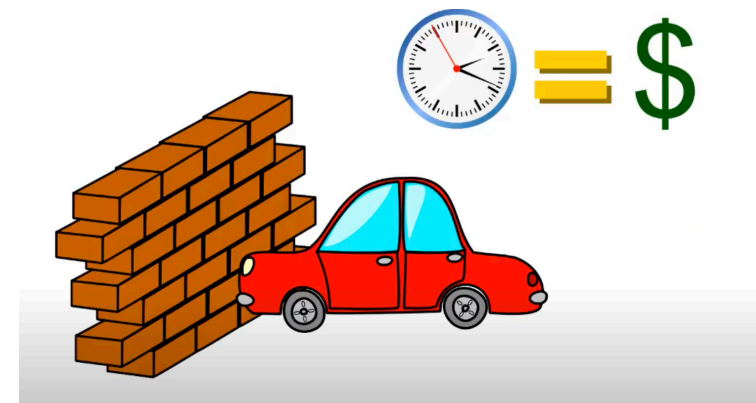
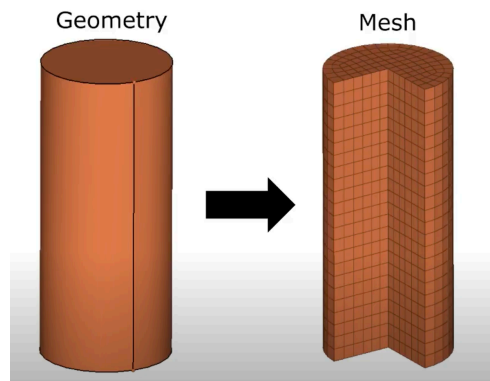
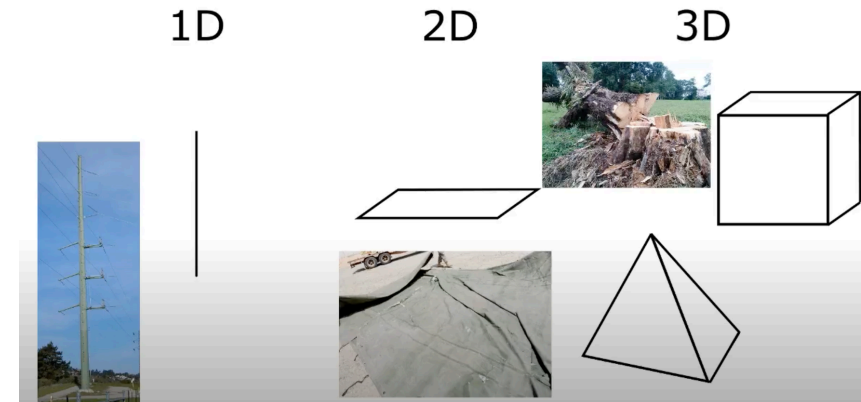
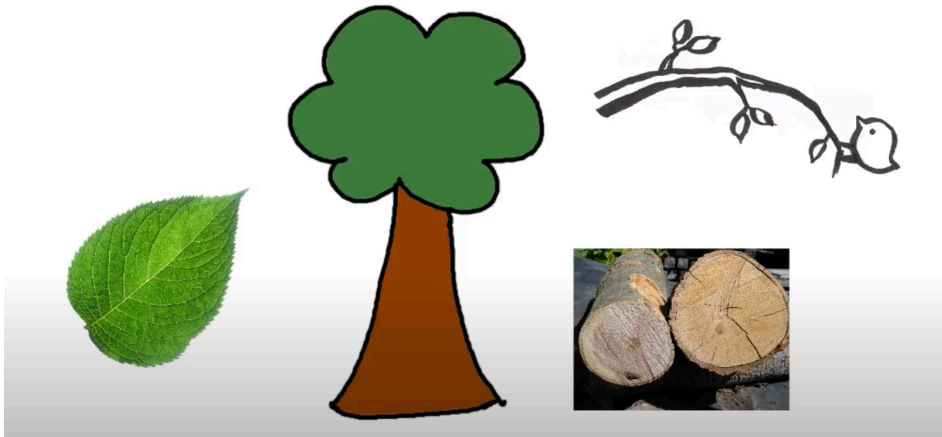
CAD- FEA –CAM- FEA/CAM

- ❑ **Objetivo é dar uma visão geral de como análises utilizando elementos finitos e softwares de apoio, como o CAD, são importantes na manufatura de componentes**

Análise utilizando elementos finitos

- FEM - <https://www.youtube.com/watch?v=boSLQYhDXoE>
- FEM - <https://www.youtube.com/watch?v=boSLQYhDXoE>
- ABAQUS
- ANSYS
- DEFORM
- MAGMA
- LS DYNA
- CONSOL
- MATLAB (otimização, machine learning)
- EXCEL (estatística e otimização)
- SOLID WORKS
- OUTDESK
- E muito mais....

Análise utilizando elementos finitos



Simulação



FUNCTIONAL GENERATIVE DESIGN



© Dassault Systèmes | Confidential Information | 4/15/2020 | ref.: 3DS_Document_2019



Simulação



Trade Off Study

Variant Names

- Satellite Bracket
 - Sim_Satellite Bracket Demo_V1
 - Design Space Analysis
 - Shape Validation.1
 - Shape Validation.2
 - Sim_Satellite Bracket Demo_V2
 - Sim_Satellite Bracket Demo_V3
 - Design Space Analysis
 - Shape Validation.1
 - Shape Validation.2
 - Shape Validation.3
 - Shape Validation.4

Advanced options

Inputs

Optimization KPIs

KPIs

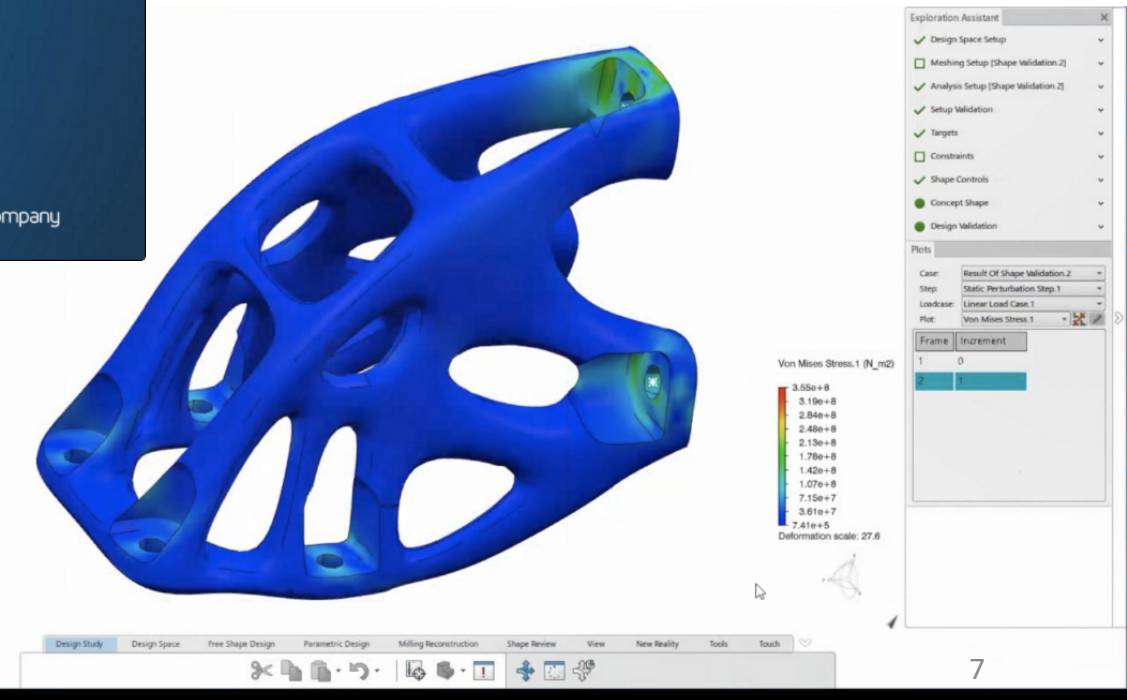
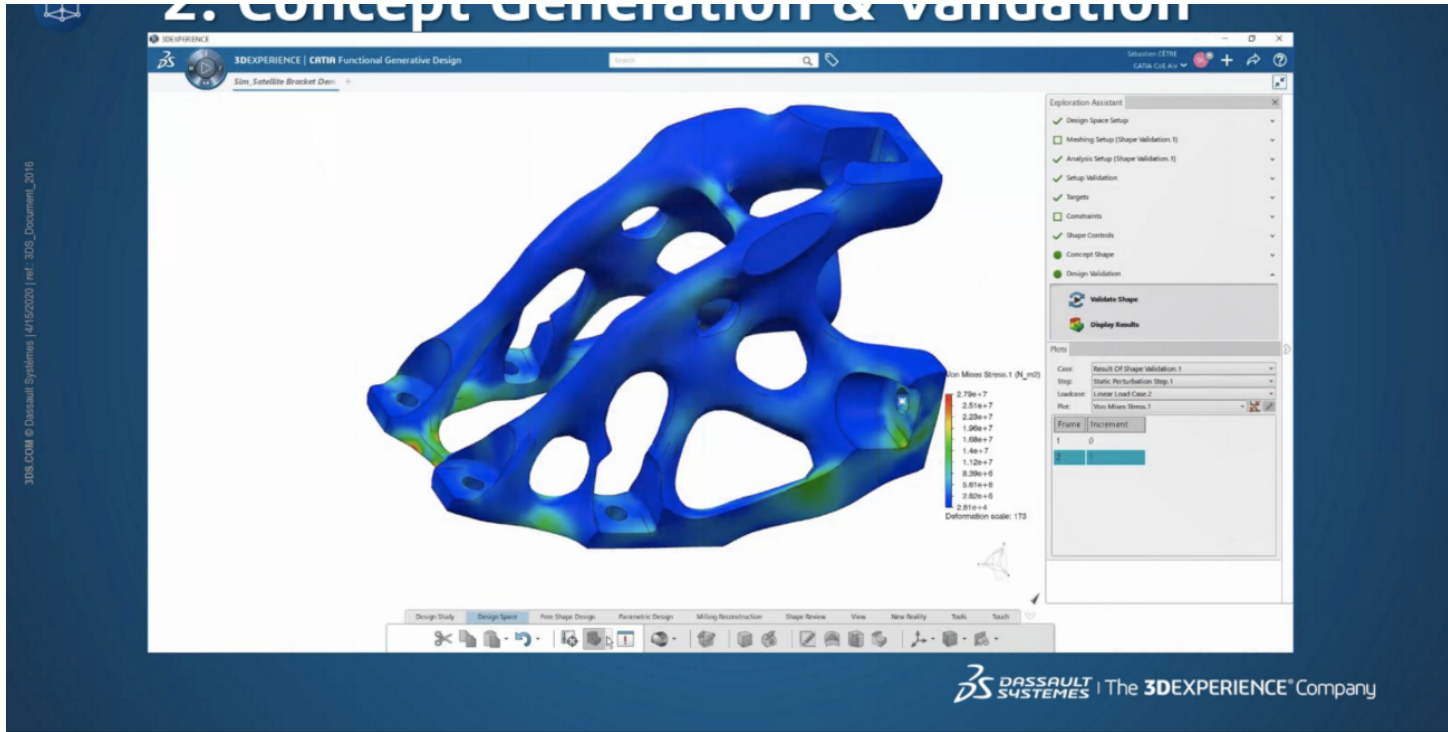
KPI	Sim_Satellite Bracket Demo_V1	Sim_Satellite Bracket Demo_V2	Sim_Satellite Bracket Demo_V3
Score	91,9406	74,6432	30
Mass	0,2319g	0,3246g	0,4346g
Von Mises Stress	4,979e+008N_m2	2,873e+008N_m2	4,543e+008N_m2
Minimum Principal Stress	1,003e+008N_m2	7,867e+007N_m2	1,308e+008N_m2
Maximum Principal Stress	5,291e+008N_m2	3,235e+008N_m2	5,967e+008N_m2
Displacement	0,527mm	0,425mm	0,875mm
Reaction Force	0N	0N	0N
Elastic Strain Energy	0,541J	0,394J	0,719J
Element Volume	52,215cm3	73,086cm3	93,37cm3
Connector Force (Axial)	4678,957N	4218,937N	4799,315N
Connector Force (Shear)	1976,890N	1604,763N	1157,832N

Von Mises Stress.1 (N_m2)

Deformation scale: 25.2

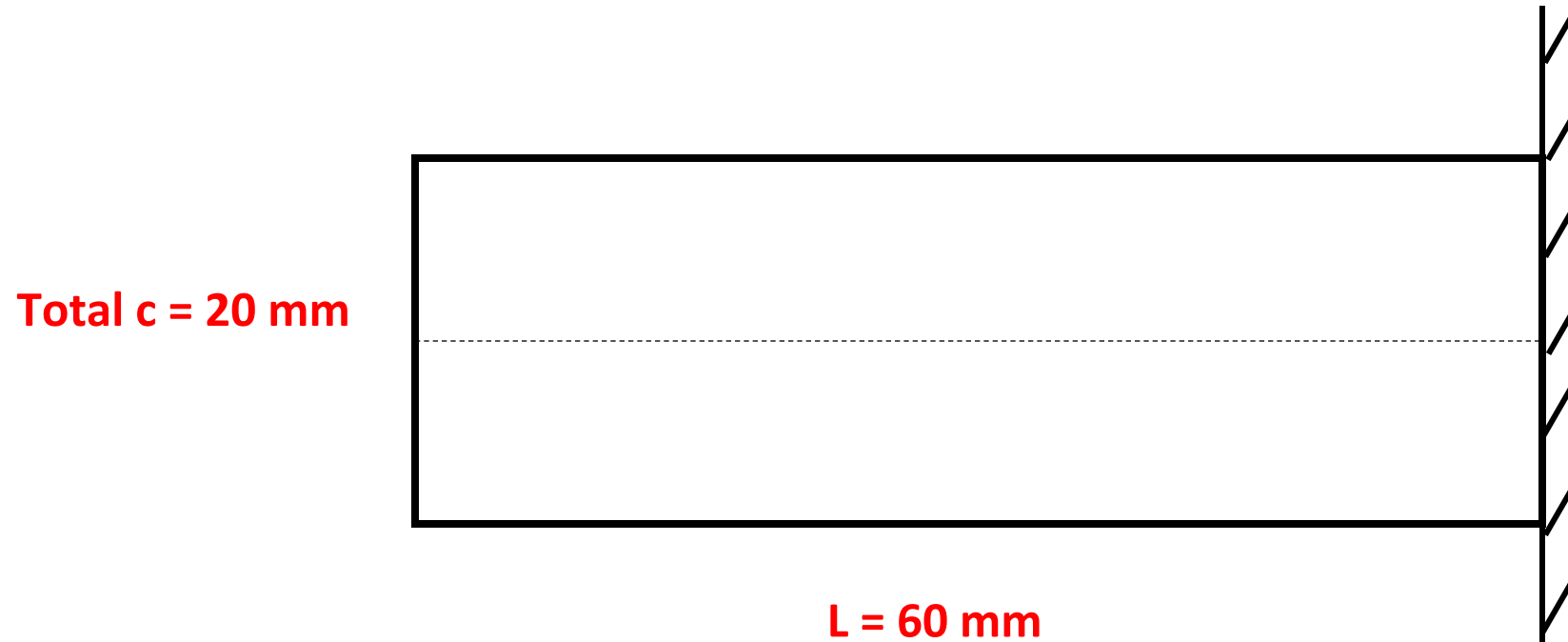
3DS.COM © Dassault Systèmes | 4/15/2020 | ref.: 3DS_Document_2016

DASSAULT SYSTEMES | The 3DEXPERIENCE® Company



Exercise 1 – Cantilever Beam

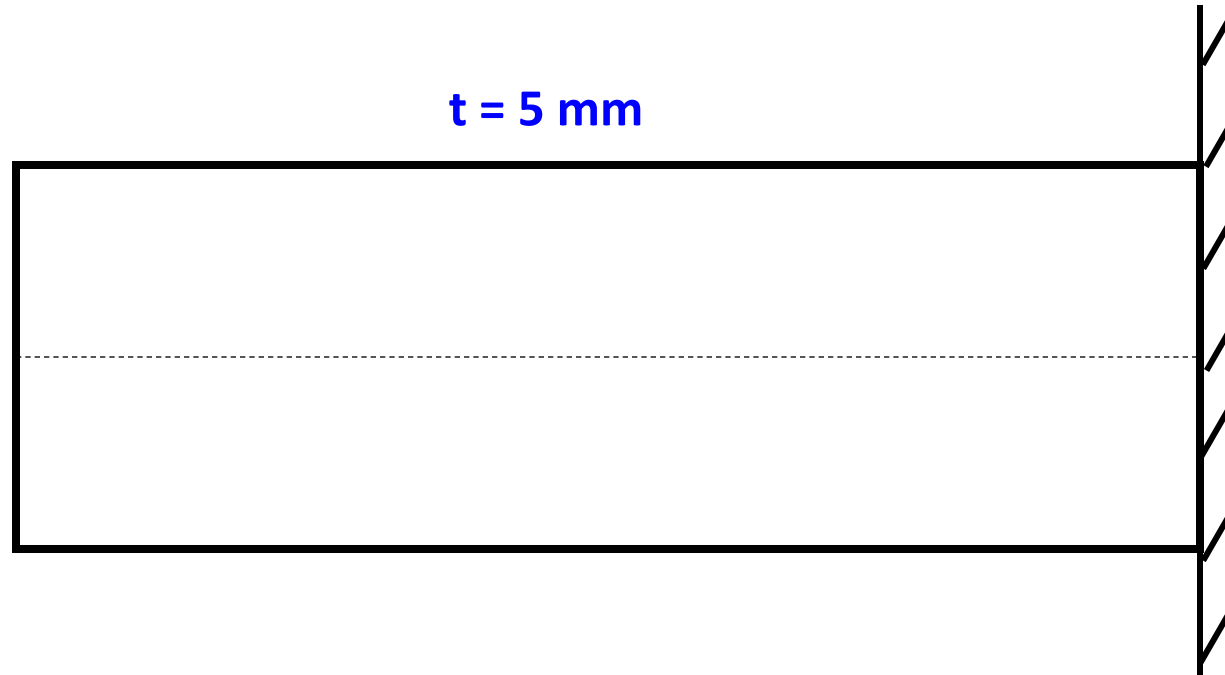
➤ **PART:** 2D – Deformable – Shell



Partition: Face – 2 points

Exercise 1 – Cantilever Beam

➤ **PROPERTIES:** Steel - $E = 200 \text{ GPa}$; $\nu = 0.3$;

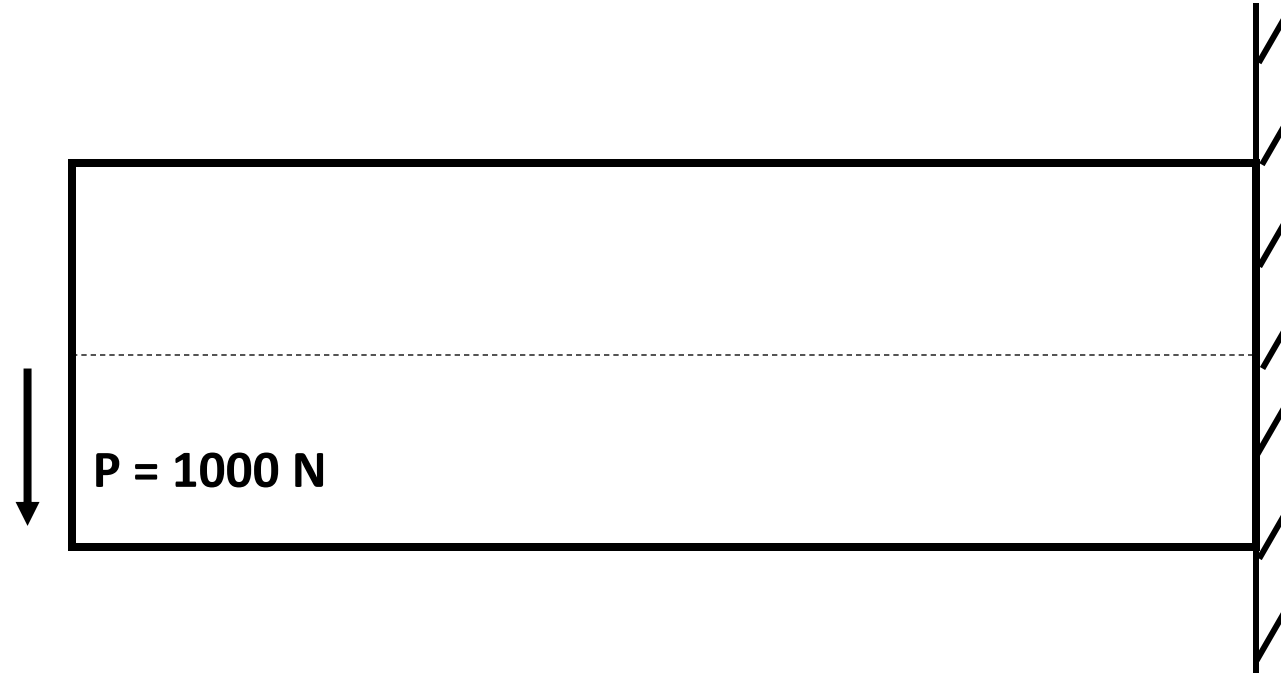


➤ **ASSEMBLY;**

➤ **STEP:** Static, General (time = 1 s); Nlgeom: OFF;

Exercise 1 – Cantilever Beam

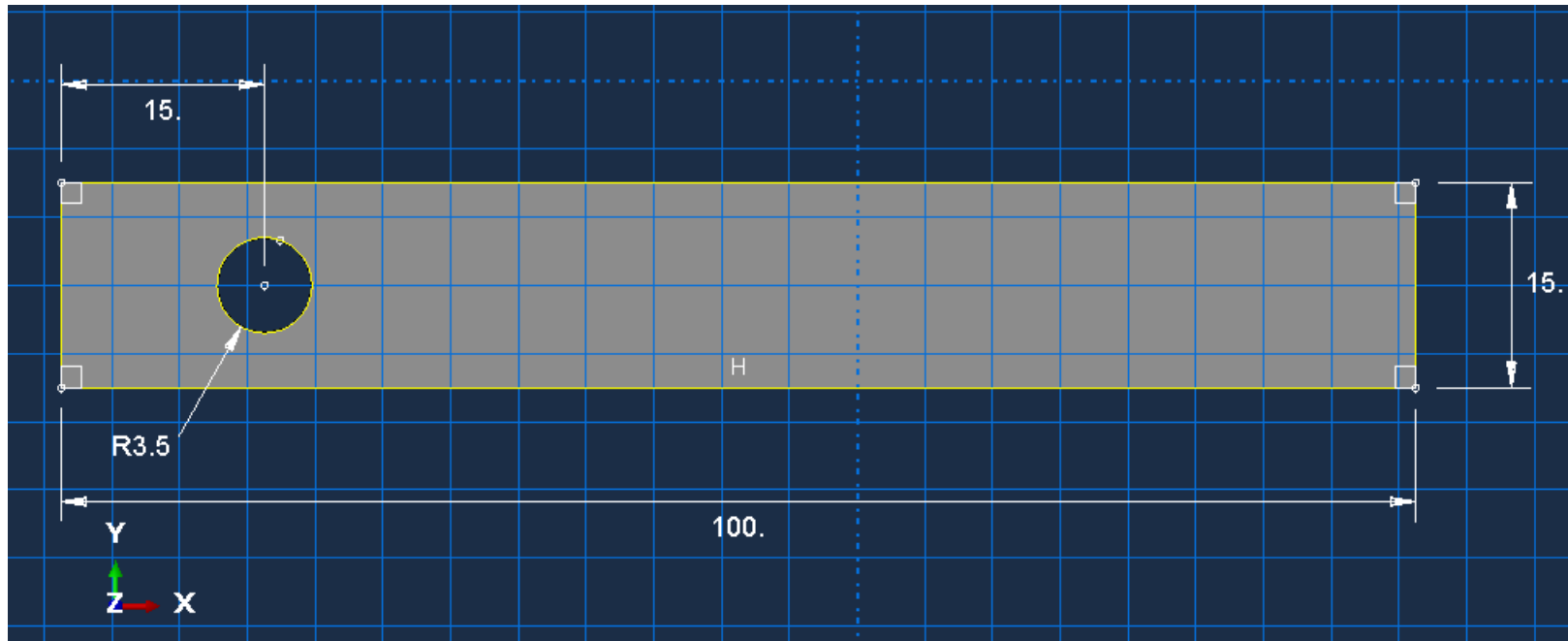
- **LOAD:** BC – encastre; Concentrated Force = 1000 N;



- **MESH:** Triangular Element – Structured Mesh;
Global Size = 5 mm.

Exercise 2 – Plasticity

➤ **PART: Bar - 2D – Deformable – Shell**



Exercise 2 – Plasticity

➤ **PROPERTIES: Steel**

Elastic: $E = 210.73 \text{ GPa}$; $\nu = 0.29$;

Plastic:

Yield Stress	Plastic Strain
200.2	0
246	0.02353
294	0.0474
374	0.09354
437	0.1377
480	0.18

Thickness (Plane Stress): 5 mm;

➤ **ASSEMBLY;**

Exercise 2 – Plasticity

➤ **STEP:** Static, General (time = 1 s); Nlgeom: ON;

Initial Increment size = 0.05

Maximum Increment size = 0.2

Field Output:

Frequency – Every x units of time: 0.01 (100 frames).

Exercise 2 – Plasticity

➤ LOAD:

$$U1 = U2 = 0$$



➤ MESH:

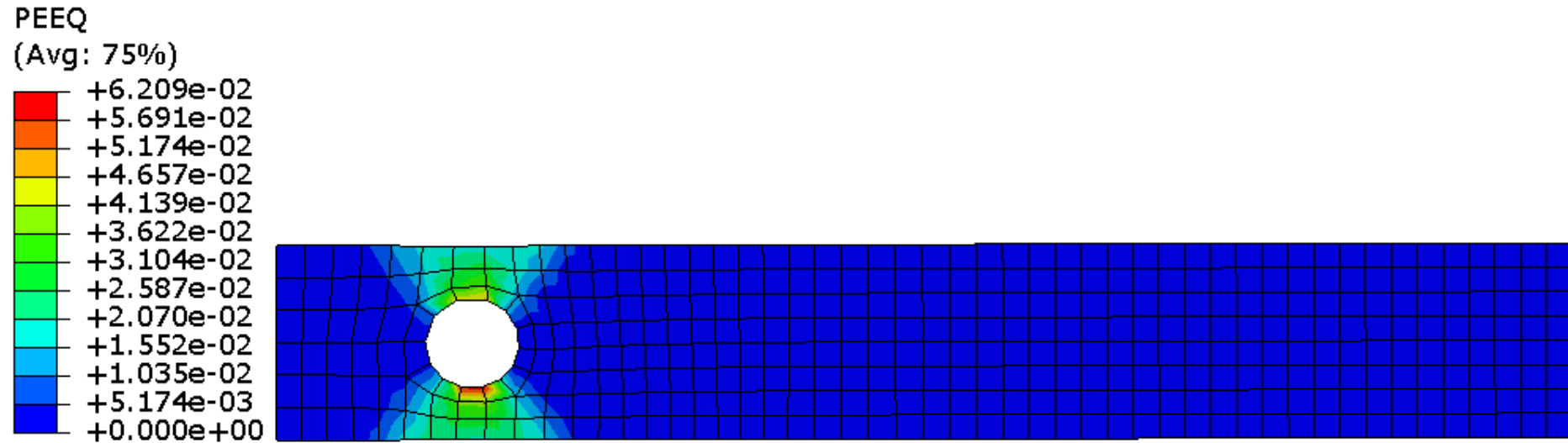
Element Type: CP4S (Plane Stress)

Controls: Quad mesh – Medial Axis

Global Size: 2

Exercise 2 – Plasticity

➤ **JOB:** Plasticity



Report: PEEQ

FEM Macroscale

➤ **PART 1:**

Workpiece - 3D – Deformable – Solid

20 x 20 x 200 **m³**

Roller - 3D – Discrete Rigid – Solid – Extrusion

∅ 100 *m*

Depth = 45 *m*

Create Reference Point (Tools).

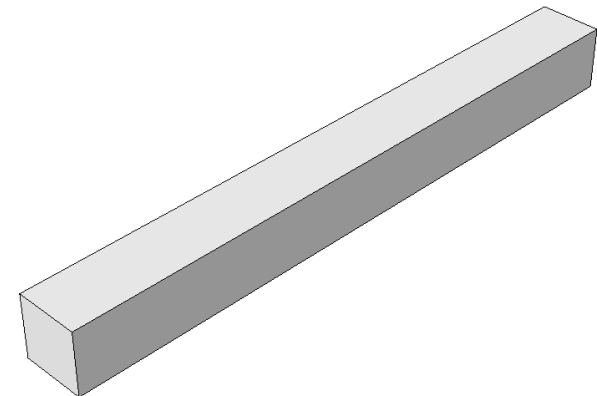
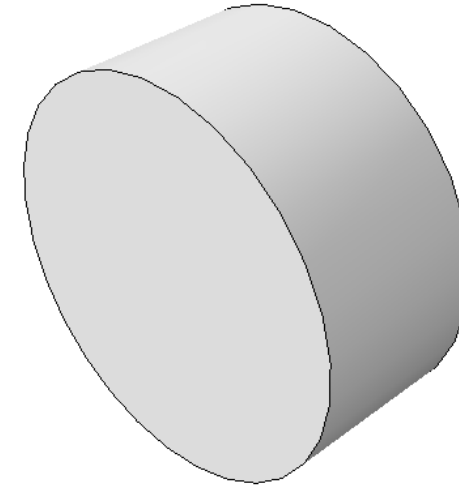
➤ **PROPERTIES:**
Workpiece - Steel

Plastic:

➤ **PROPERTIES:**

Workpiece - Steel

Elastic: $E = 200 \text{ GPa};$
 $\nu = 0.3;$

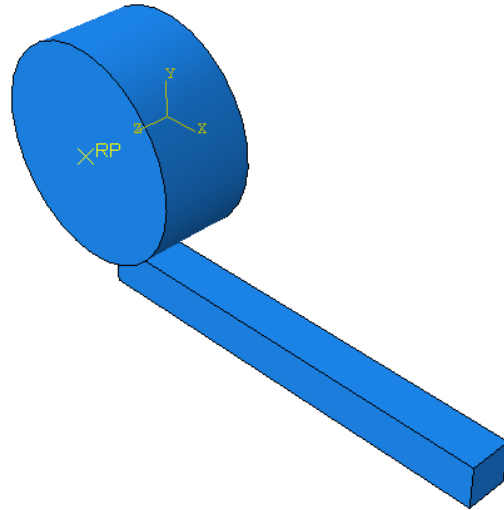


Yield Stress	Plastic Strain
380e6	0
420e6	0.04
470e6	0.12
500e6	0.19
530e6	0.25

FEM Macroscale

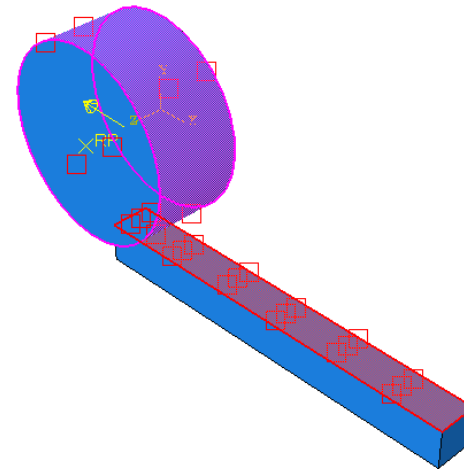
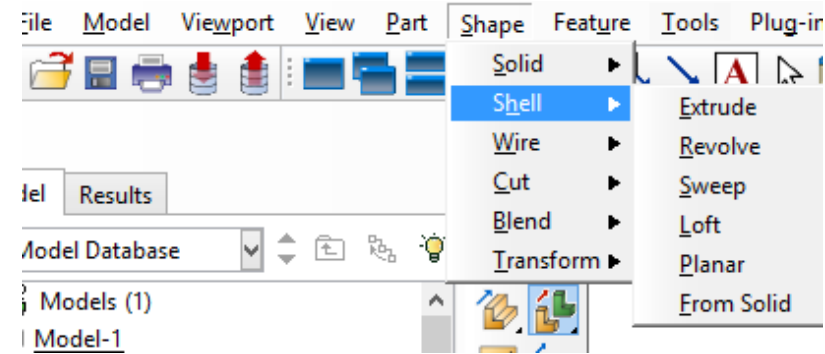
➤ **ASSEMBLY:**

Rotate and Translate the Workpiece



➤ **INTERACTION:**
Surface-to-surface;

Penalty: COF = 0.3;



FEM Macroscale

➤ **LOAD:**

Workpiece

Pre-defined field ($V_1 = -70$ m/s);

ZSymm;

YSymm.

RP – Roller:

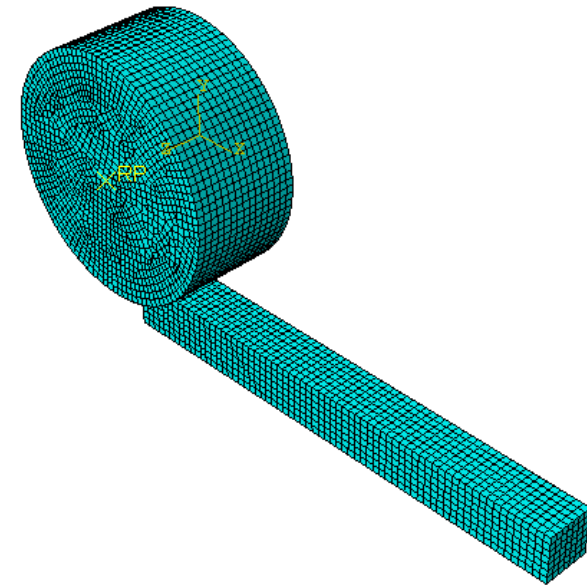
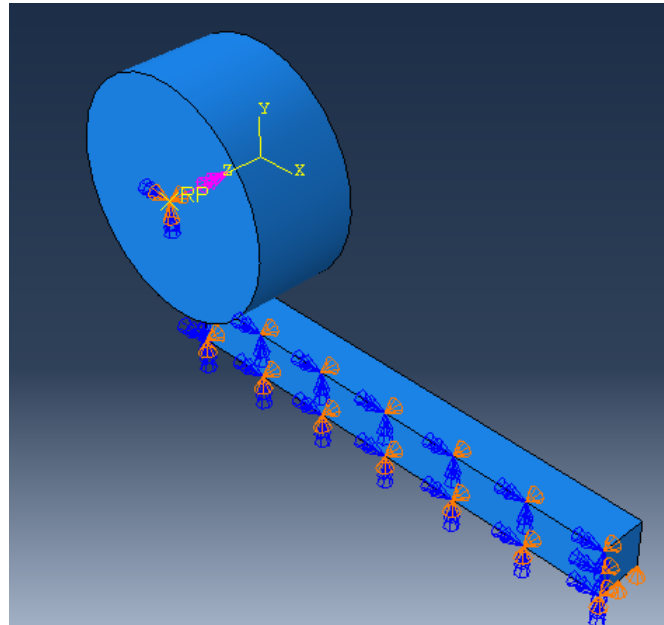
Initial Step - $U_1 = U_2 = U_3 = UR_1 = UR_2 = 0$

Step -1: $VR_3 = -5$ rad/s

➤ **MESH:**

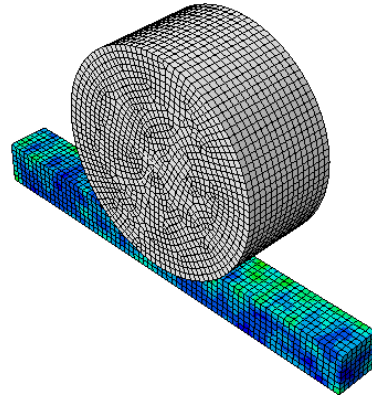
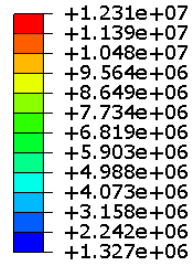
Workpiece: Hex (C3DR8) – Global Size: 3;

Roller: R3D4 – Global Size: 3;

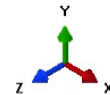
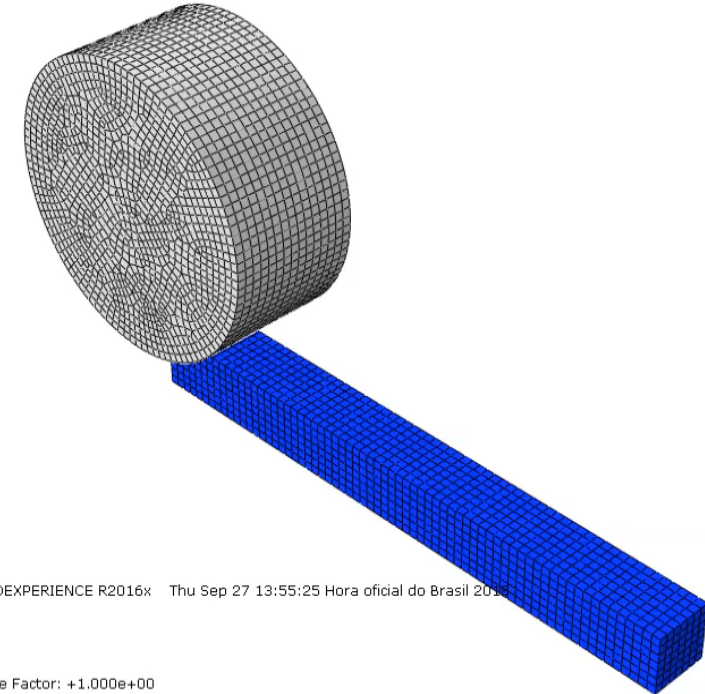
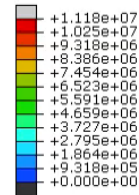


FEM Macroscale

S, Mises
(Avg: 75%)



S, Mises
(Avg: 75%)

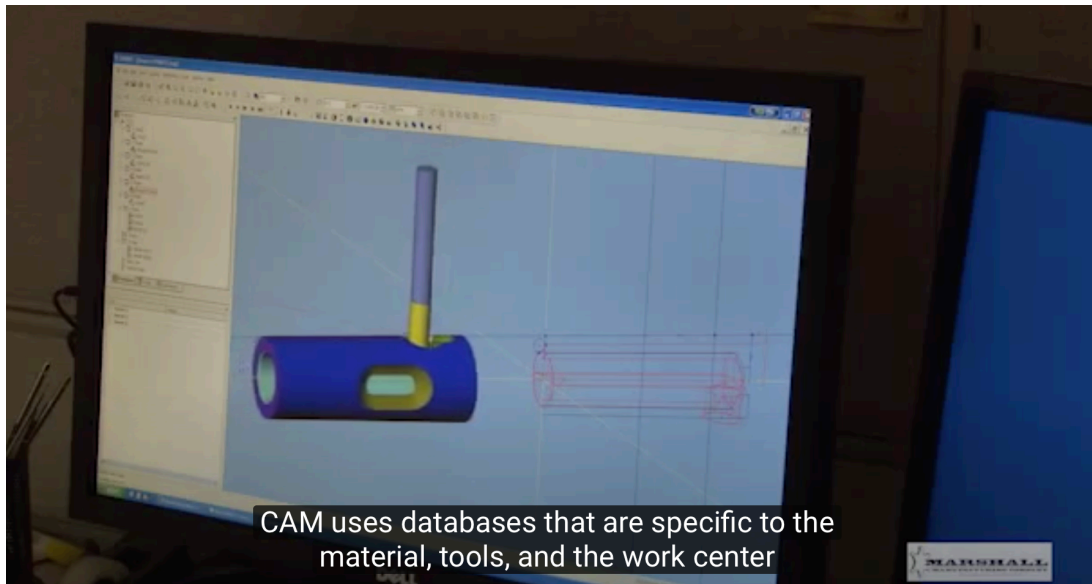
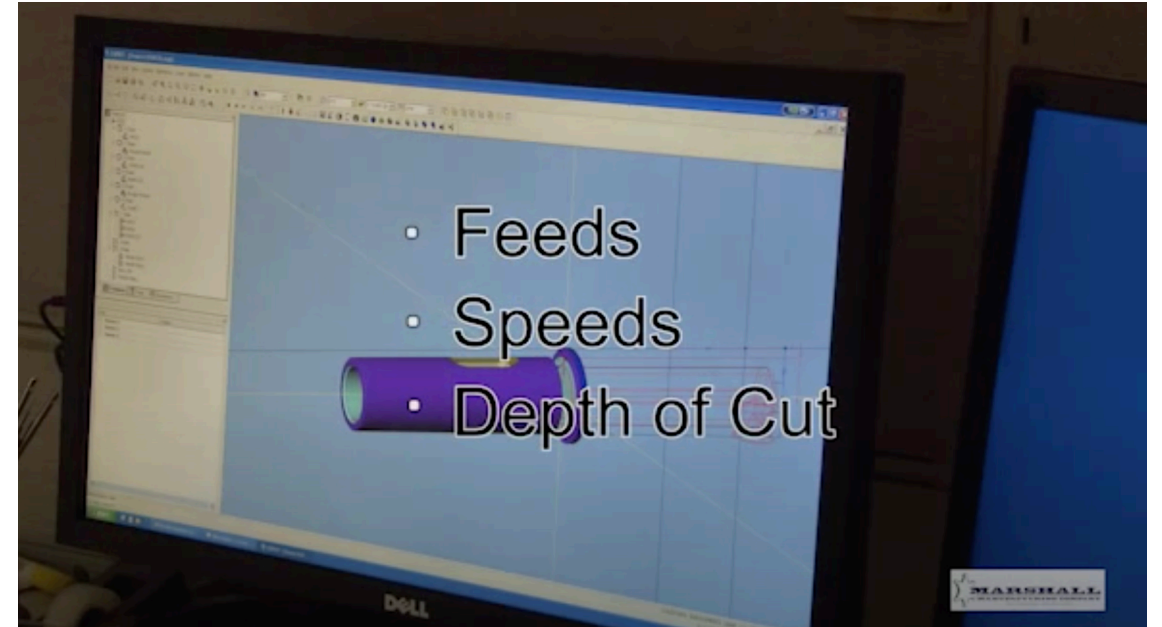
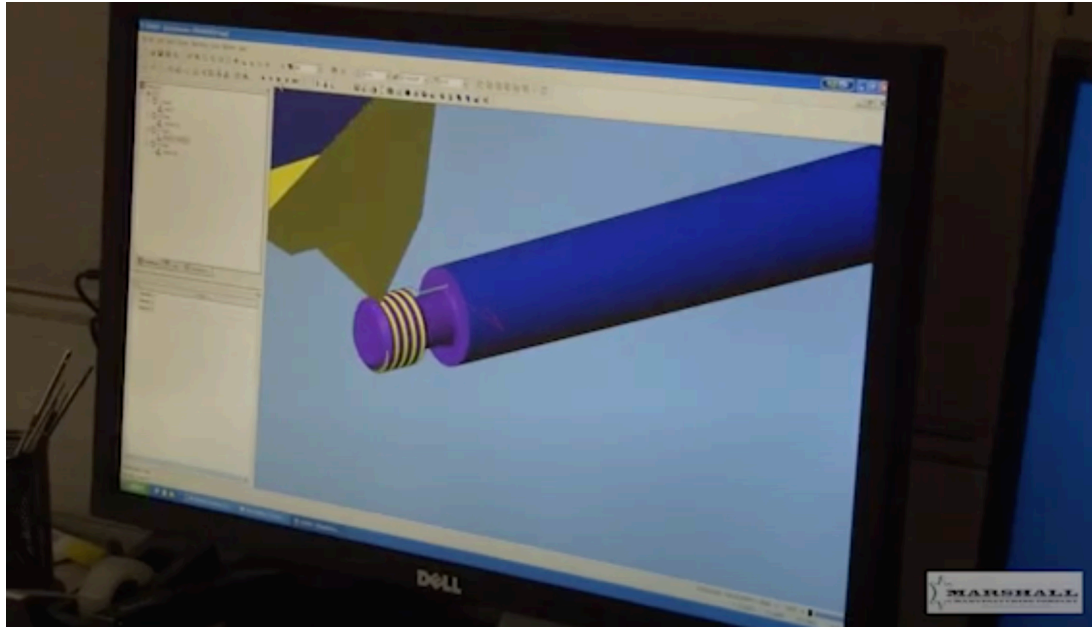


ODB: Ex_3.odb Abaqus/Explicit 3DEXPERIENCE R2016x Thu Sep 27 13:55:25 Hora oficial do Brasil 2016

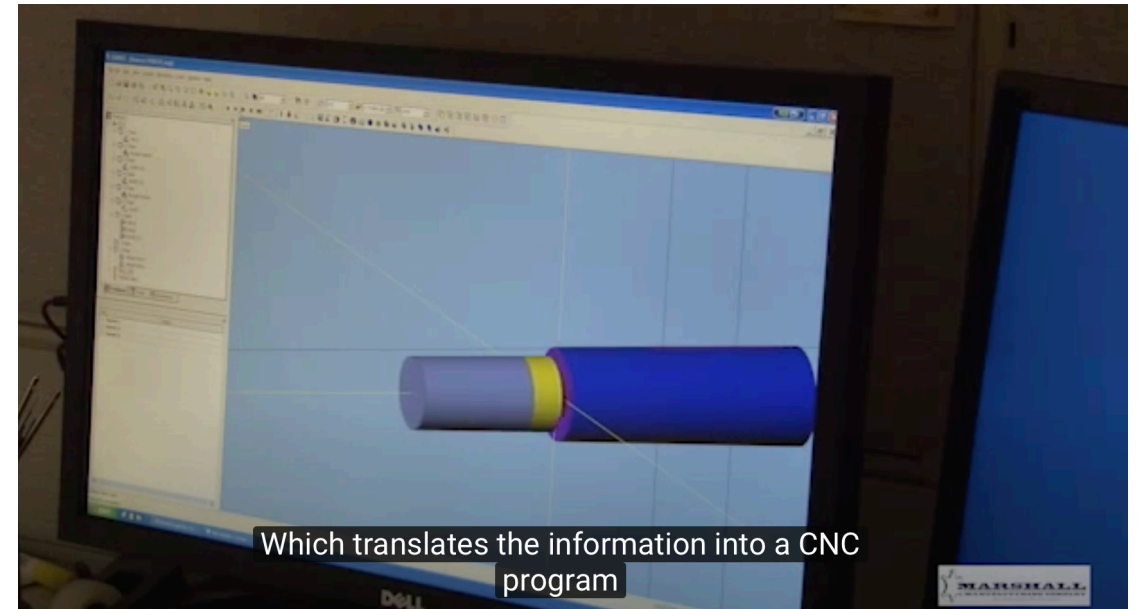
Step: Step-1
Increment: 0: Step Time = 0.0
Primary Var: S, Mises
Deformed Var: U Deformation Scale Factor: +1.000e+00

CAM

- https://www.youtube.com/watch?v=FdipJNG_vV8



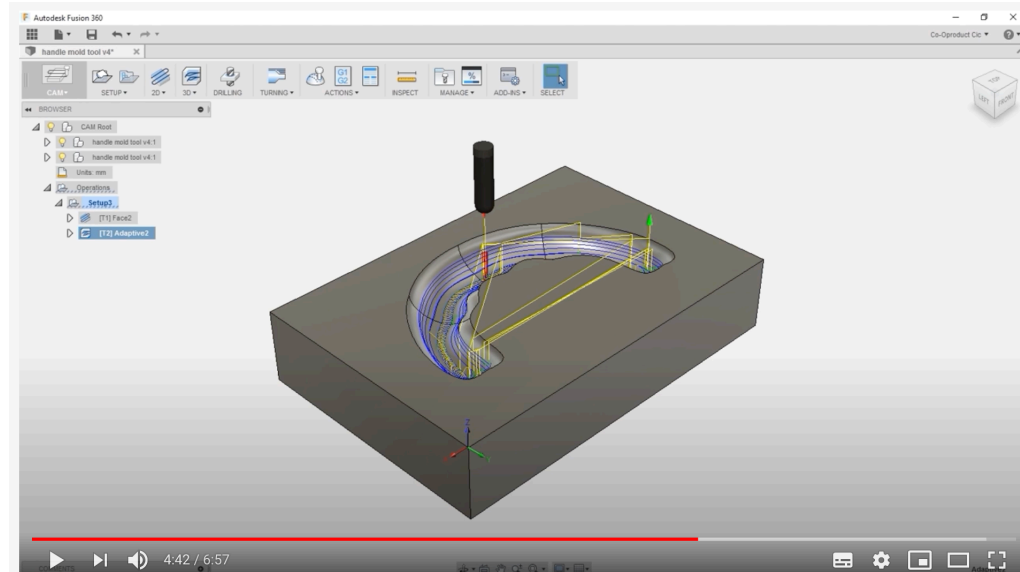
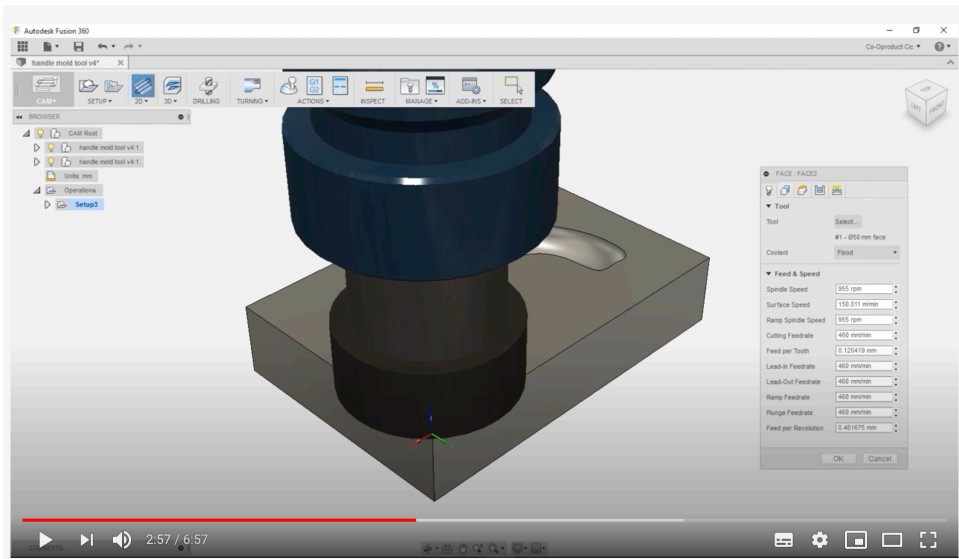
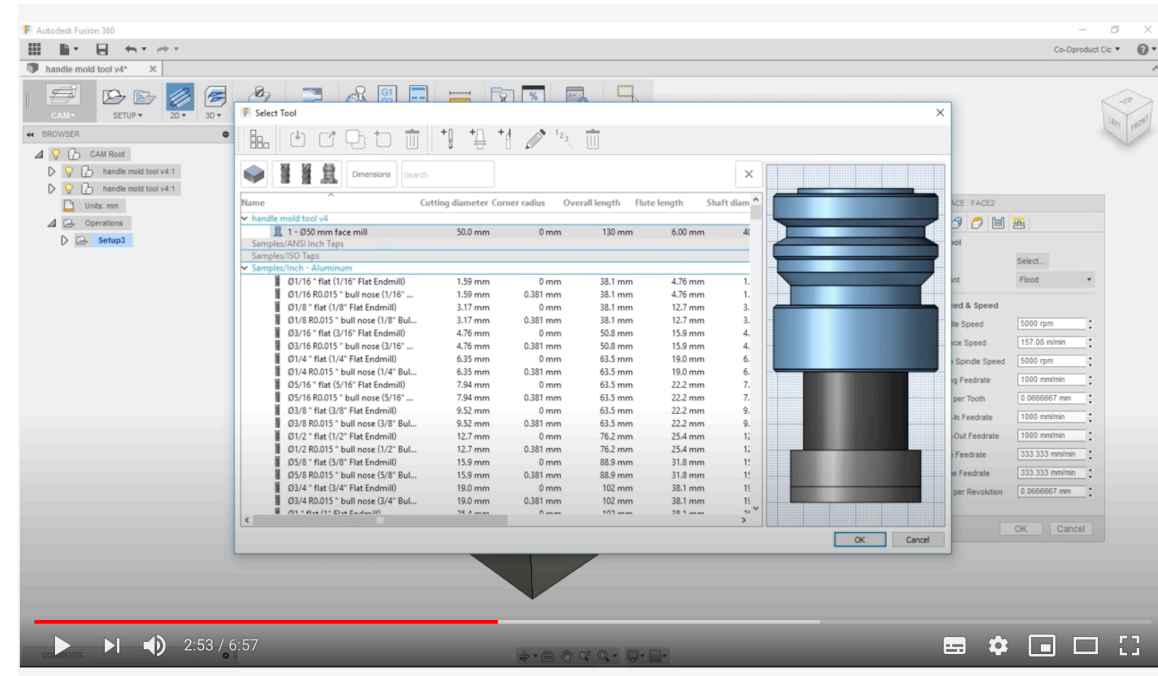
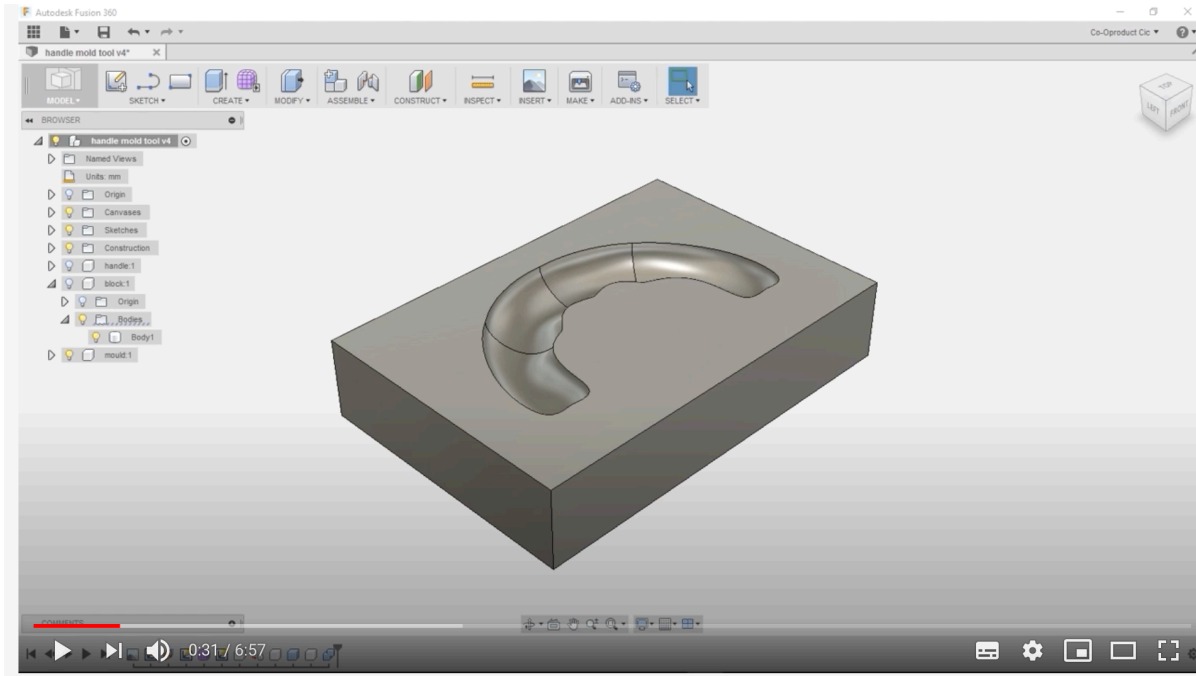
CAM uses databases that are specific to the material, tools, and the work center



Which translates the information into a CNC program

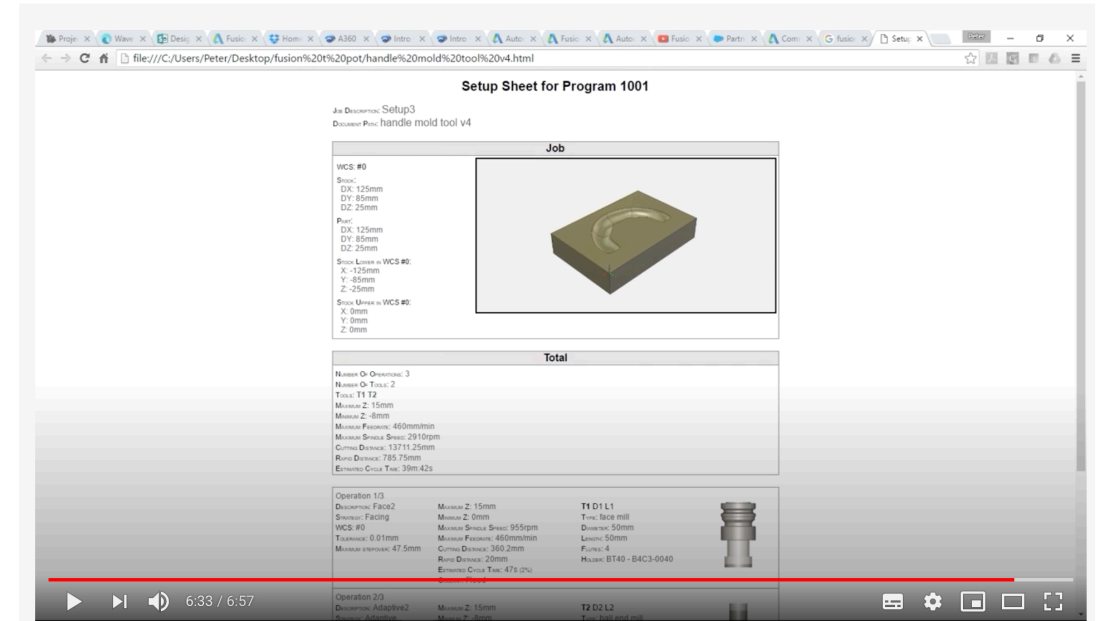
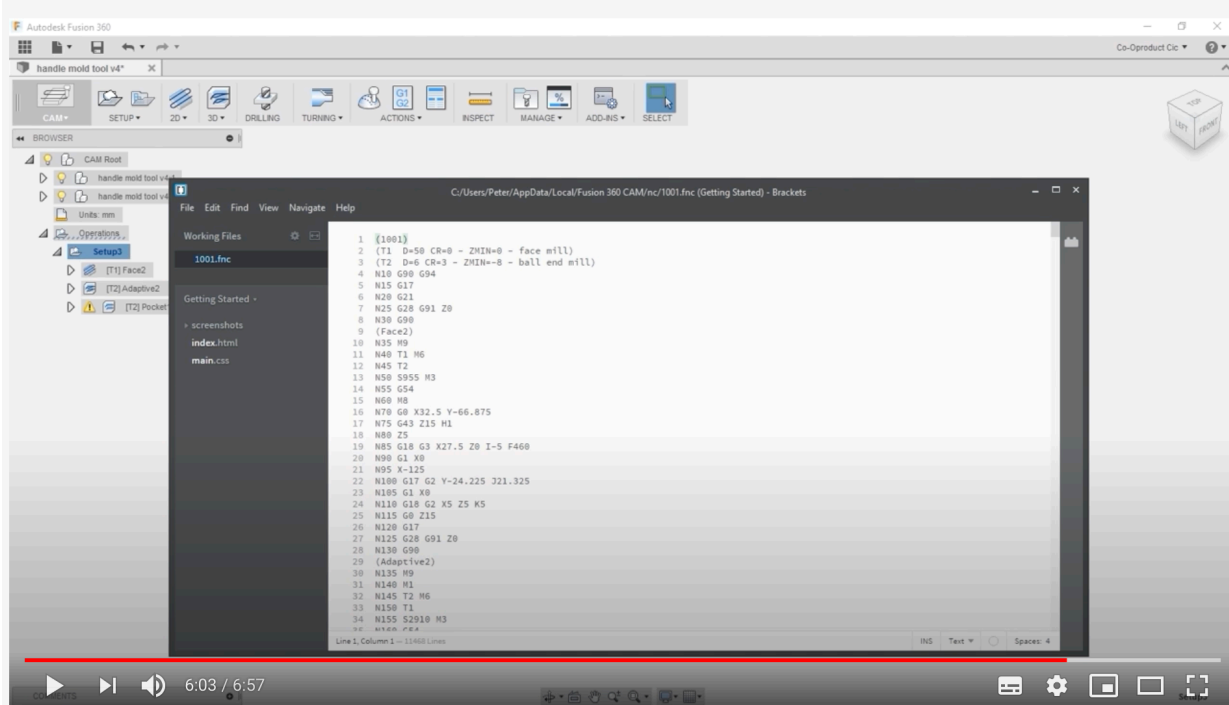
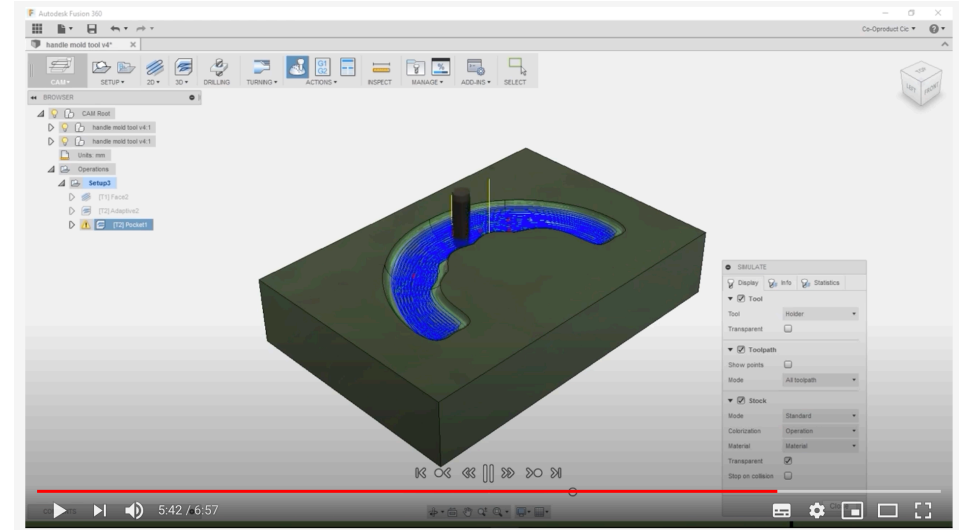
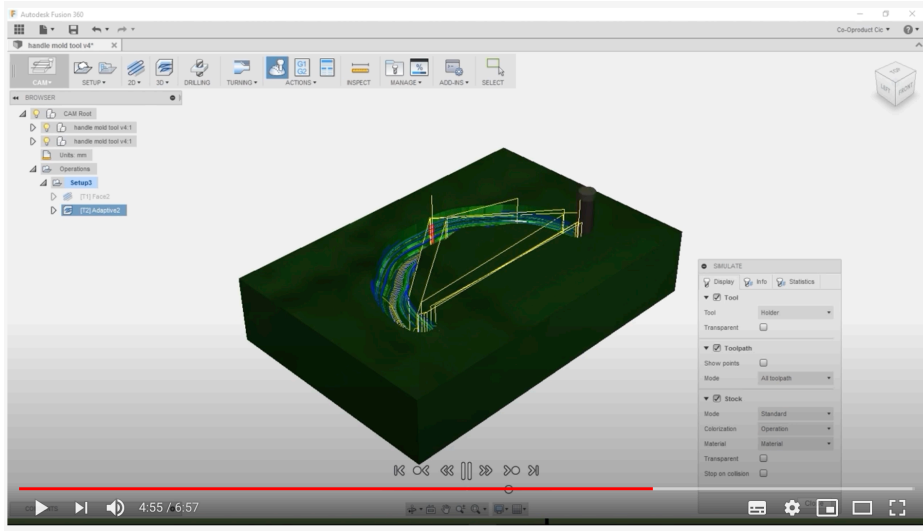
CAM

- <https://www.youtube.com/watch?v=JrmYZIrcuMs>



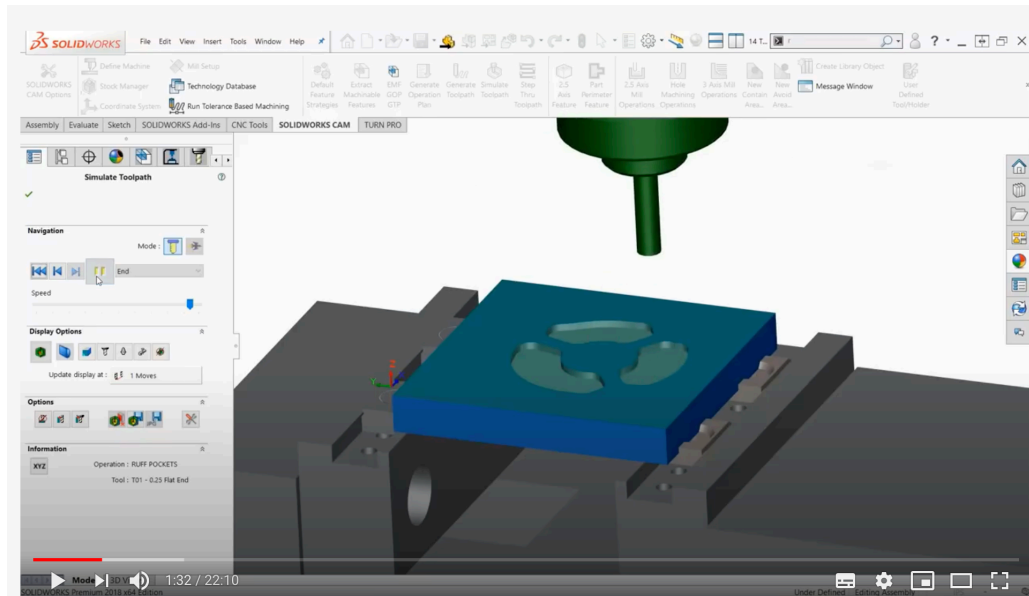
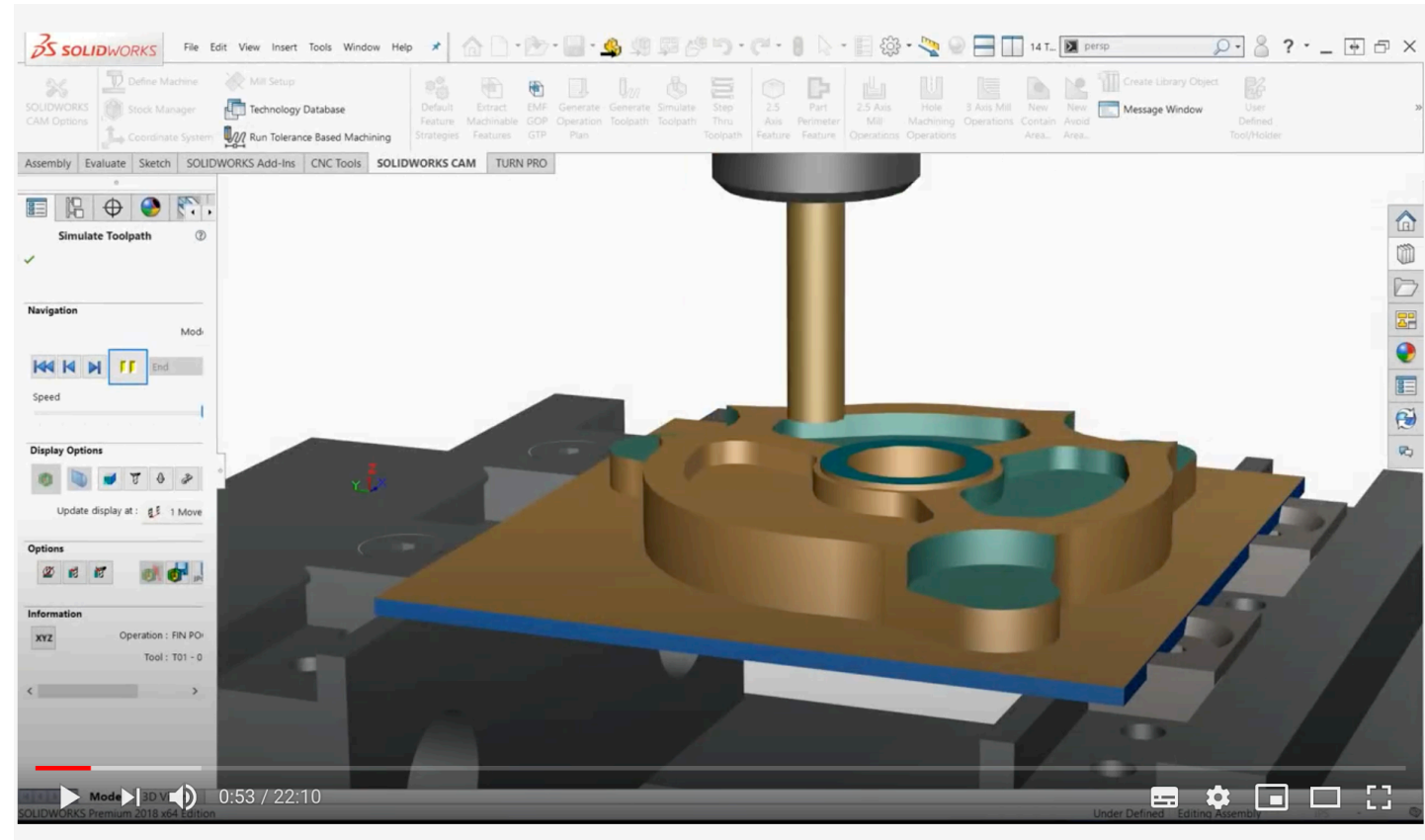
CAM

• <https://www.youtube.com/watch?v=JrmYZIrcuMs>



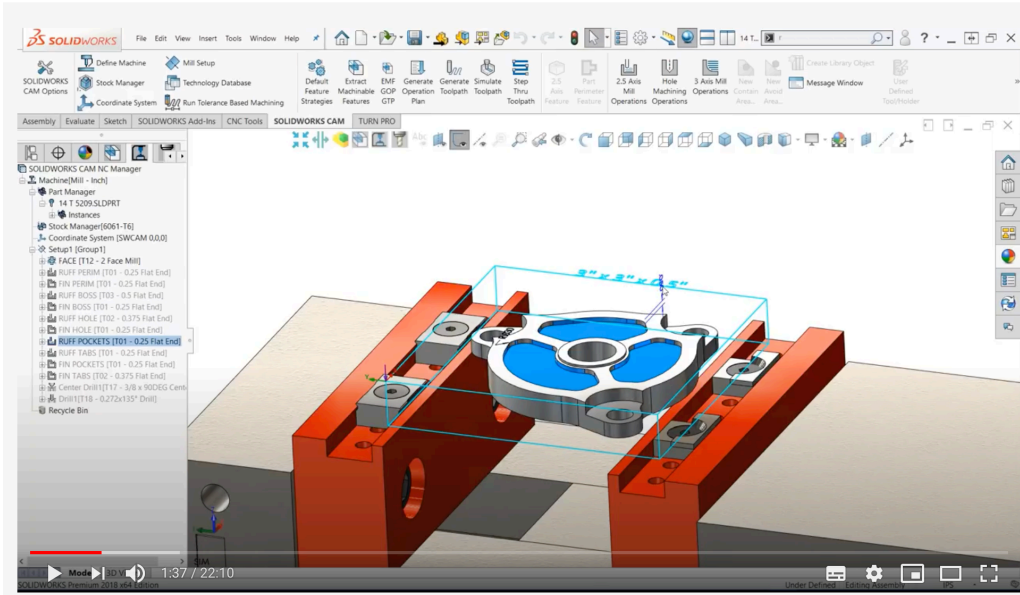
CAM

- <https://www.youtube.com/watch?v=00TqO1pBEro>

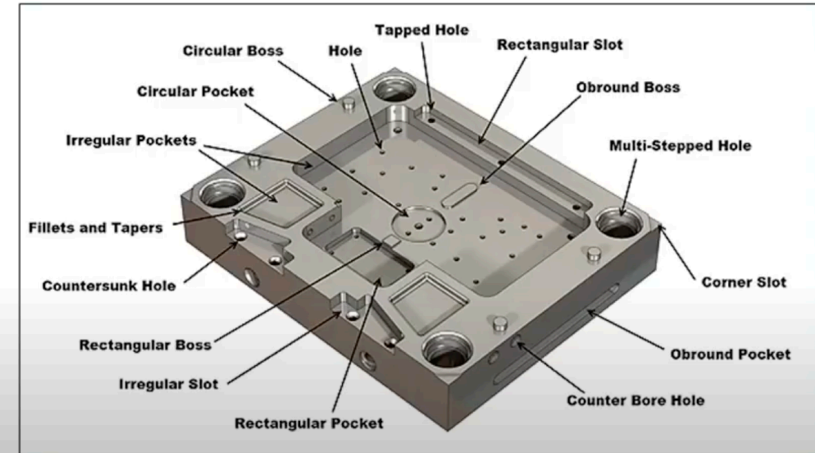


CAM

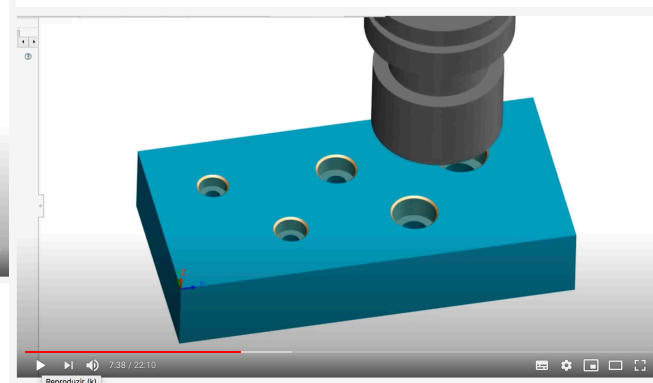
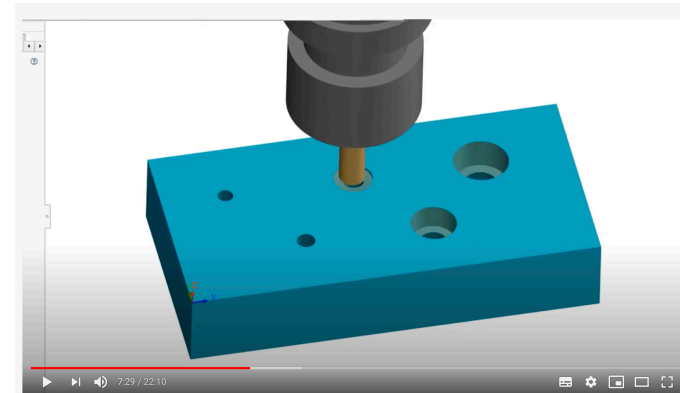
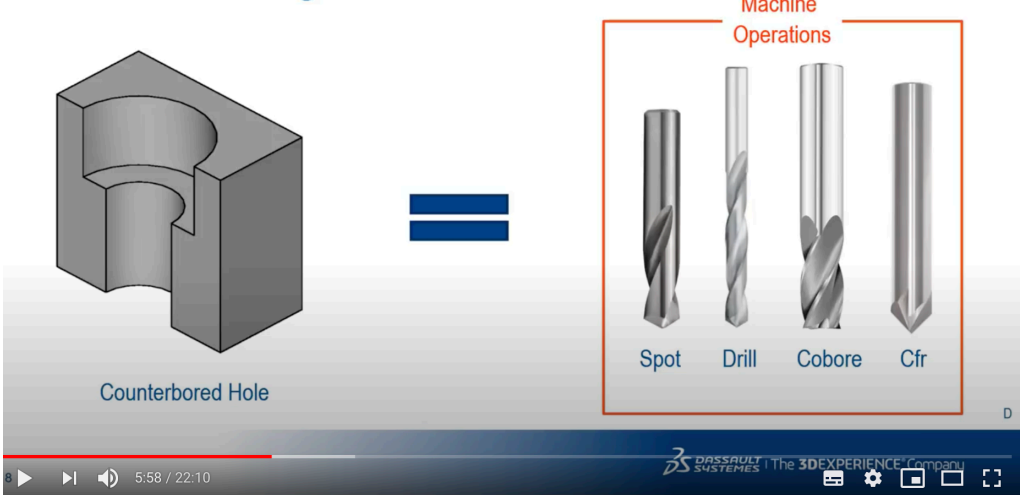
- <https://www.youtube.com/watch?v=00TqO1pBEro>



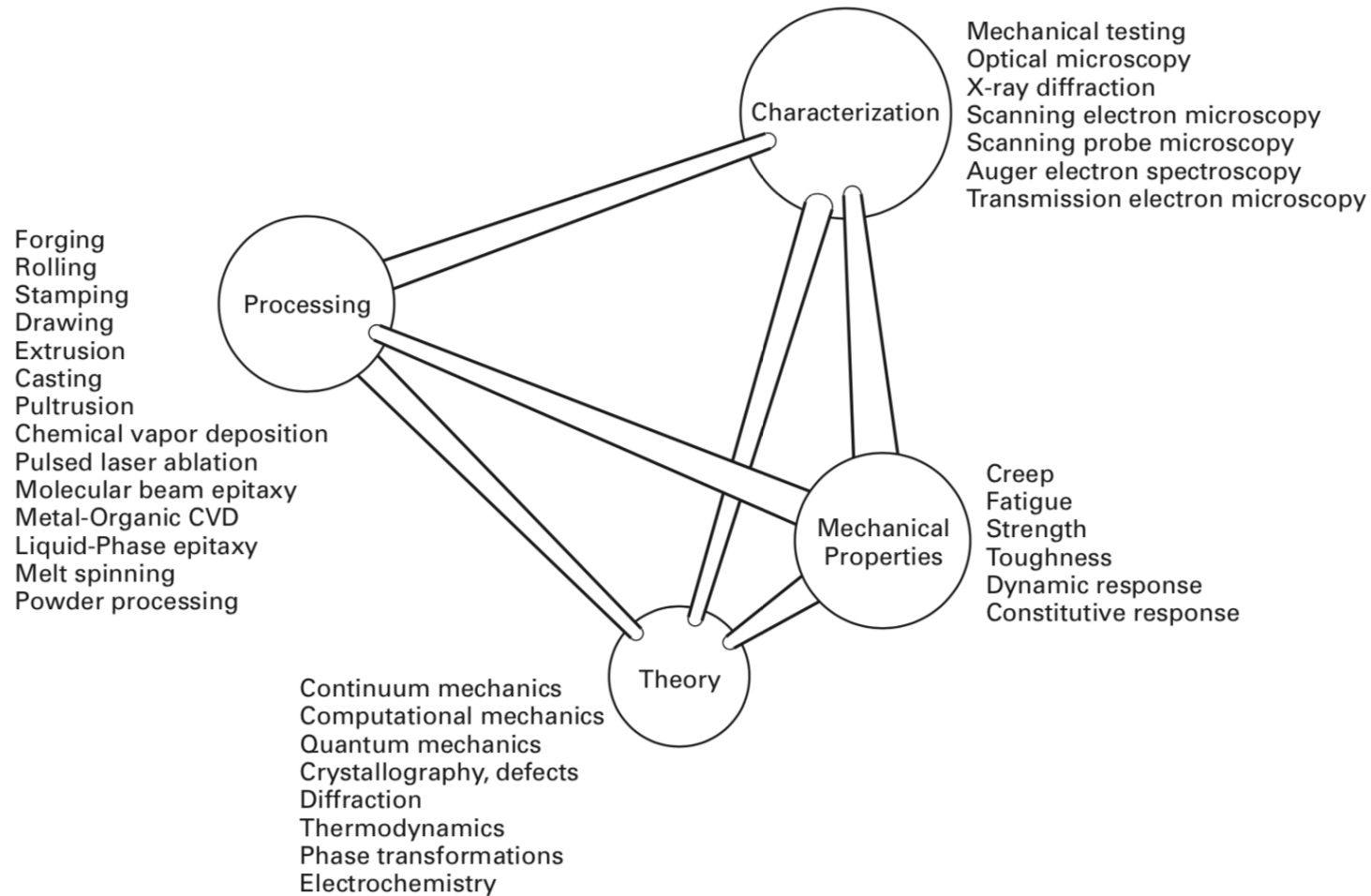
Automatic Feature Recognition



Manufacturing Features

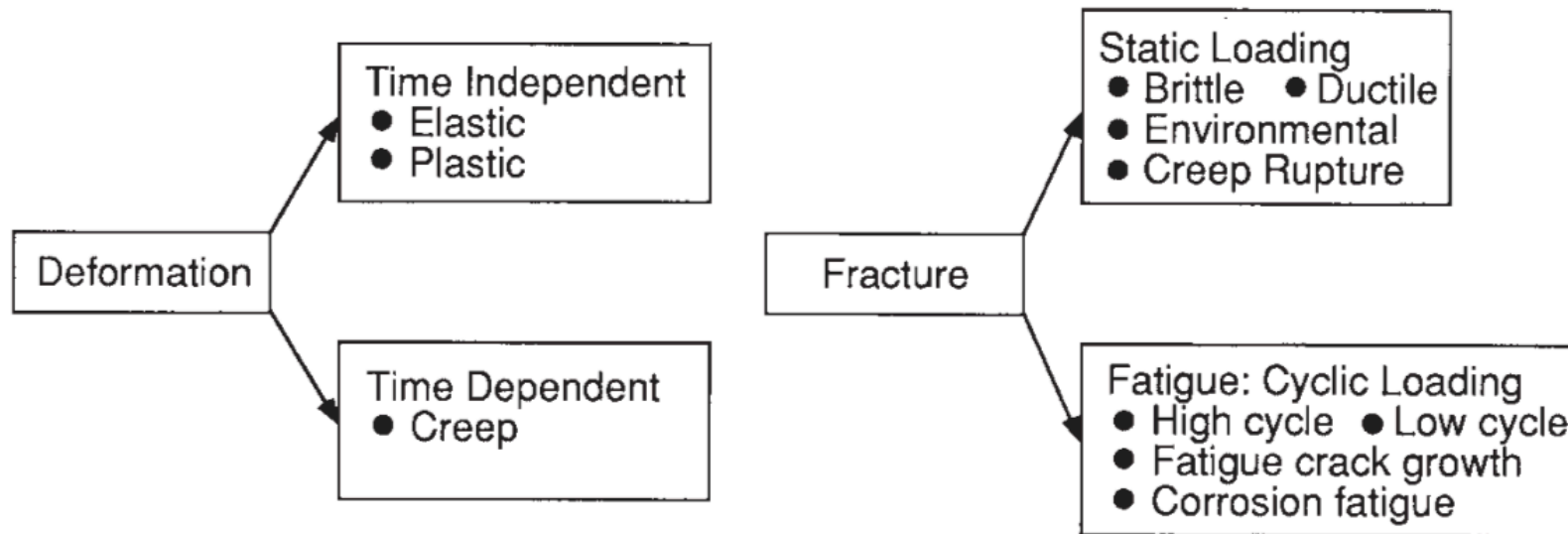


Mechanical and Tribological (Micro) Behavior Assessment using Finite Element Method Tools



Stress constrains that can cause failure!

Basic types of deformation and failure (Dowling, 2012)



How can we connect all possible mechanisms and conditions ???

Knowledge, characterization, experiments models and computational tools ...

And the effect stress constraints influence on damage



Mechanical Approach X Metallurgical/Materials Approach

1. **Materials are usually considered homogenous and isotropic**
2. Plastic deformation is based on **tension tests**
3. Failure deformation Principles
4. State
5. Strain rate and **constitutive equations** such as Johnson-Cook are important to describe the mechanical behavior
6. Damage is mainly evaluated during crack growth - Macro
7. Focus on Design of components

1. **Materials are usually considered heterogeneous and anisotropic**
2. Plastic deformation is based on **dislocations theory**, crystalline structure

Everything has to be considered!!!

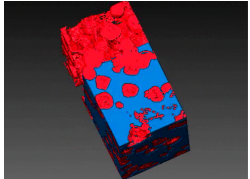
And the tool is FEM

3. Microstructural characterization (Macro and Micro levels) is an important tool
6. Mechanical behavior (mechanical properties and processing) – Micro
7. Focus on Design of Materials

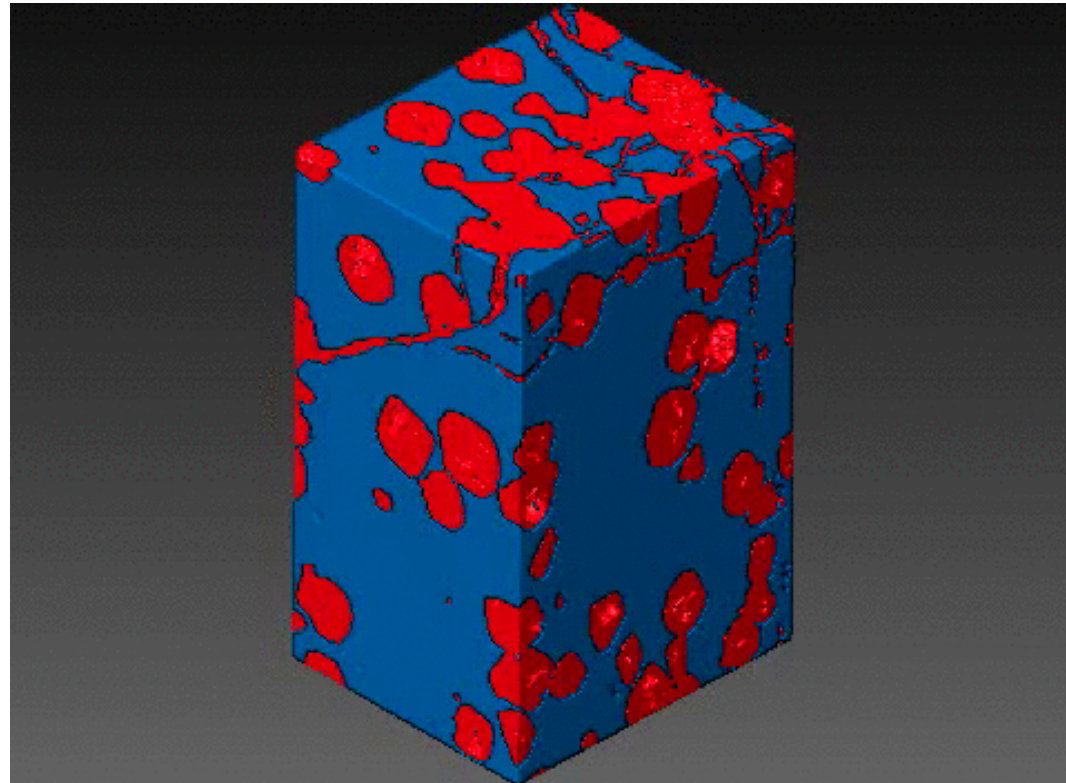
FEM Microescale

CAD, Parameters, MICROSTRUCTURE

X-Ray Tomography : resolution, density of phases



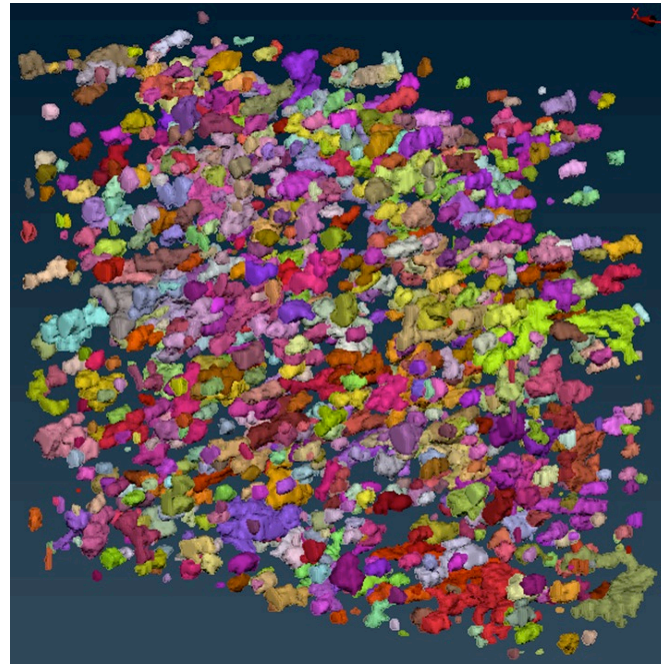
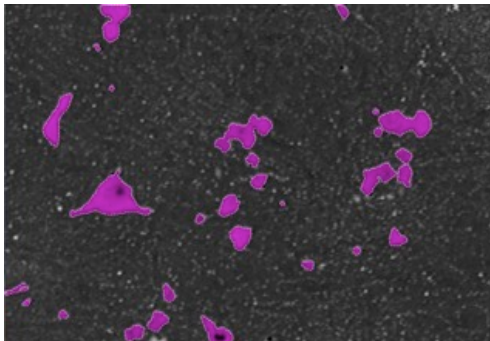
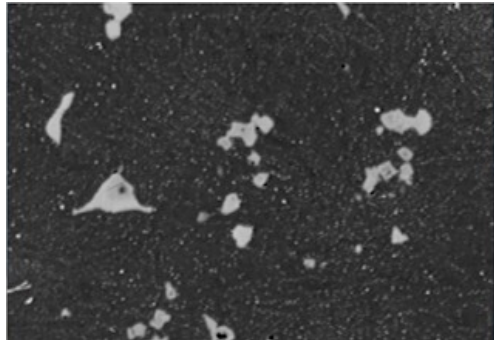
https://commons.wikimedia.org/wiki/File:Micro_CT_analysis_of_Ti2AlC_and_Al_composite.gif



FEM Microescale

CAD, Parameters, MICROSTRUCTURE

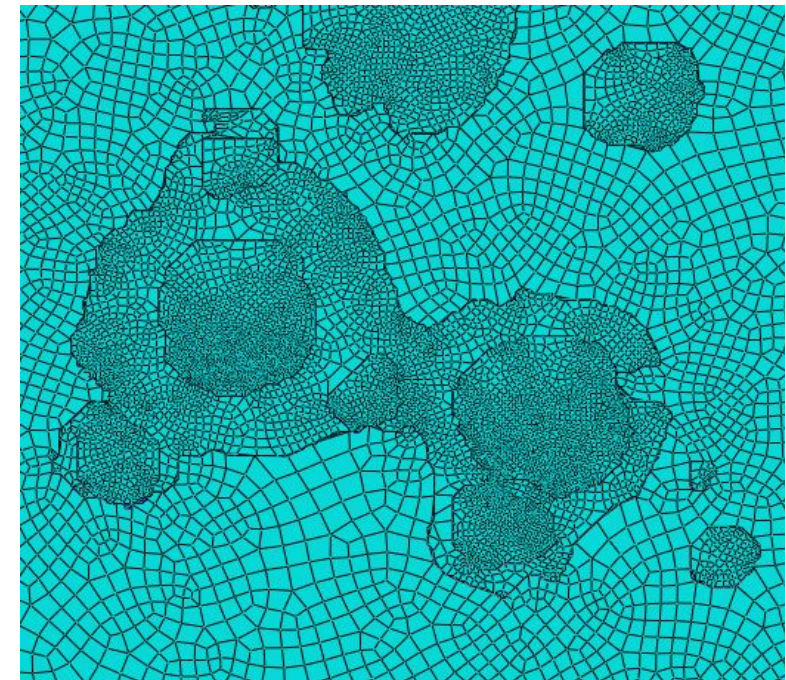
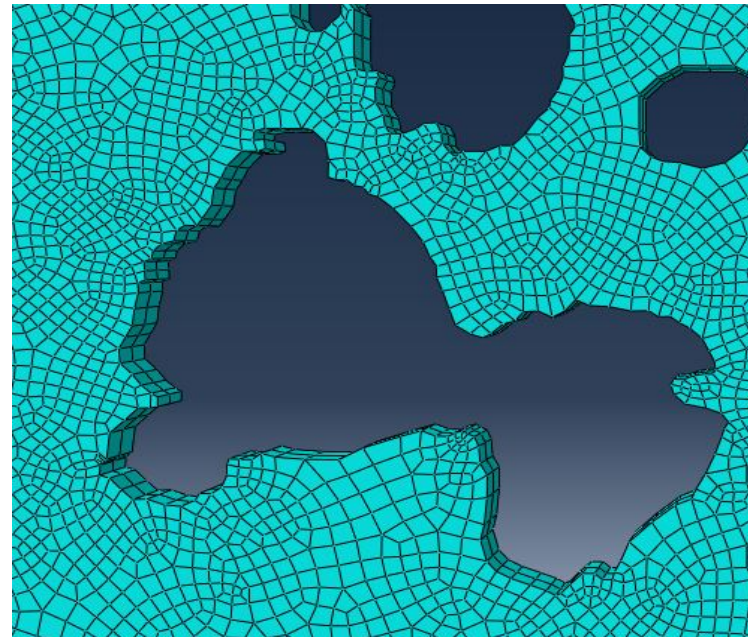
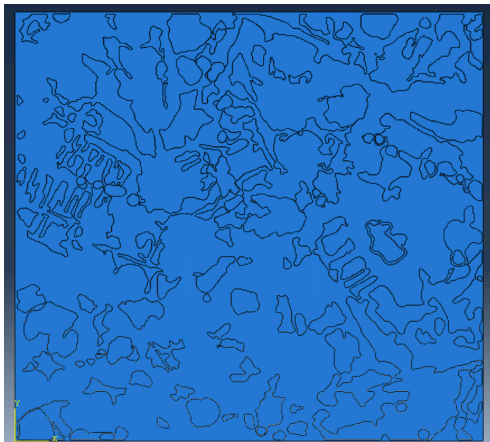
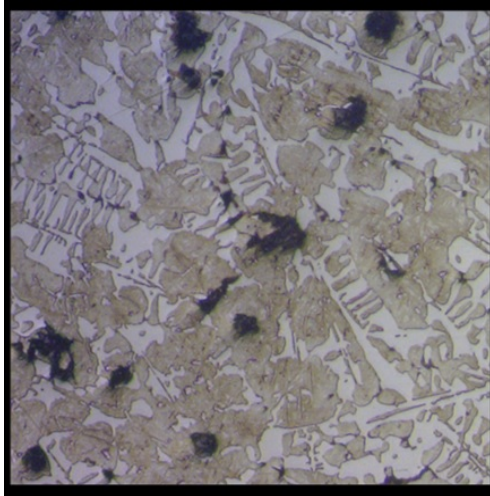
Softwares



FEM Microescale

CAD, Parameters, MICROSTRUCTURE

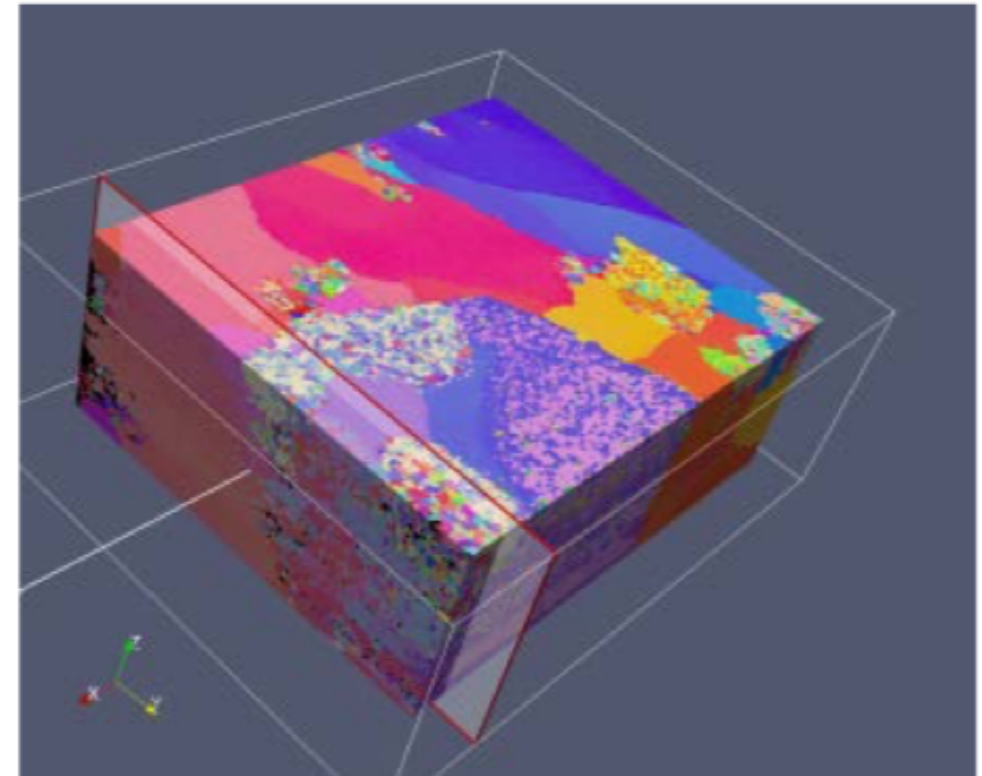
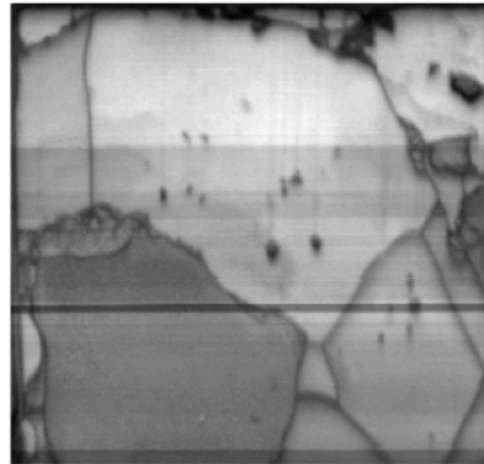
Softwares



FEM Microescale

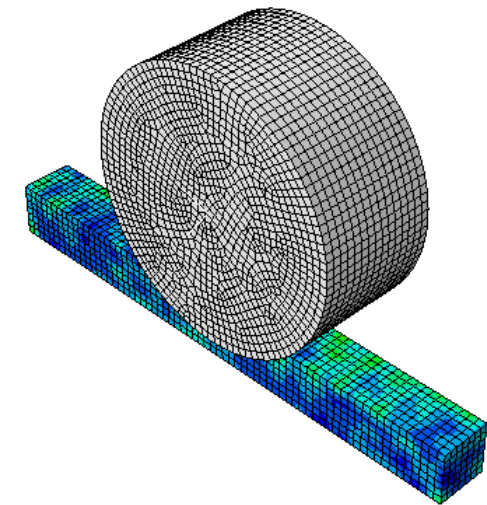
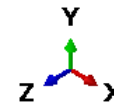
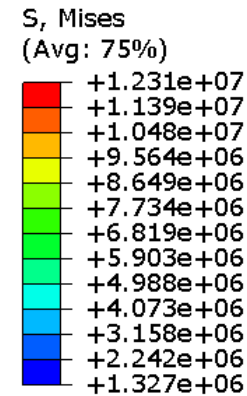
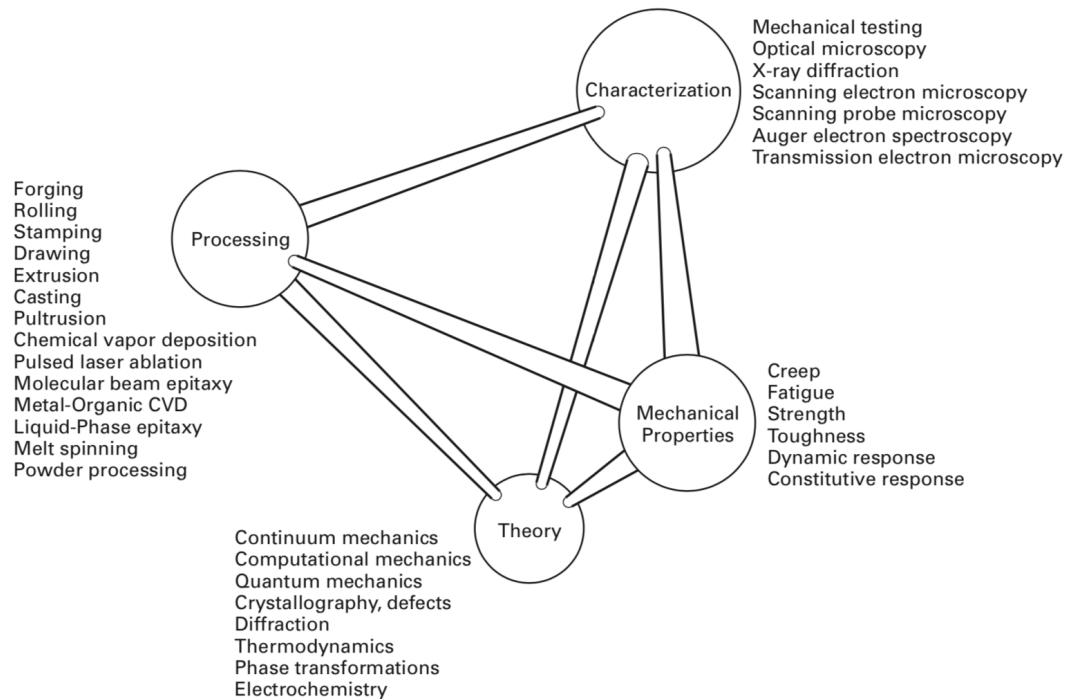
CAD, Parameters, MICROSTRUCTURE

FIB - EBDS



<https://www.osti.gov/servlets/purl/1358236>

Mechanical and Tribological (Micro) Behavior Assessment using Finite Element Method Tools



Meyers and Chawla, Mechanical behavior of Materials , 2009

1

Finite element analysis of the effects of thermo-mechanical T loadings on a tool steel microstructure

V. Seriacopi*, N.K. Fukumasu, R.M. Souza, I.F. Machado, Engineering Failure Analysis, <https://doi.org/10.1016/j.engfailanal.2019.01.006>

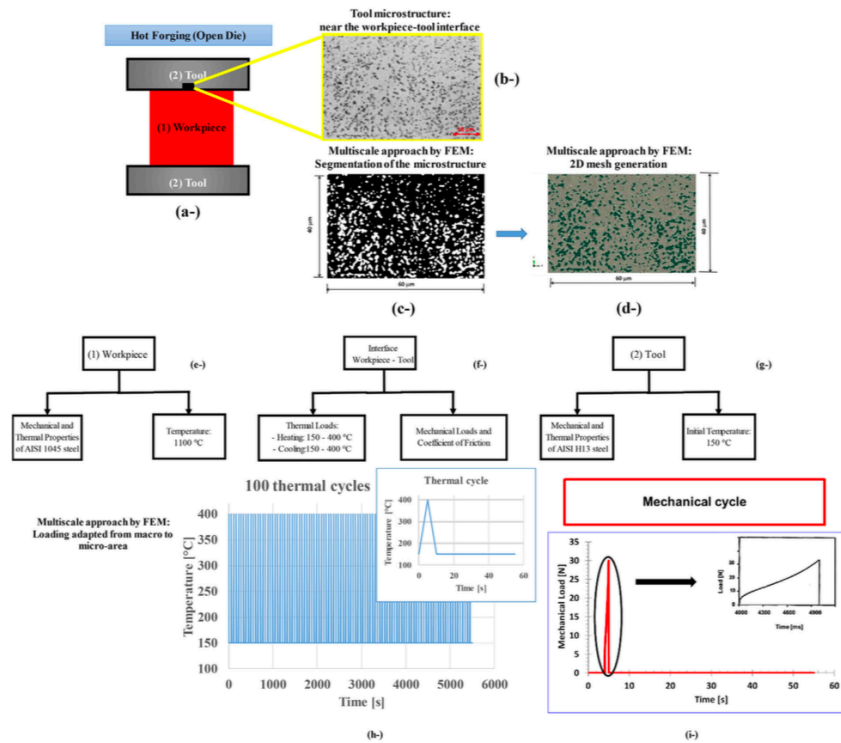


Fig. 1. Schematic representation containing the assumption of the micro-analyses conducted from the macroscopic system, mainly focused on the hot forging tool. Simplified frames are provided to specify the inputs of the models: purely thermal and thermo-mechanical loadings: (a-) general layout of the open die forging process, where (1) is the workpiece and (2) is the tool; (b-) microstructure of the tool steel studied; (c-) micrograph after segmentation, considering gray scales; (d-) 2D mesh assigned to the microstructural region evaluated; (e-) inputs of the numerical model regarding the workpiece - AISI 1045 steel; (f-) inputs of the numerical model regarding the interface between tool and workpiece; (g-) inputs of the numerical model regarding the tool - AISI H13 steel; (h-) thermal cycle considered on the analyses; and (i-) mechanical cycle evaluated by numerical modelling.

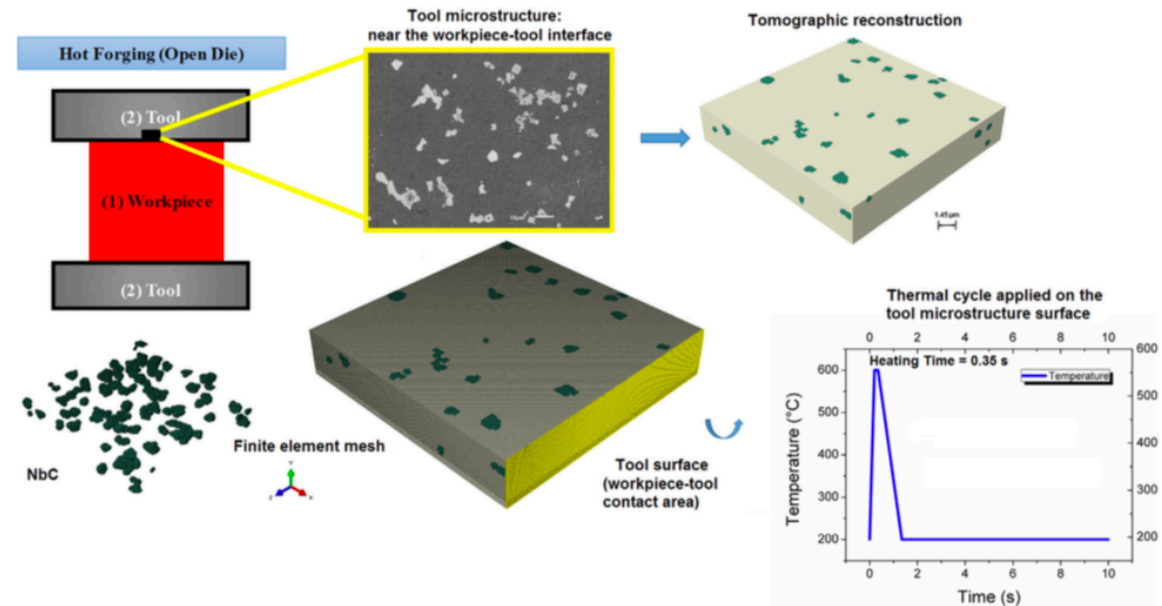


Fig. 8. Microstructure of the hot forging tool steel, consisting of martensitic matrix and niobium carbides (in green), and a detail of these carbides with the finite element mesh. Also, thermal cycle applied during the heat transfer analysis on the tool microstructure surface (yellow area) is shown. (For interpretation of the references to colour in this figure legend, the reader is referred to the web version of this article.)

Finite element analysis of the effects of thermo-mechanical loadings on a tool steel microstructure

V. Seriacopi*, N.K. Fukumasu, R.M. Souza, I.F. Machado, Engineering Failure Analysis , <https://doi.org/10.1016/j.engfailanal.2019.01.006>

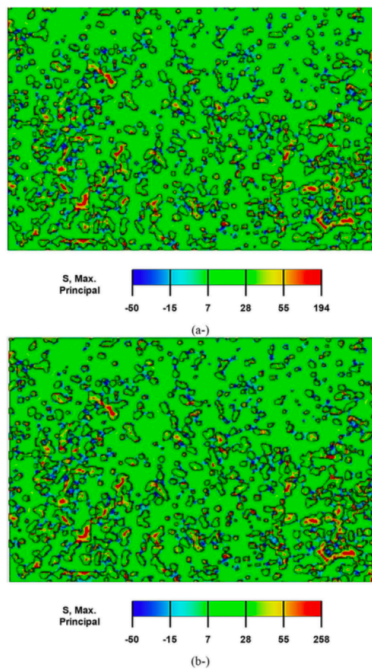


Fig. 6. Thermo-mechanical Loading results: Evolution of the results for Maximum Principal Stress [MPa] obtained during the post-cooling: (a-) First cycle; (b-) Hundredth Cycle.

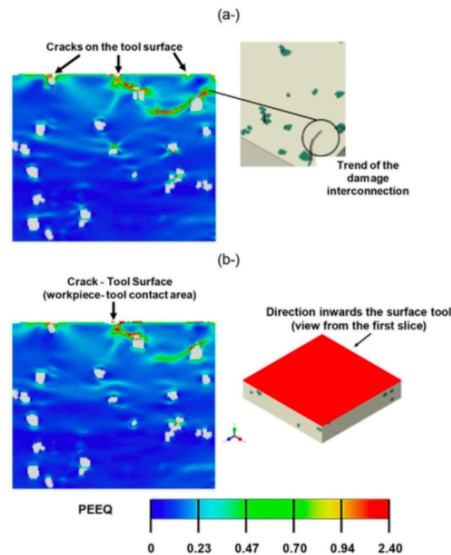


Fig. 11. View from the first slice in the direction inwards the surface tool - Equivalent plastic strain (PEEQ) field after the cooling for the following cases of NbC fracture toughness: 5 MPam^{1/2} (a) and 7 MPam^{1/2} (b).

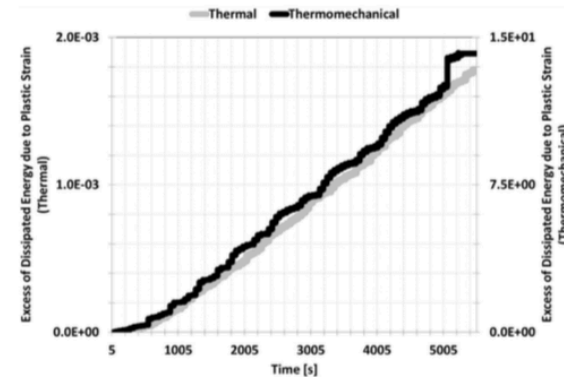
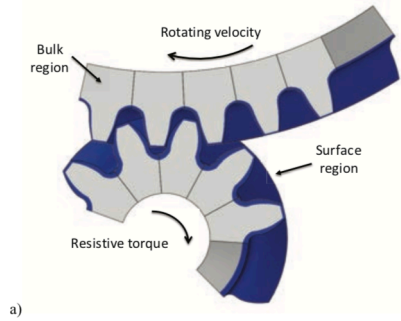


Fig. 7. Excess of the energy dissipated due to plastic strain along the time during 100 thermal cycles. This parameter was calculated from the normalized relation by 5 first seconds of heating.

2

Stress Analysis to Improve Pitting Resistance in Gear Teeth

Newton K.Fukumasu Guilherme A.A.Machado Roberto M.Souza Izabel F.Machado
<https://doi.org/10.1016/j.procir.2016.02.349>



a)



b)

Fig. 1 – Finite Element Model of the helical gears: a) numerical model of five pairs of helical gear tooth, in which blue indicates the near surface region while the light gray indicates the bulk region of gear teeth; b) central point and path of numerical results extraction.

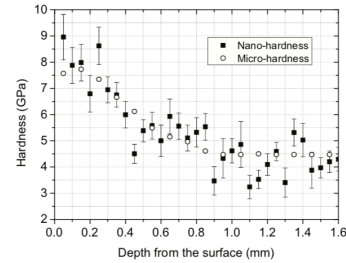
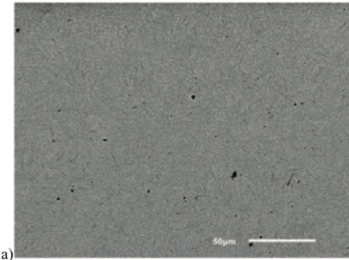
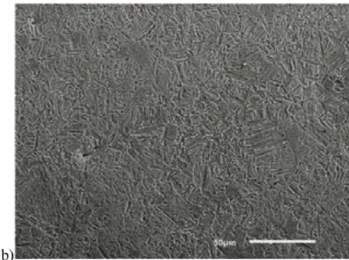


Fig. 3 – Hardness profile from surface towards the inner region of the helical gear measured by micro and nano-indentation techniques.

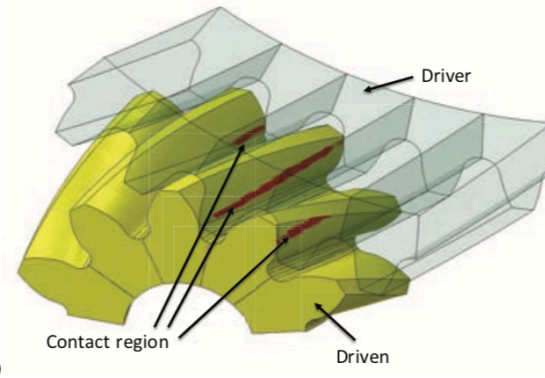


a)

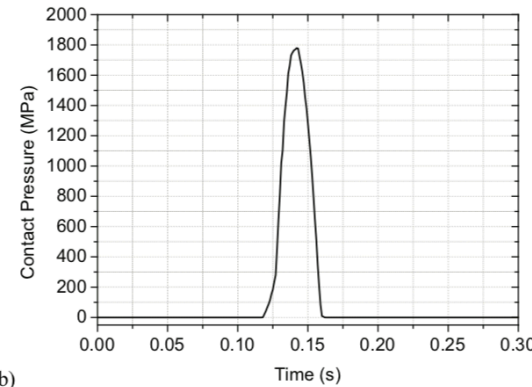


b)

Fig. 2 – Back scattering SEM image of the microstructure of one gear tooth: a) bainitic inner region and b) martensitic surface region.

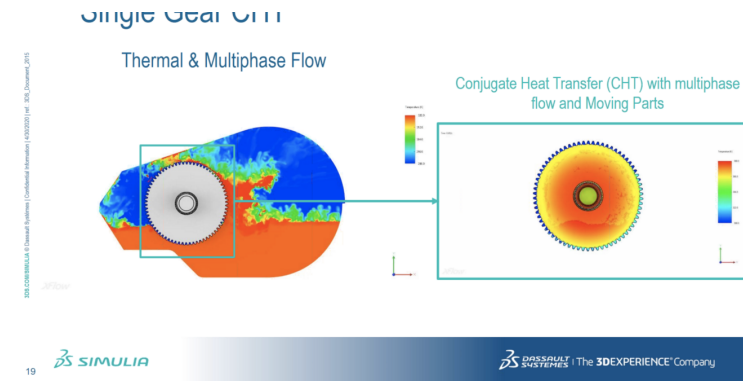


a)



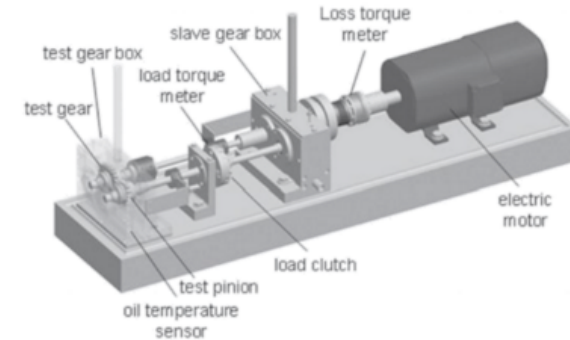
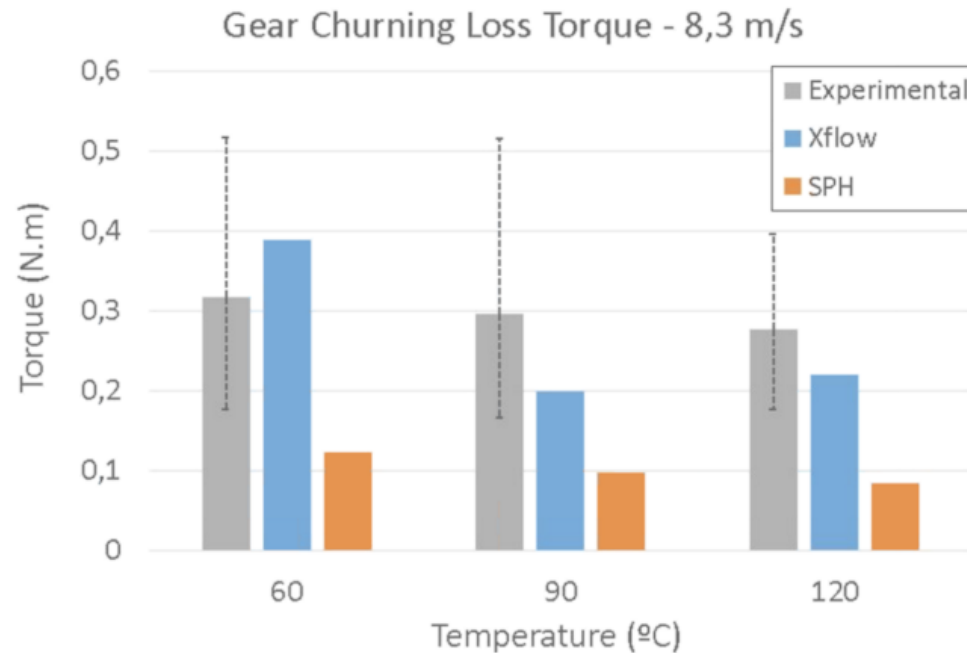
b)

Fig. 4 – Contact in an engaged helical gear pair: a) contact region distributed in three pairs of gear tooth (red region) and b) evolution of contact pressure in the central point of the gear tooth (Fig. 1b).



Simulação do funcionamento de engrenagens

1.20 Gear Test Rig



Liu et al., Numerical modelling of oil distribution and churning gear power losses of gearboxes by SPH, J. of Engineering Tribology, 2019

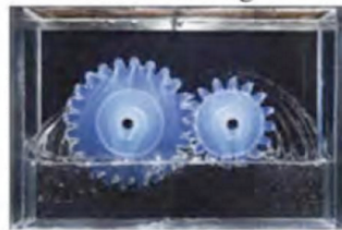
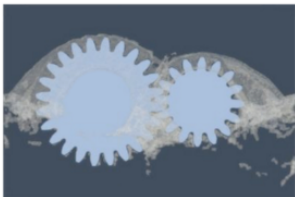
3DS.COM/SIMULIA © Dassault Systèmes | Confidential Information | 4/30/2020 | ref.: 3DS_Document_2015

FGZ – churning losses

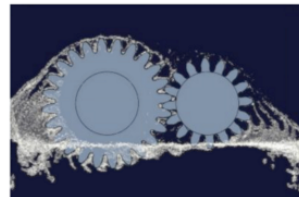
1/2 G Gear Testing



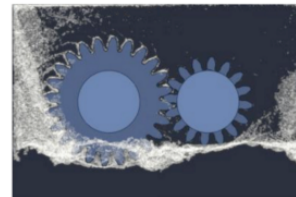
$v_t = 0.88$ m/s
IOL = centerline



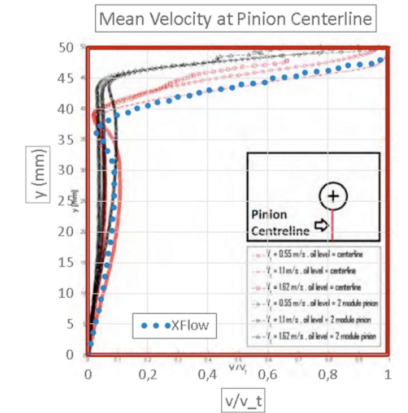
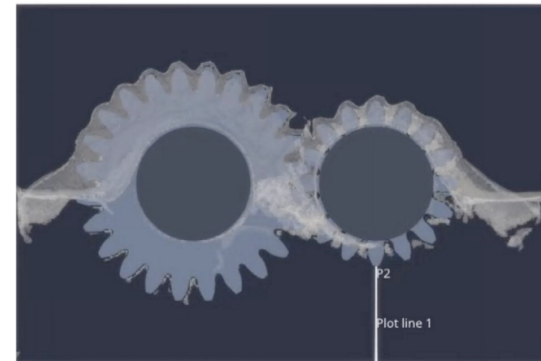
$v_t = 0.88$ m/s
IOL = pinion pitch radius



$v_t = 2.64$ m/s
IOL = pinion pitch radius

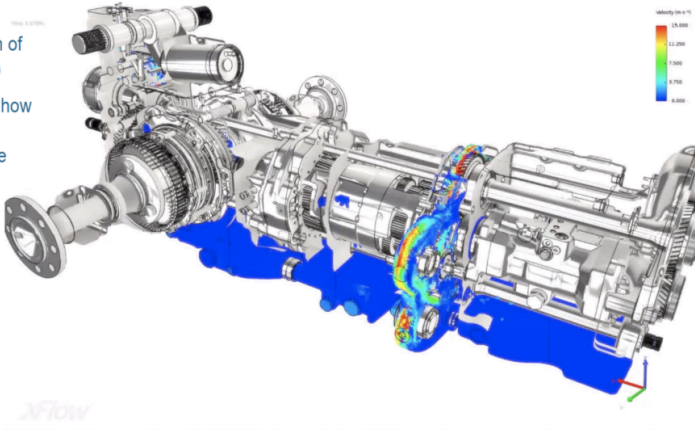


1/2 G Gear Testing



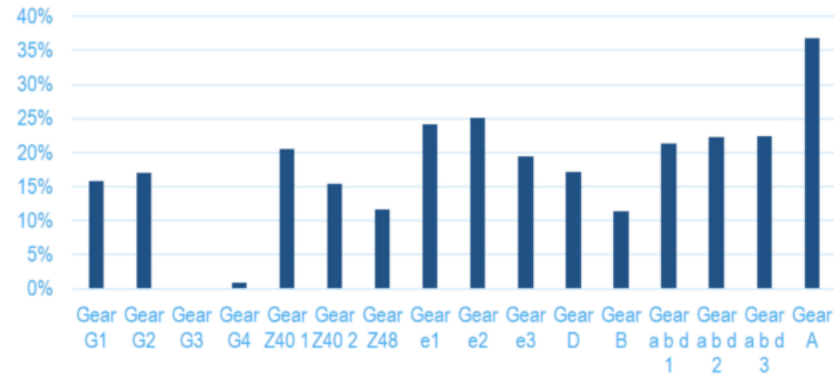
MARKERS - COLORED BY VELOCITY

- ▶ Markers provide an indication of where the liquid phase (oil is)
- ▶ In this animation we can see how the oil behaves and how it transitions from rest to regime

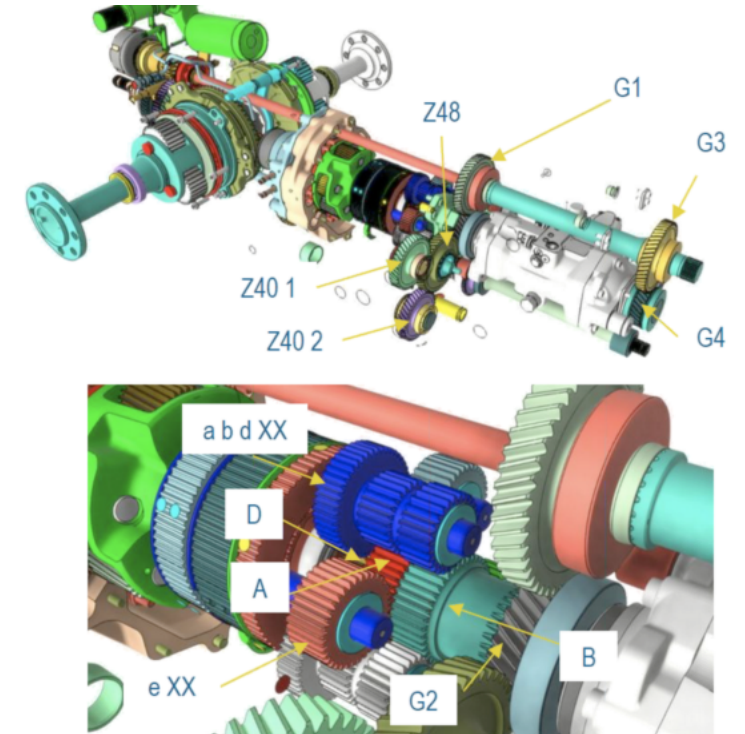


Gears Wet Surface

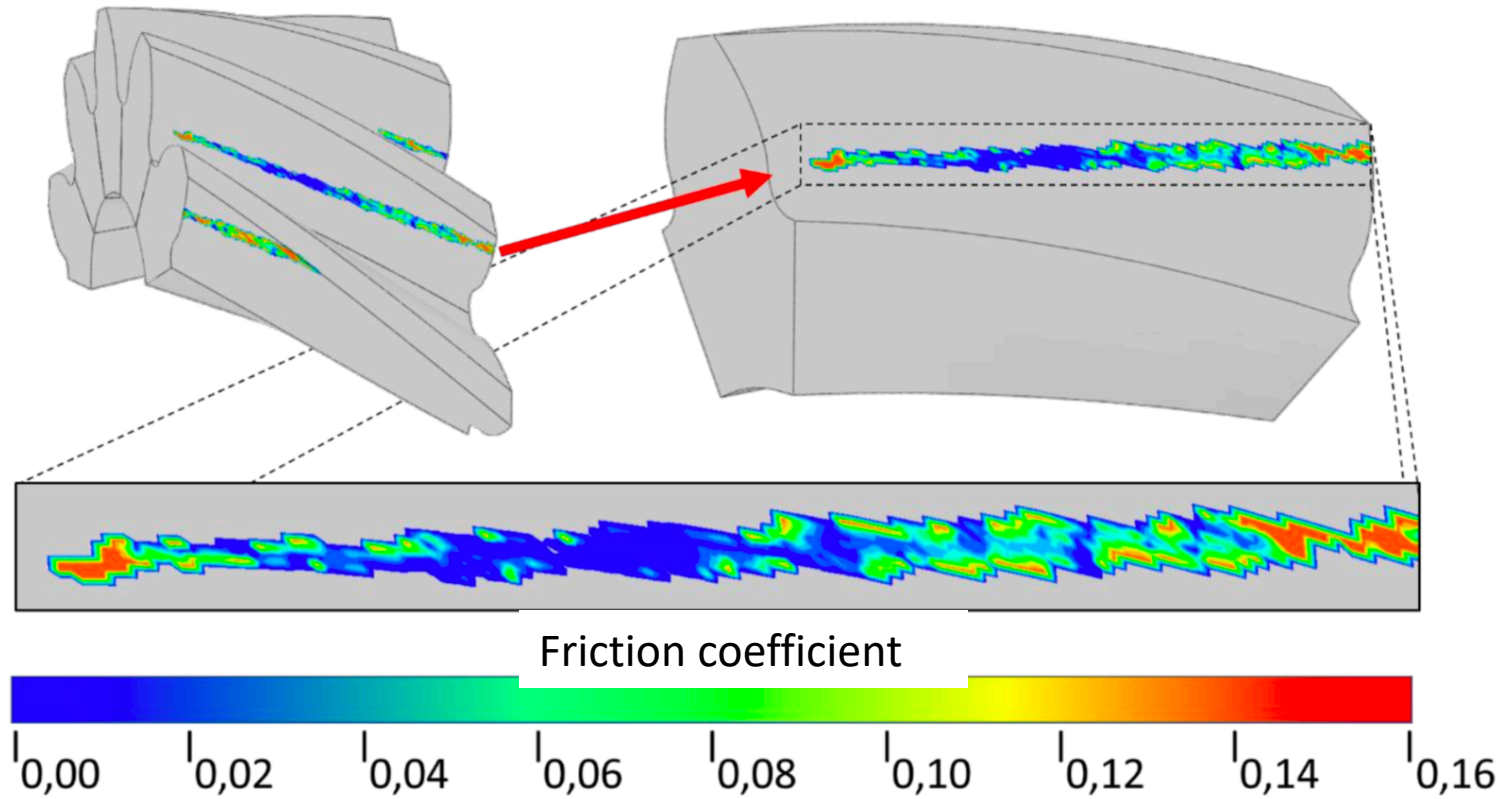
Gears Wet Surface, % of total



- ▶ The chart reports the % of wet surface for the rotating gears
- ▶ Note how Gears G3 and G4 are not lubricated at all



Friction evaluation during contact – manual transmission



3



Experimental and numerical analysis of dry contact in the pin on disc test

E.M. Bortoleto, A.C. Rovani, V. Seriacopi, F.J. Profito, D.C. Zachariadis, I.F. Machado, A. Sinatora, R.M. Souza, WEAR.
<http://dx.doi.org/10.1016/j.wear.2012.12.005>

Table 2
 Material properties of the pin (AISI 4140 steel) and disc (AISI H13 steel) [14].

	Material	
	AISI 4140 (wt%)	AISI H13 (wt%)
Density [kg/m ³]	7885	7800
Elastic modulus [GPa]	210	210
Poisson's ratio	0.29	0.3
Yield stress [MPa]	1370	1410

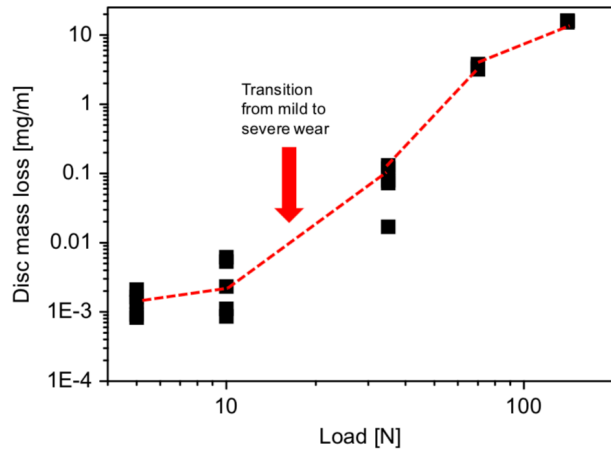


Fig. 6. Disc mass loss of the experimental results for the 5, 10 35, 70 and 140 N.

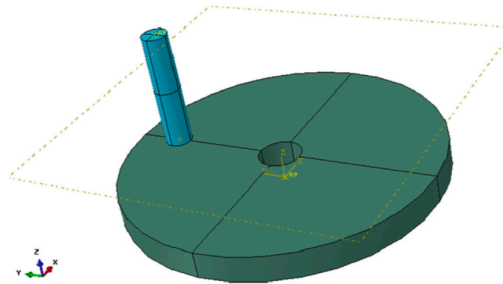


Fig. 1. Geometry of the contact pair pin on disc (tribological system).

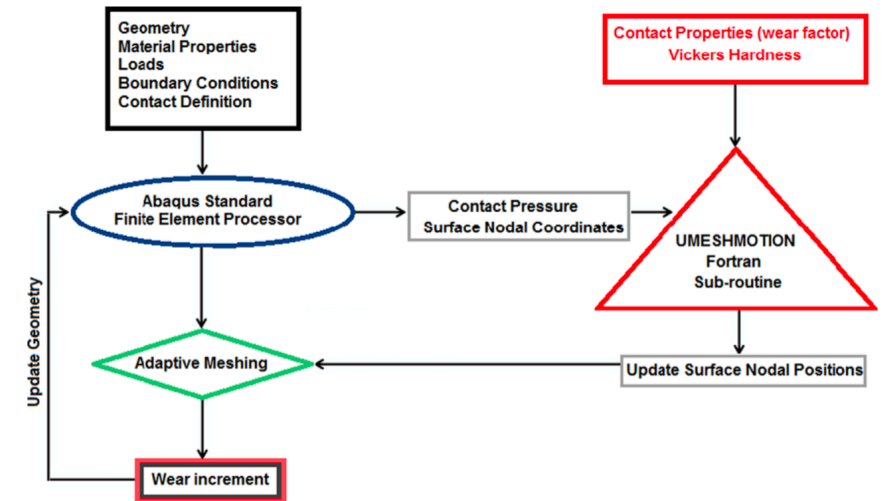


Fig. 4. Flowchart for the UMESHMOTION subroutine.

Experimental and numerical analysis of dry contact in the pin on disc test

E.M. Bortoleto, A.C. Rovani, V. Seriacopi, F.J. Profito, D.C. Zachariadis, I.F. Machado, A. Sinatora, R.M. Souza, WEAR.

<http://dx.doi.org/10.1016/j.wear.2012.12.005>

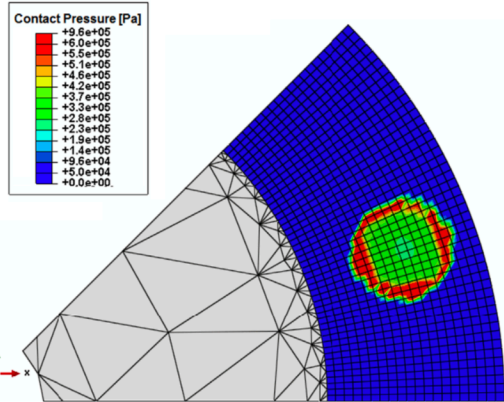


Fig. 8. Contact pressure on the disc surface during pin sliding with 10 N normal load.

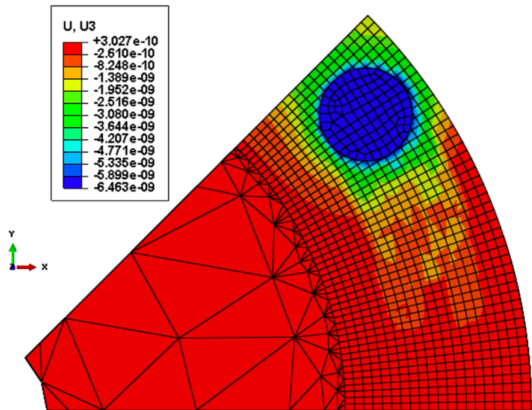


Fig. 12. Superposition of elastic deformation effects and wear after pin sliding over disc surface.

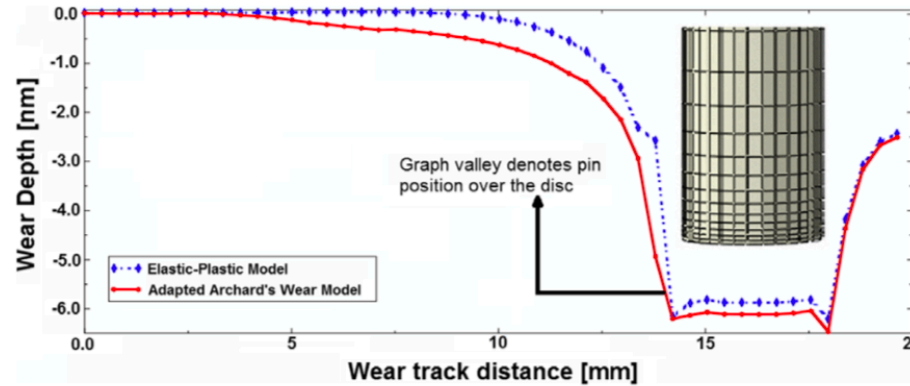


Fig. 11. Comparison between wear profile (continuous line) and elastic deformation (dashed line) during pin sliding over disc under 10 N load along movement direction.

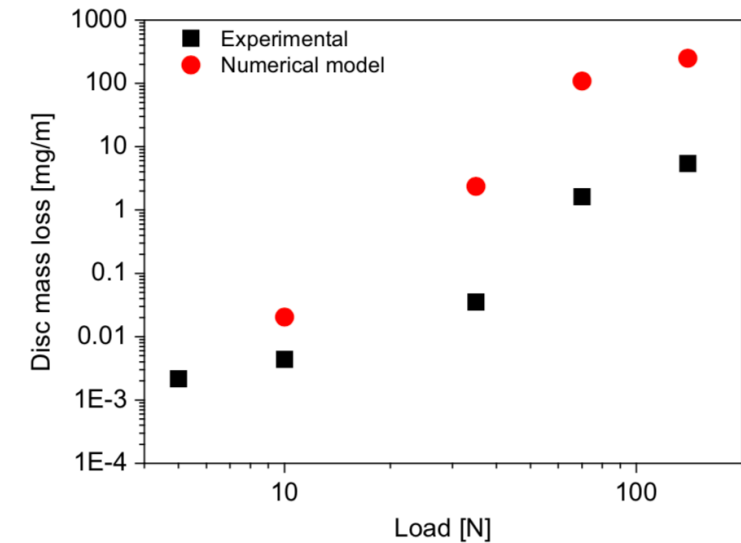


Fig. 10. Comparison between mass losses of experimental and numerical results after the sliding wear.

4

Numerical Model of Machining Considering the Effect of MnS Inclusions in an Austenitic Stainless Steel

G.M.P.Chagas, I.F.Machado

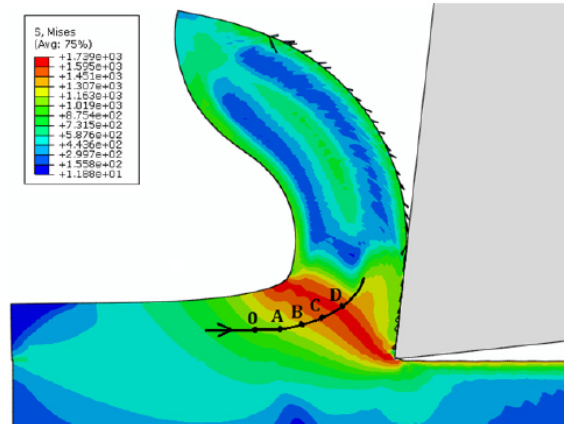
<https://doi.org/10.1016/j.procir.2015.04.093>


Fig. 4. Von Mises stress with positions evaluated along the flow line

Table 4. Maximum and minimum plane stress

Distance	σ_1 (MPa)	σ_2 (MPa)
0-A	59	-1267
A-B	118	-1229
B-C	470	-1151
C-D	615	-1187

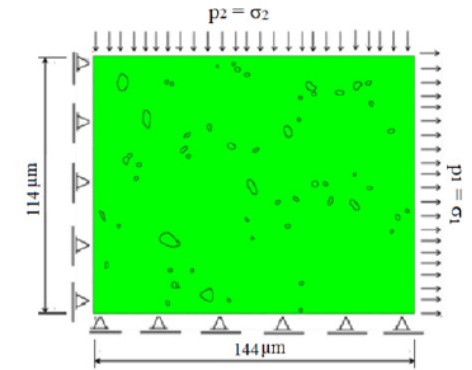
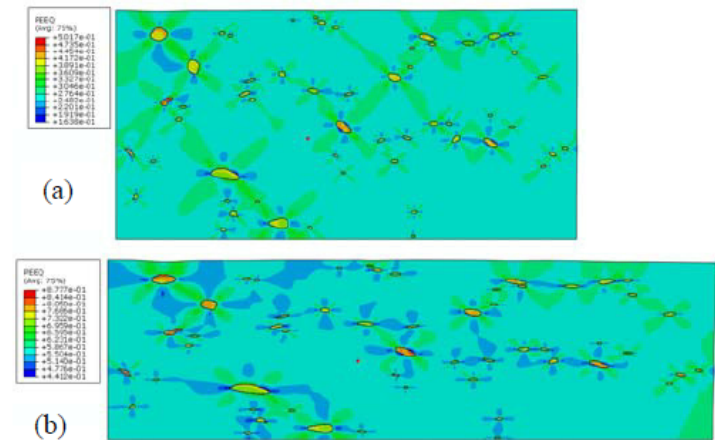
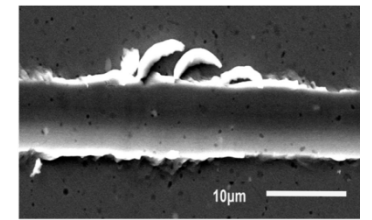
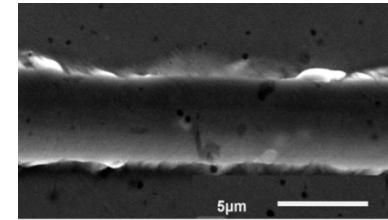


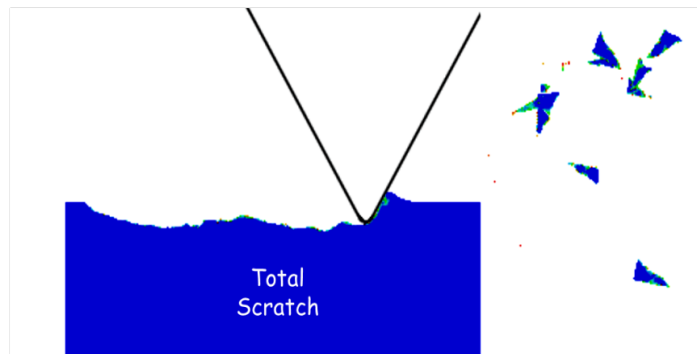
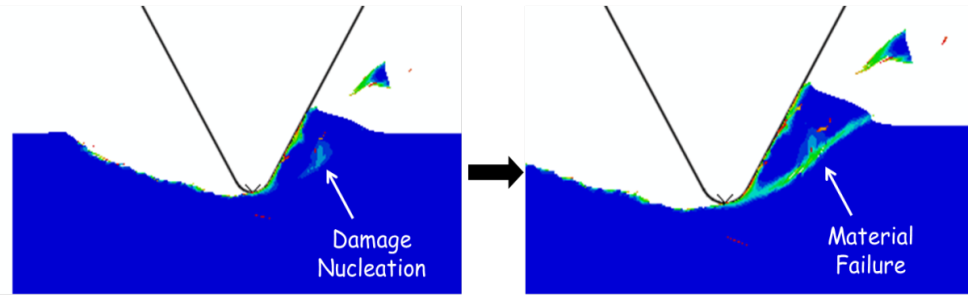
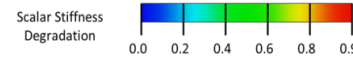
Fig.7. Microstructure boundary conditions and loads applied


 Fig. 11 Equivalent plastic strain behavior:
 (a) in the instant time of 8.083×10^{-3} s, (b) instant of time of 2.546×10^{-4} s.

Phenomena – Abrasion, 2D analysis

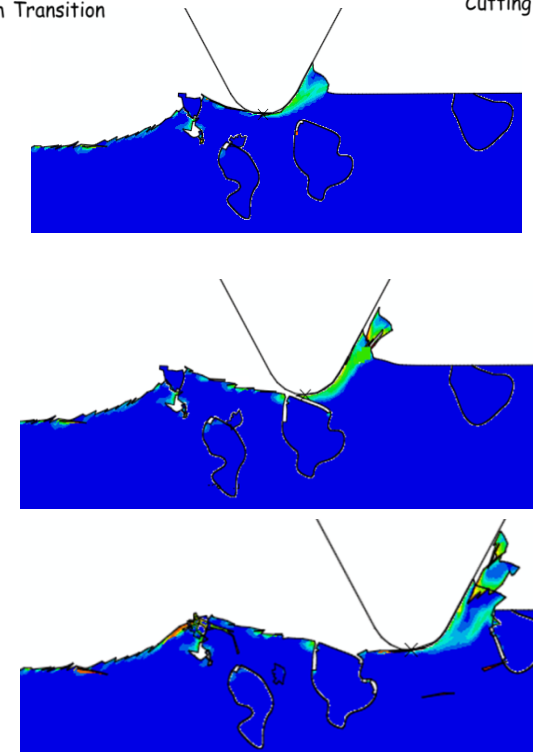


Chip formation mechanism during cutting: When the scalar stiffness degradation is unity, the material failure will occur promoting debris such as discontinuous chips agreement with the experimental results.

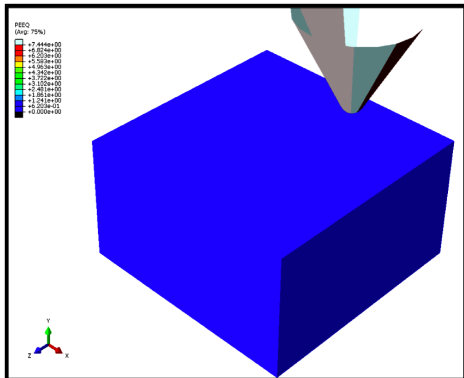


50 mN - Mechanism Transition

100 mN - Cutting



Homogeneous material



Analysis of abrasion mechanisms in the AISI 303 stainless steel: Effect of deformed layer

V. Seriacopi, N. K. Fukumasu, R. M. Souza, I. F. Machado

10.1016/j.procir.2016.02.326

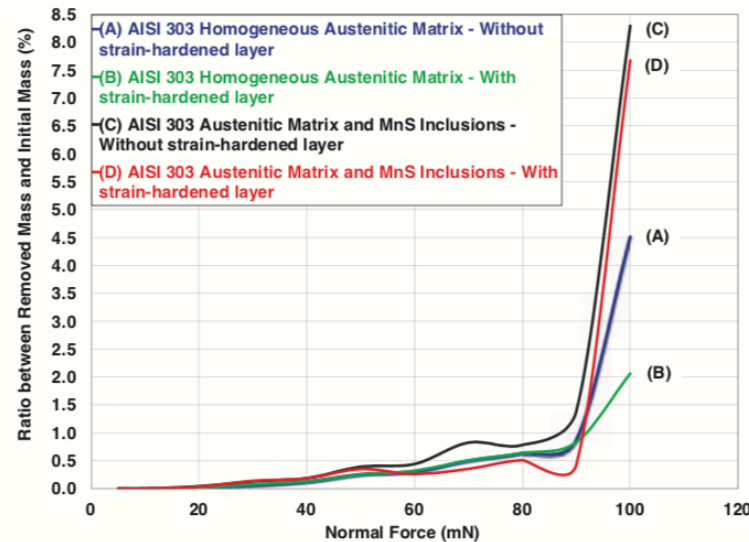
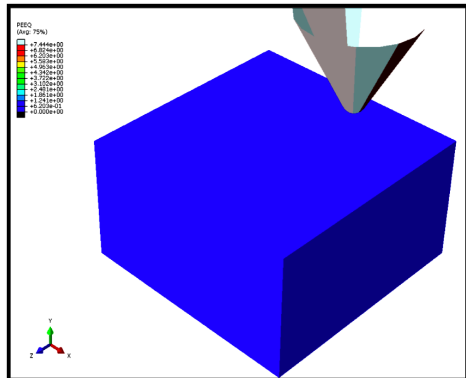
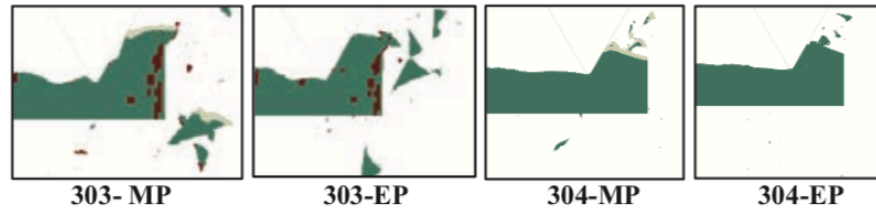


Fig. 6. Numerical results of mass removal by abrasion, obtained considering difference in surface finishing and microstructure.

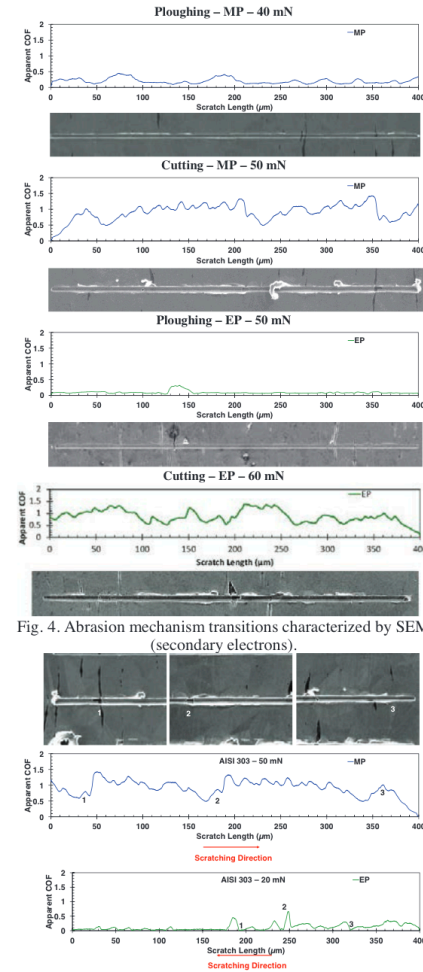


Fig. 4. Abrasion mechanism transitions characterized by SEM (secondary electrons).

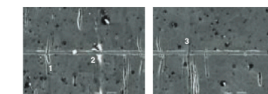


Fig. 5. Experimental results of scratch test at the microscale: details of AISI 303 microstructural behavior.

Vanessa Seriacopi. Evaluation of abrasive mechanisms in metallic alloys during scratch tests: a numerical-experimental study in micro-scale. 2017.

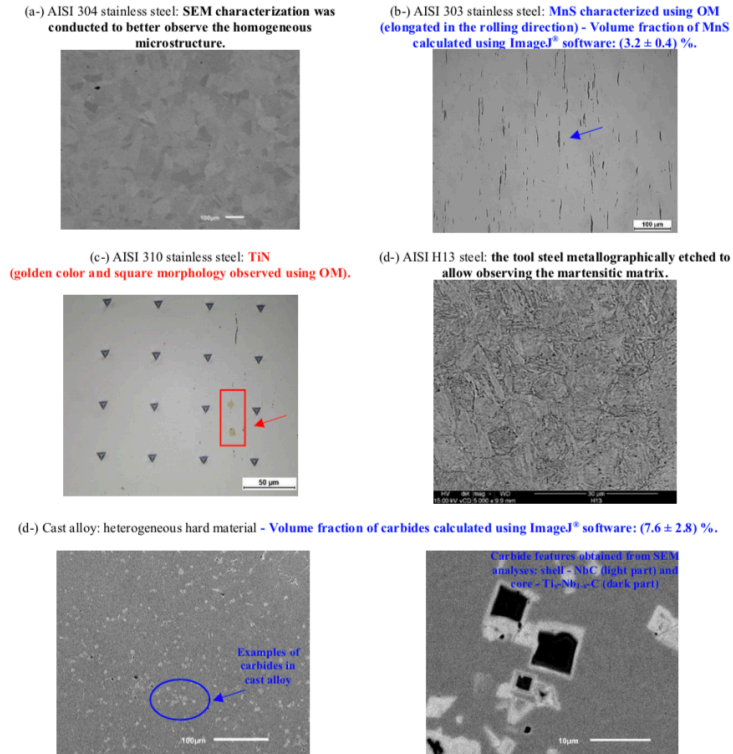


Figure 1. Characterization microstructural using different techniques (SEM – Scanning Electron Microscopy – and OM – Optical Microscopy) of the materials evaluated in the present work.

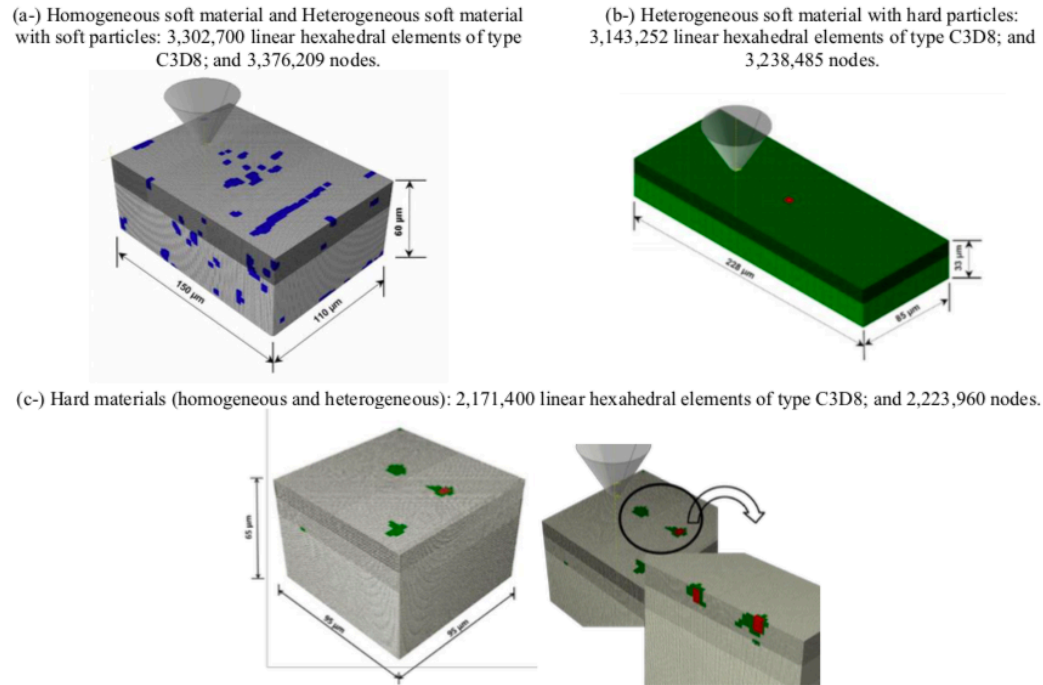


Figure 2. Finite element meshes generated from the microstructures of the materials studied: (a-) details of the heterogeneous soft material with soft precipitates (Group 2), composed by austenitic matrix and manganese sulfides; and (b-) heterogeneous soft material with hard precipitate (Group 3): austenitic matrix and titanium nitride; (c-) details of the heterogeneous hard material (Group 5), composed by martensitic matrix and niobium carbides, which are divided into a shell (in green – rich in Nb) and a core (in red – rich in Ti) [16].

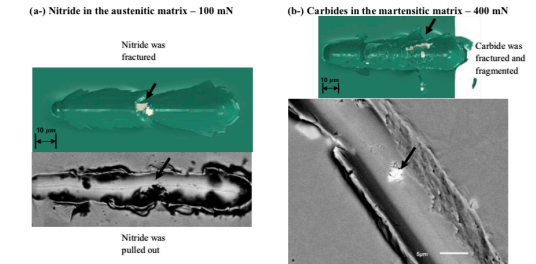
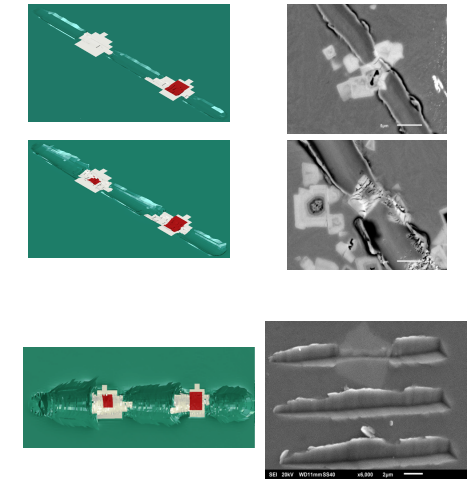
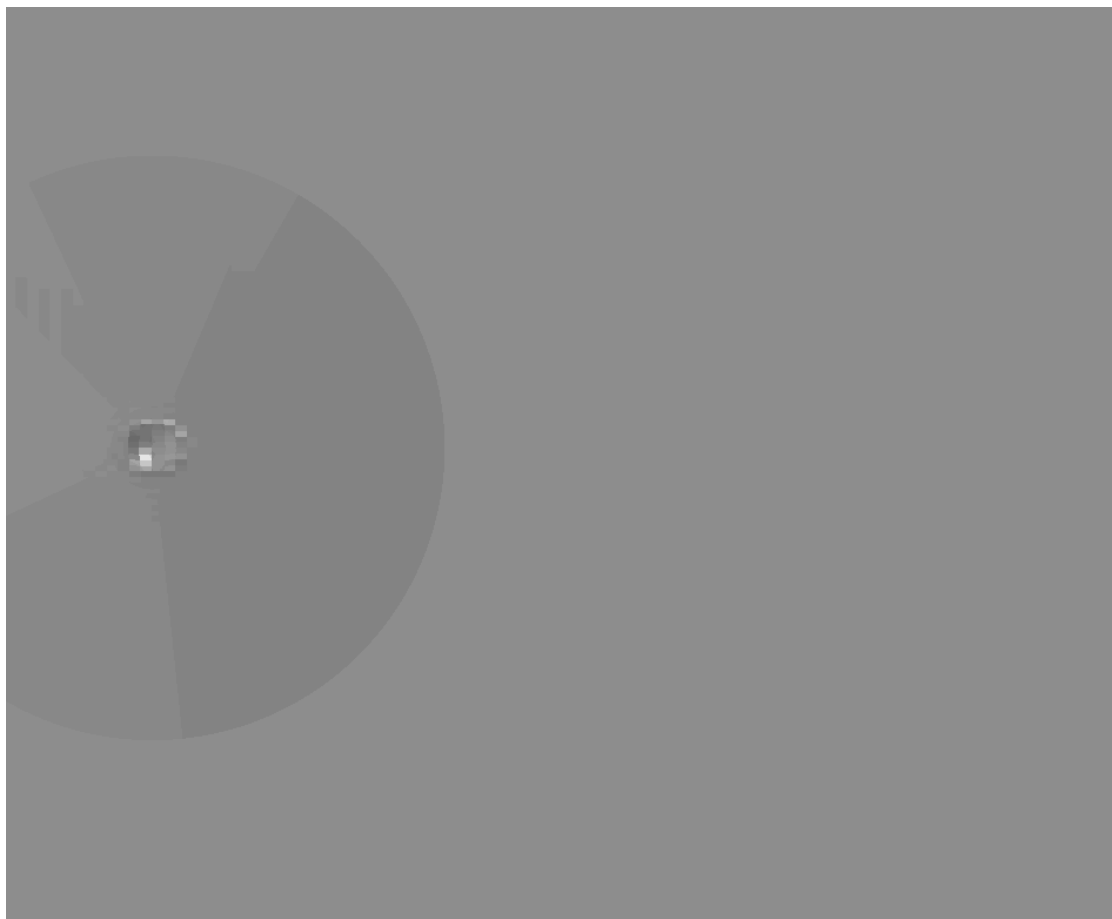


Figure 8. The reduction of the material removal resistance since the hard second phase particles tend to fracture, shear and/or fragment under higher normal loads applied during the micro-scratch tests.



Riscamento



Vanessa Seriacopi. Evaluation of abrasive mechanisms in metallic alloys during scratch tests: a numerical-experimental study in micro-scale. 2017.

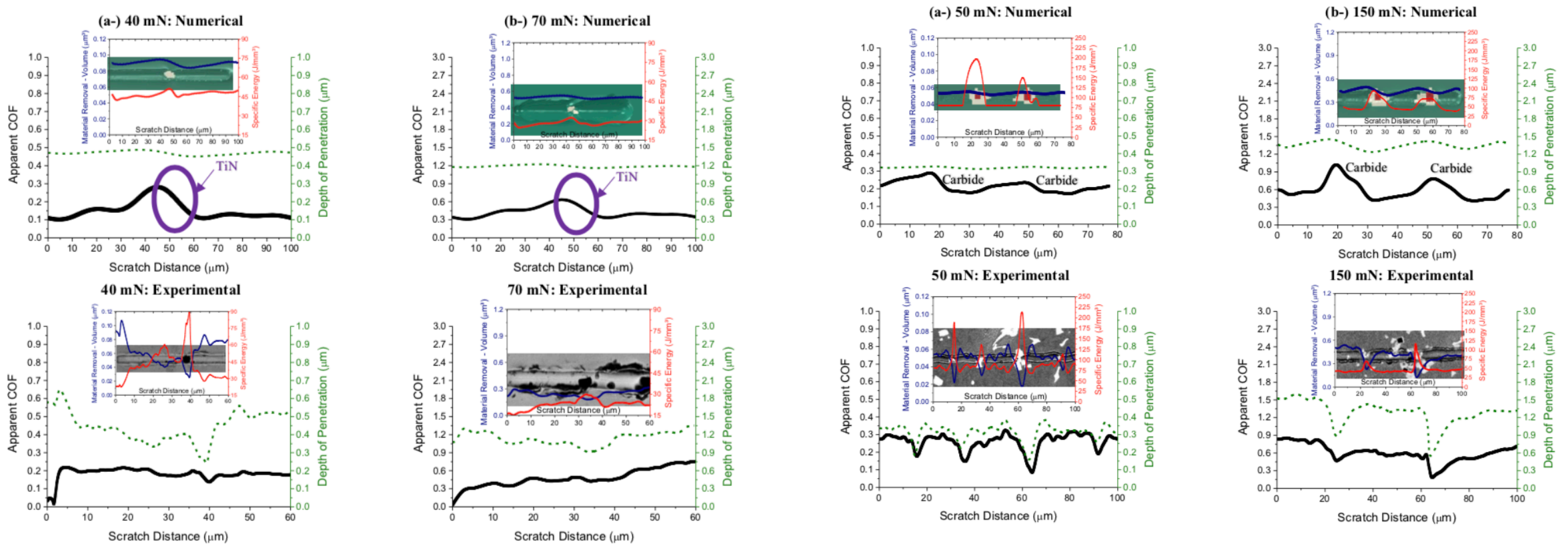
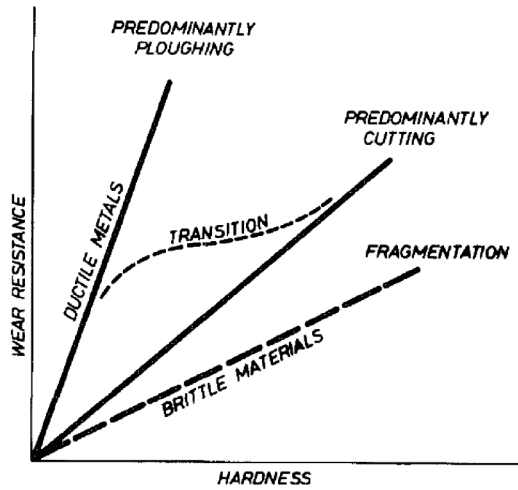


Figure 3. Particle abrasive - heterogeneous soft material with hard second phase (group 3) contact pair: numerical and experimental results of the apparent coefficient of friction, depth of penetration, material removal and specific energy along the scratch length, based on different normal load conditions: (a-) 40 mN; and (b-) 70 mN.

Figure 4. Particle abrasive - heterogeneous hard material (group 5) contact pair: numerical and experimental results of the apparent coefficient of friction, depth of penetration, material removal and specific energy along the scratch length, based on different normal load conditions: (a-) 50 mN; and (b-) 150 mN.



(MURRAY; MUTTON; WATSON, 1979)

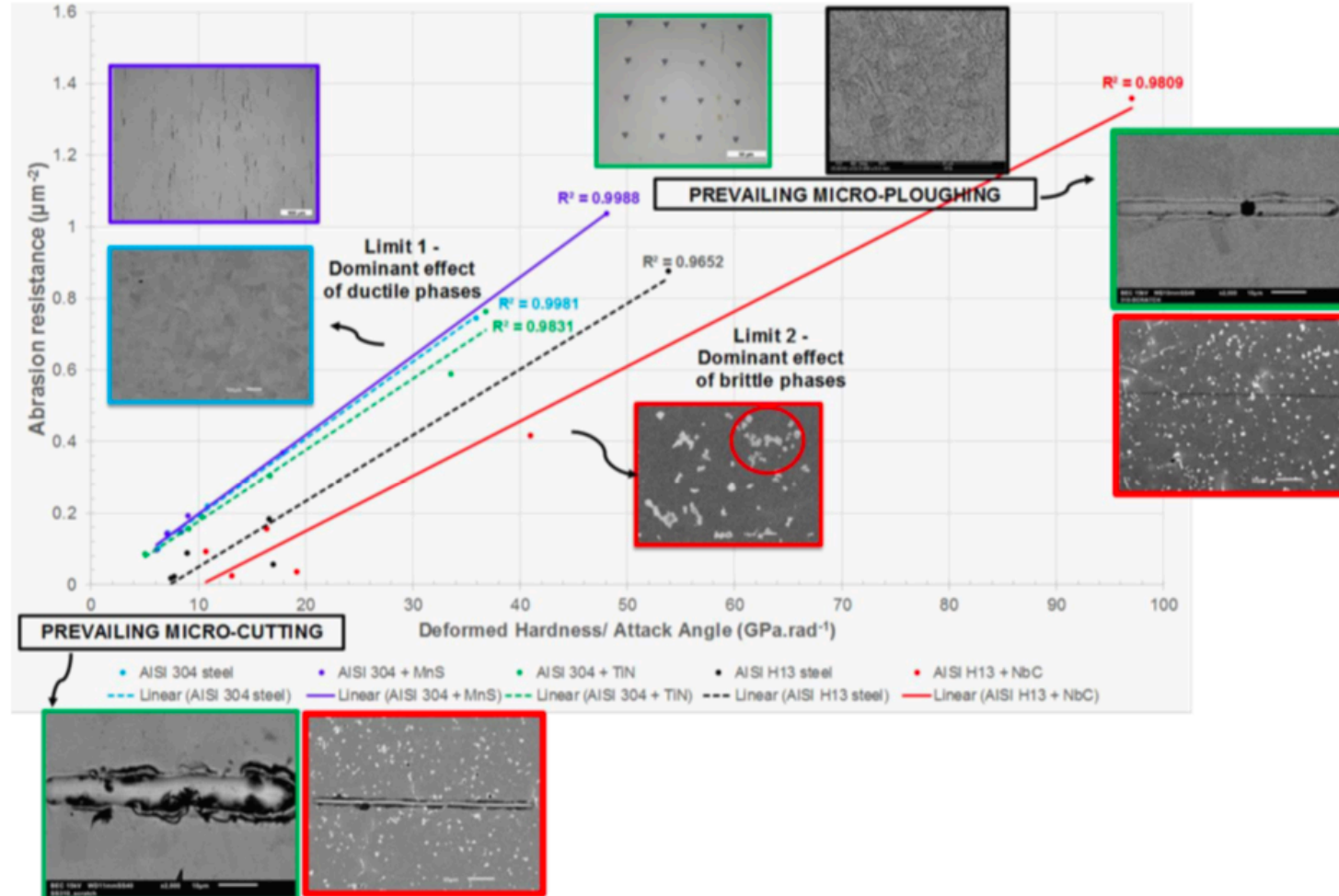


Figure 10. Quantitative map developed from the numerical results, in which frontiers can be delineated to determine the dominant ductile or brittle features (mechanical and damage behavior), and the prevailing abrasive micro-mechanism: abrasion resistance as a function of $H_{dec}/\text{Attack Angle}$.

Study of angular cutting conditions using multiple scratch tests onto low carbon steel: An experimental-numerical approach

V. Seriacopi, S. Mezghani, S. Crequy, I.F. Machado, M. El Mansori, R.M. Souza, *Wear*

<https://doi.org/10.1016/j.wear.2019.01.101>

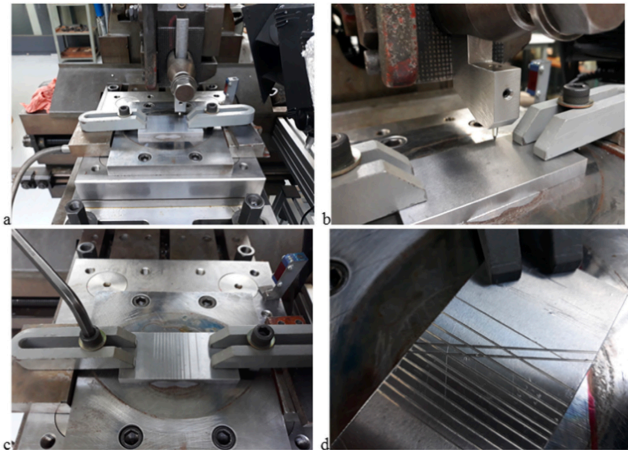


Fig. 1. Experimental setup of the scratch tests onto the 1020 steel conducted in the sequence a-d. Parallel scratches were carried out (a-c) and later a second set of parallel scratches was run at a specific angle (10, 20 or 30°) with respect to the previous one (d).

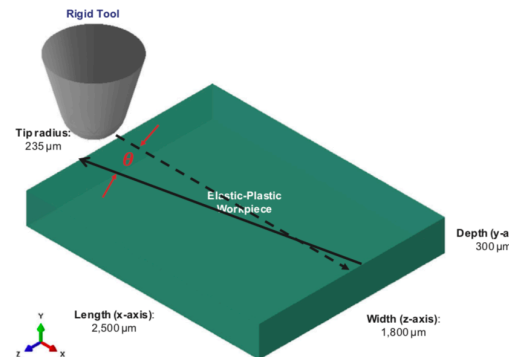


Fig. 2. Numerical modelling created to study the angled scratches. The following successive steps can be predicted here: (i-) first scratch due to the tool movement along x-direction; (ii-) tool moving along z-direction; and finally (iii-) angular scratches in the x-z plane ($\theta = 10, 20$ and 30°), resulting in a V-shape or a X-shape depending on the angle and the consequent final scratch length.

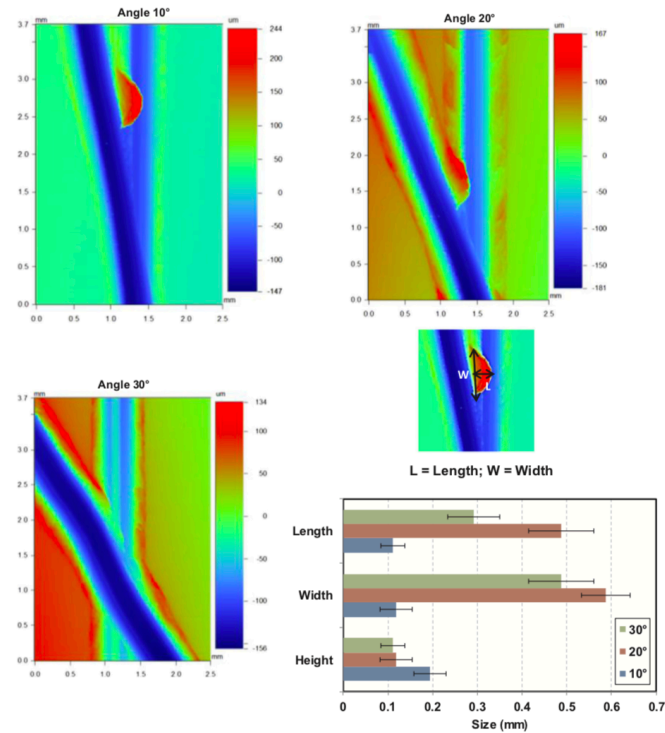


Fig. 5. Experimental results: topography characterization for all orientations. The burr features – length, width and height - are also displayed here.

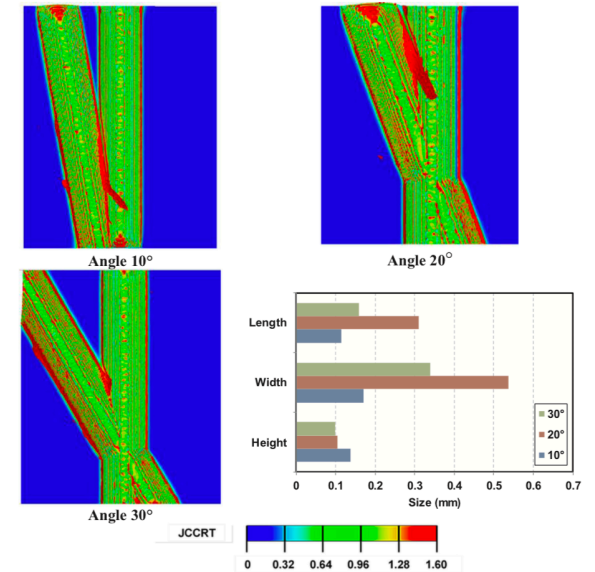


Fig. 6. Numerical results: Equivalent plastic strain at the onset of the fracture, defined by the Johnson-Cook damage criterion (JCCRT) for all orientations. The burr features – length, width and height - obtained from the numerical analyses are available here.

Study of angular cutting conditions using multiple scratch tests onto low T carbon steel: An experimental-numerical approach

V. Seriacopi, S. Mezghani, S. Crequy, I.F. Machado, M. El Mansori, R.M. Souza, *Wear*

<https://doi.org/10.1016/j.wear.2019.01.101>

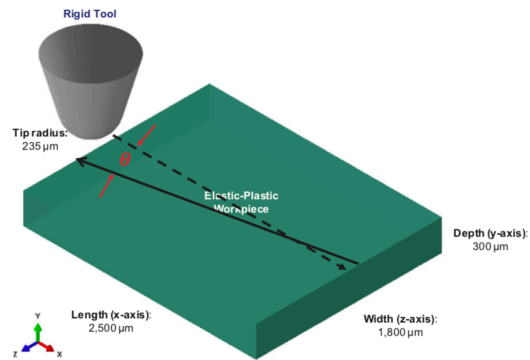


Fig. 2. Numerical modelling created to study the angled scratches. The following successive steps can be predicted here: (i-) first scratch due to the tool movement along x-direction; (ii-) tool moving along z-direction; and finally (iii-) angular scratches in the x-z plane ($\theta = 10, 20$ and 30°), resulting in a V-shape or a X-shape depending on the angle and the consequent final scratch length.

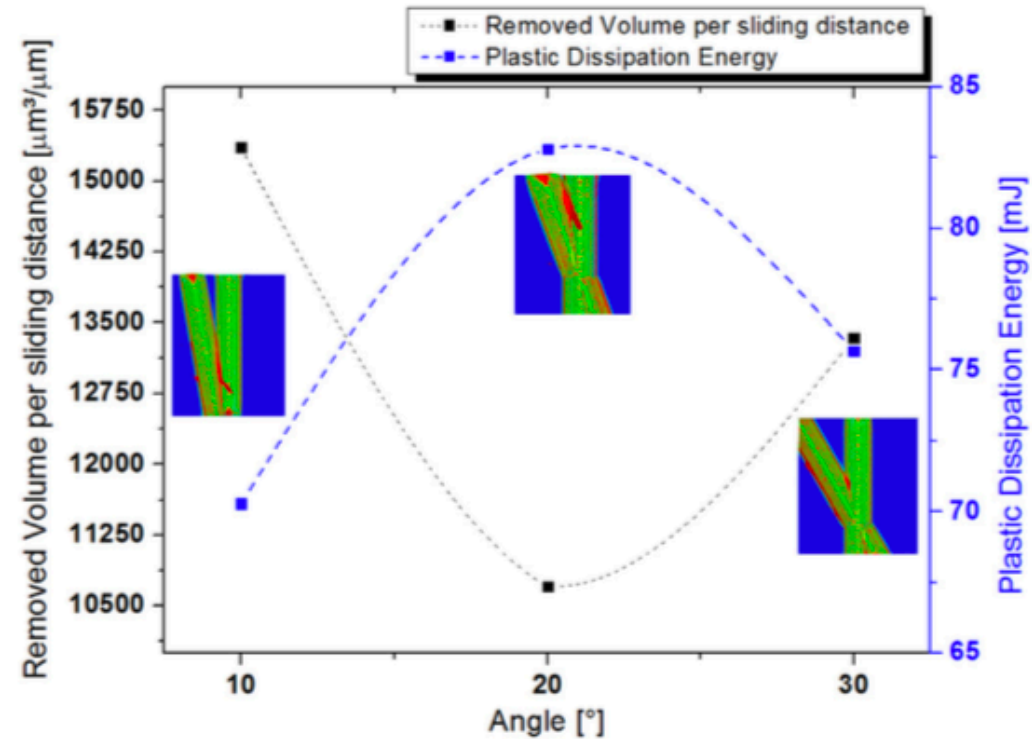
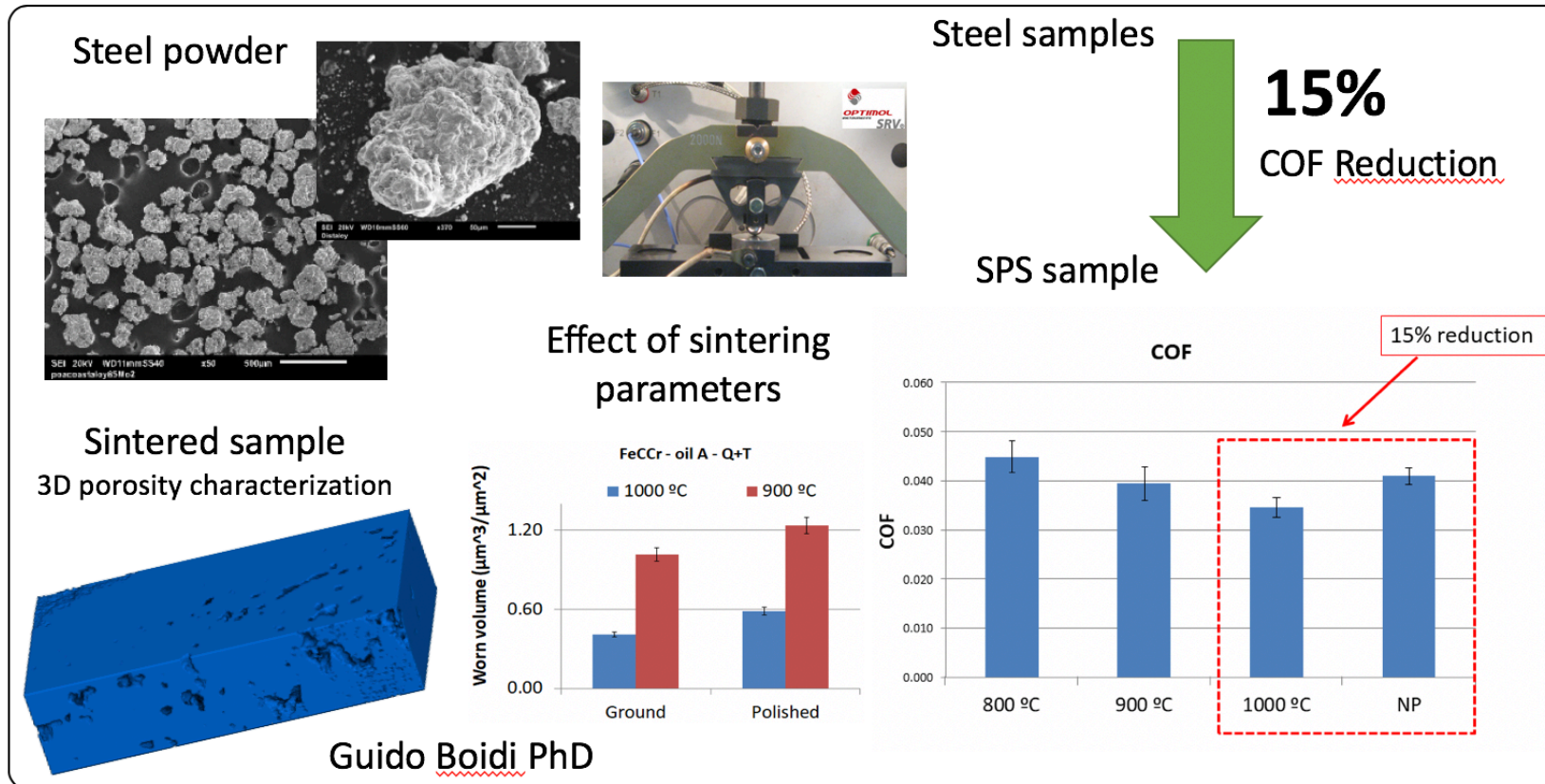


Fig. 7. Numerical results of the material removal and plastic dissipation energy as a function of the orientation of the angular scratch.

Numerical analyses of stress induced damage during a reciprocating lubricated test of FeCMo SPS sintered alloy

N.K.Fukumasu, G.Boidi, V.Seriacopi, G.A.A.Machado, R.M.Souza, I.F.Machado, Tribology International

<https://doi.org/10.1016/j.triboint.2016.12.025>



Numerical analyses of stress induced damage during a reciprocating lubricated test of FeCMo SPS sintered alloy

N.K.Fukumasu, G.Boidi, V.Seriacopi, G.A.A.Machado, R.M.Souza, I.F.Machado, Tribology International

<https://doi.org/10.1016/j.triboint.2016.12.025>

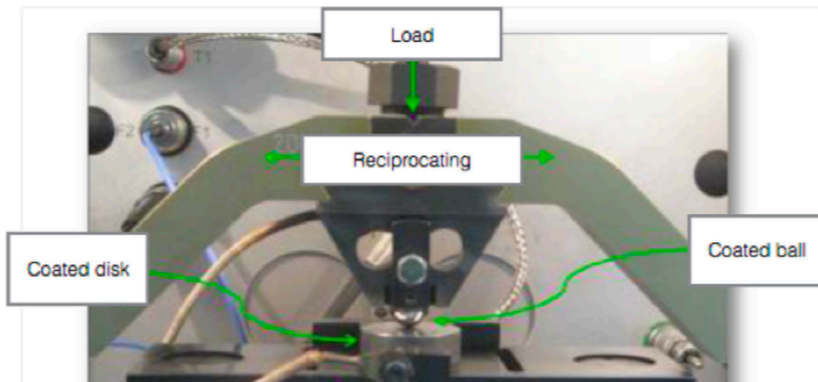


Fig. 1. Macroscale reciprocating test configuration analyzed in this work, in which both sphere and disk were coated.

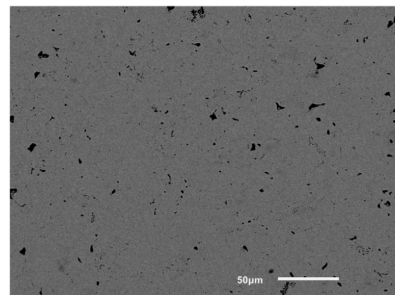


Fig. 3. Back scattered SEM image of the sintered FeCMo material presenting less than 2% porosity.

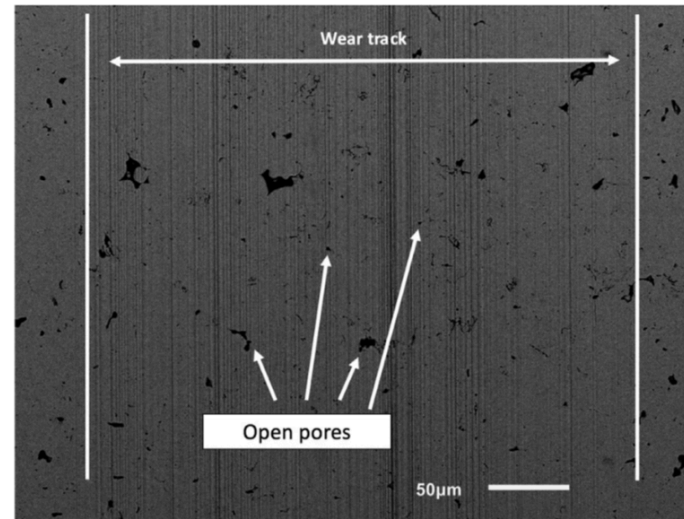


Fig. 5. Back scattered SEM image of the wear track from the experimental reciprocating test with contact pressure of 2.5 GPa.

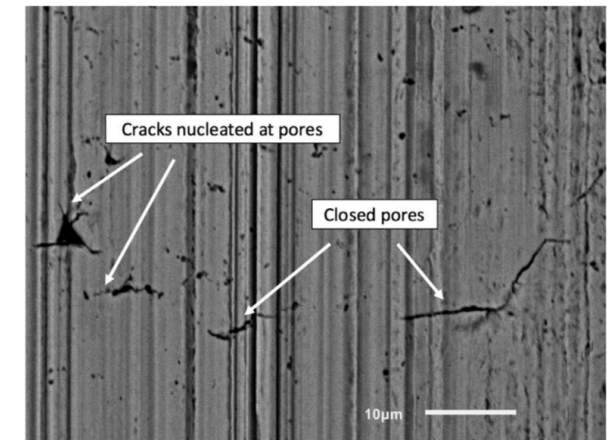


Fig. 8. Higher magnification of the back scattered SEM image of the white ellipses in Fig. 7.

Numerical analyses of stress induced damage during a reciprocating lubricated test of FeCMo SPS sintered alloy

N.K.Fukumasu, G.Boidi, V.Seriacopi, G.A.A.Machado, R.M.Souza, I.F.Machado, Tribology International

<https://doi.org/10.1016/j.triboint.2016.12.025>

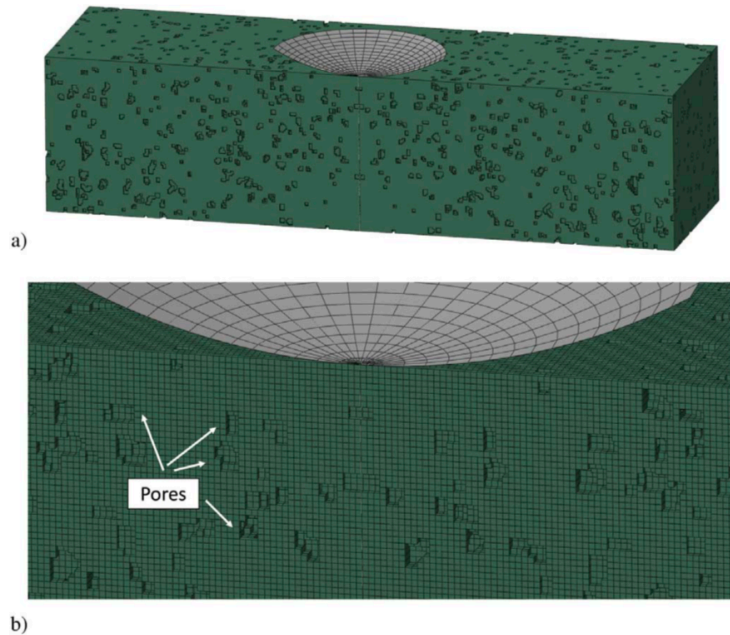


Fig. 1. Computational domain for the reciprocating test analyses: a) system composed by an analytical rigid sphere (gray) and a plane counterbody (dark green); b) detail of the system indicating the porosity represented as small voids (regions without elements) in the numerical mesh. (For interpretation of the references to color in this figure legend, the reader is referred to the web version of this article.)

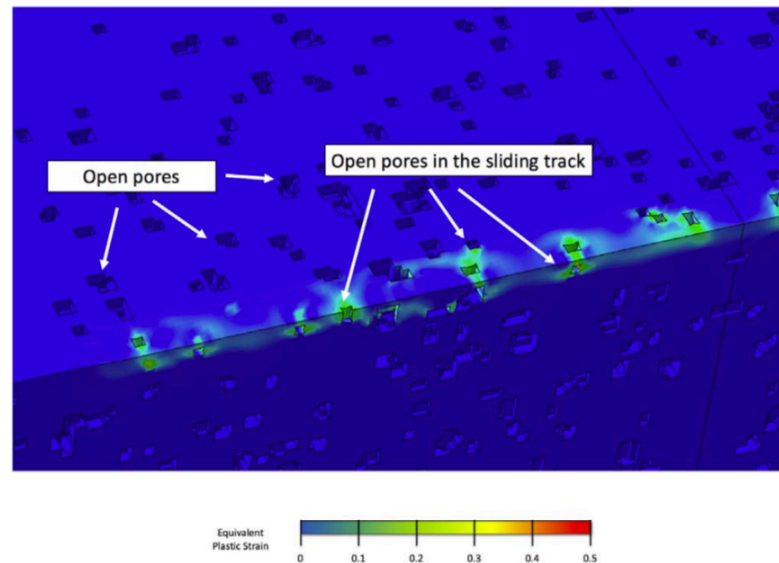


Fig. 4. Localized plastic deformation induced by the pores during the sliding of the sphere. The color field indicates the level of plastic deformation.

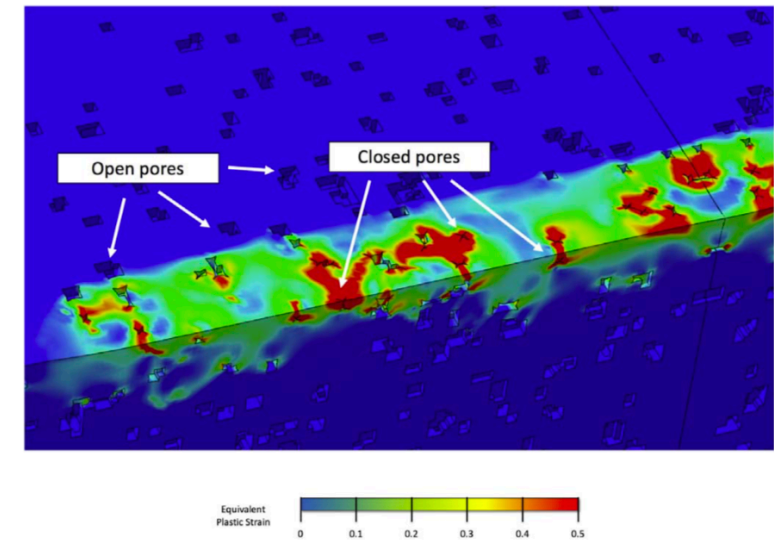
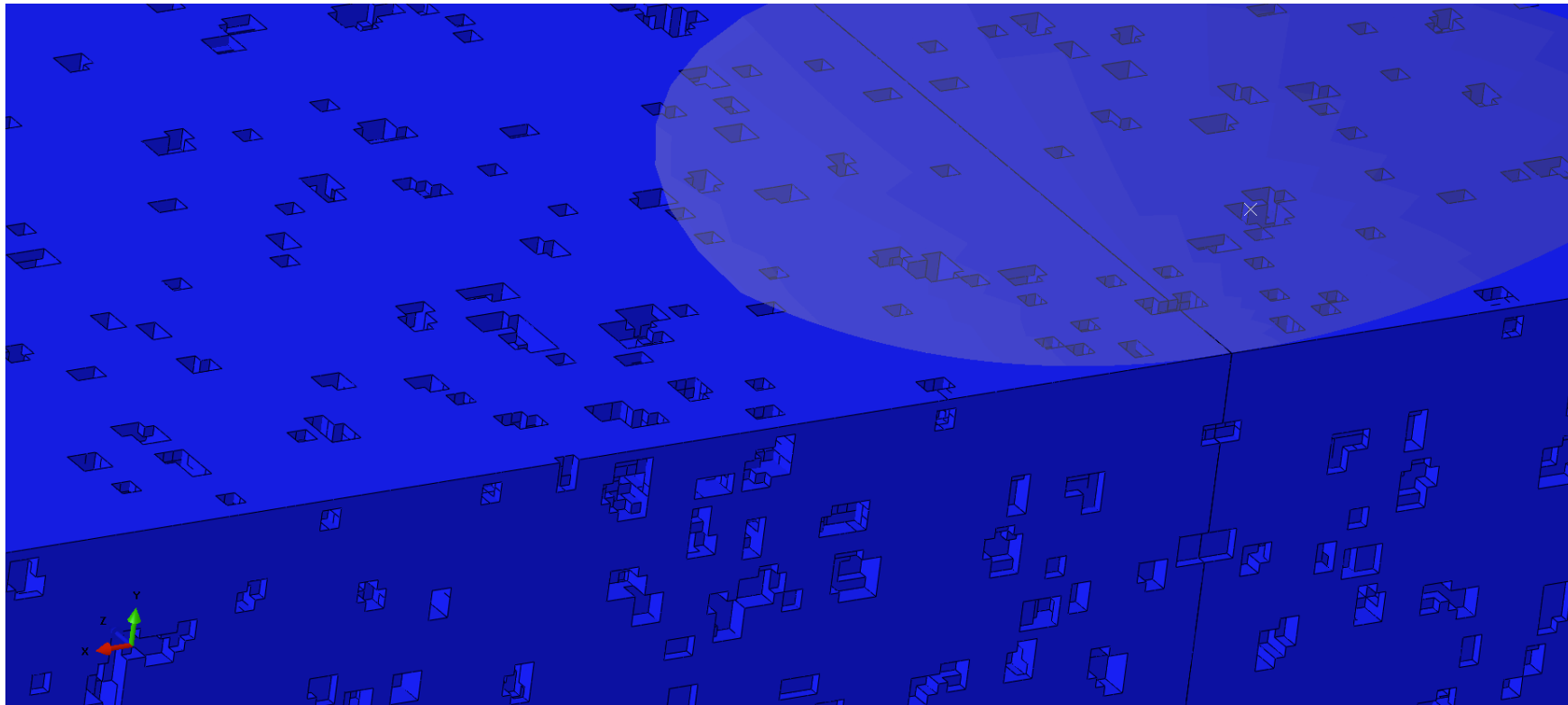


Fig. 6. Collapse of the pores by the plastic deformation during the sliding of the sphere. The color field indicates the level of plastic deformation and red regions indicate plastic deformation higher than 50%.

Numerical analyses of stress induced damage during a reciprocating lubricated test of FeCMo SPS sintered alloy

N.K.Fukumasu, G.Boidi, V.Seriacopi, G.A.A.Machado, R.M.Souza, I.F.Machado, Tribology International

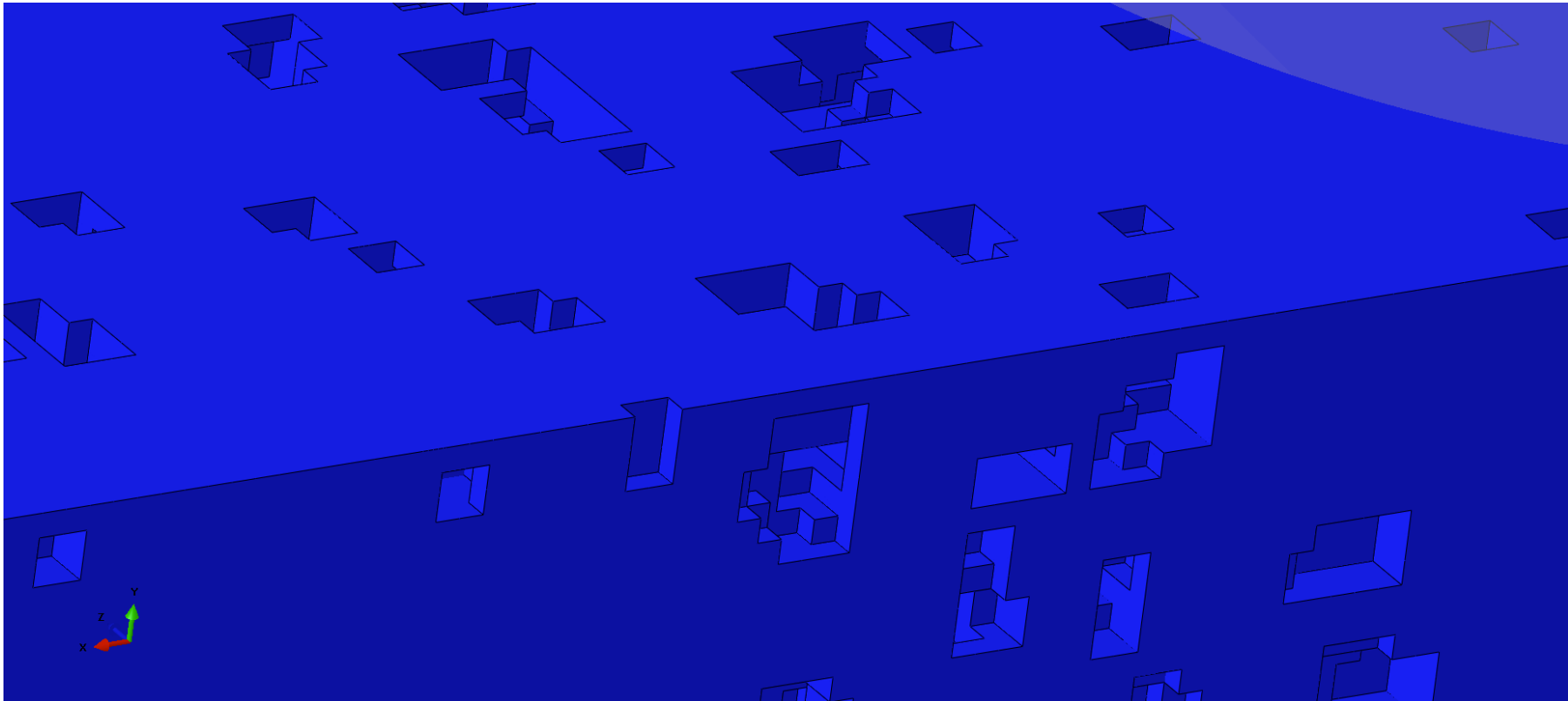
<https://doi.org/10.1016/j.triboint.2016.12.025>



Numerical analyses of stress induced damage during a reciprocating lubricated test of FeCMo SPS sintered alloy

N.K.Fukumasu, G.Boidi, V.Seriacopi, G.A.A.Machado, R.M.Souza, I.F.Machado, Tribology International

<https://doi.org/10.1016/j.triboint.2016.12.025>

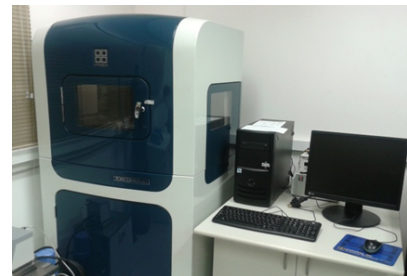
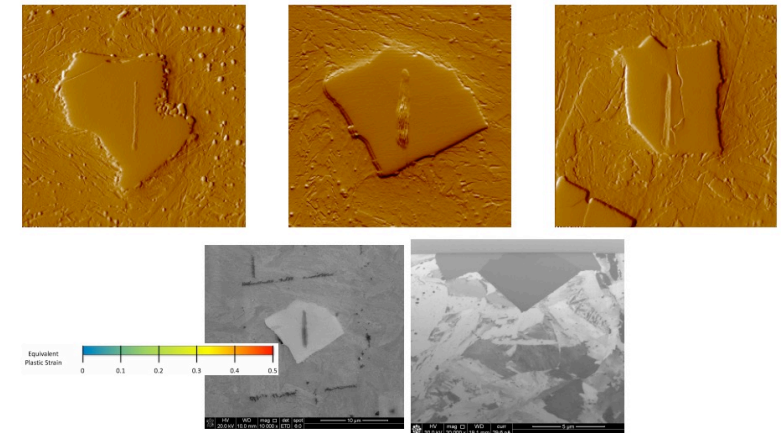
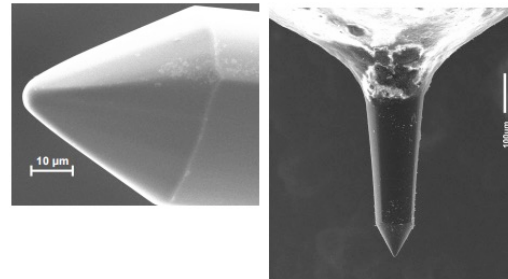
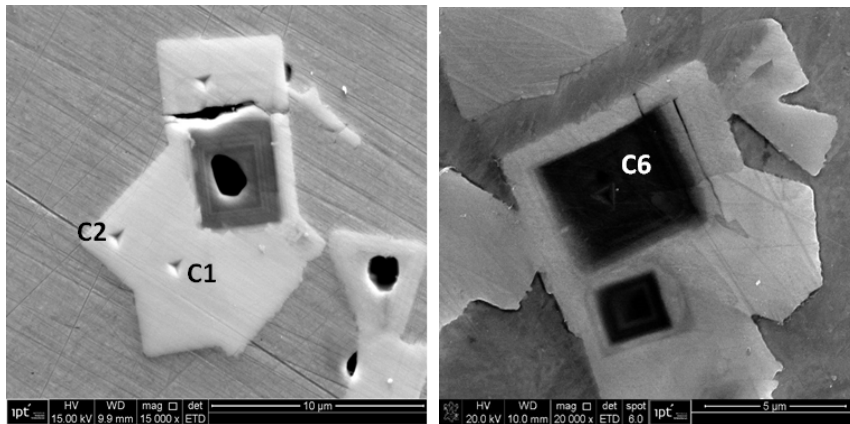


9

Influence of Sintering Parameters on Micro-Scale Mechanical and Tribological Behavior of Niobium Carbides

N.K. Fukumasu, A.J.O.Tertuliano, C.F. Bernardes, V. Seriacopi, R.M. Souza, I.F. Machado
Plansee Seminar - 2017

Motivation: Previous studies to evaluate the mechanical properties and influence on wear of NbC on the AISI H13 steel with 5% volume fraction of NbC –, design of materials and multiscale analysis - evaluate bulk properties



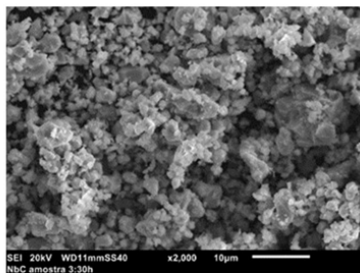
Tribointenter Hysitron - TI950

Influence of Sintering Parameters on Micro-Scale Mechanical and Tribological Behavior of Niobium Carbides

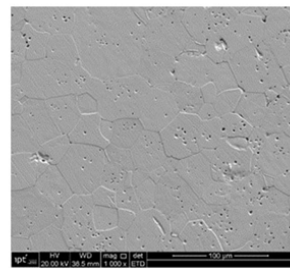
N.K. Fukumasu, A.J.O.Tertuliano, C.F. Bernardes, V. Seriacopi, R.M. Souza, I.F. Machado
Plansee Seminar - 2017

Motivation: Previous studies to evaluate the mechanical properties and influence on wear of NbC on the AISI H13 steel with 5% volume fraction of NbC –, design of materials and multiscale analysis - evaluate bulk properties

Pressure applied during the consolidation was 60MPa of maximum pressure, vacuum range was between 10 and 15 Pa, the average heating rate was 50°C/min, The temperature reached was 1600°C and the holding time

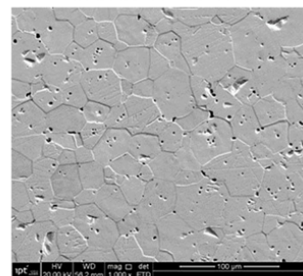


NbC Powder features

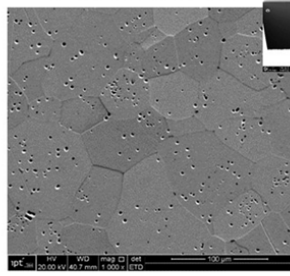


95% densified (7.40 g/cm³)

Pores (FEG-FIB)



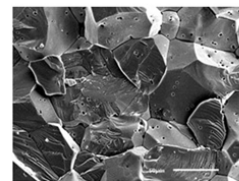
97% densified (7.60 g/cm³)



99% densified (7.76 g/cm³)



Fracture



Sample	Holding time (min)	Cooling
NbC95	5	Free cooling in the die
NbC97	10	Free cooling in the die
NbC99	10	100°C/min from 1600°C to 1100°C and free cooling in the die.



Influence of Sintering Parameters on Micro-Scale Mechanical and Tribological Behavior of Niobium Carbides

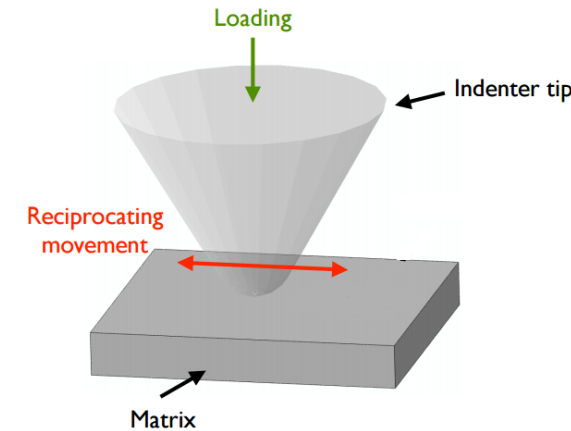
N.K. Fukumasu, A.J.O. Tertuliano, C.F. Bernardes, V. Seriacopi, R.M. Souza, I.F. Machado
Plansee Seminar - 2017

Wear tests

- Procedure and details of this method development and description can be found elsewhere [E. Broitman, Francisco J. Flores-Ruiz, Journal of Vacuum Science & Technology [A 33], 043201 (2015)]
- Wear tests were conducted in different grains after EBSD analysis. Indentation marks were made previously to identify the grains scanned.

Finite element method simulation

- The Finite Element Method (FEM), using the Abaqus® commercial package, is used to build a 3D
- The numerical simulations have focused on the influence of mechanical and failure properties on the wear behavior of the NbC. An explicit time integration
- Rigid cono-spherical indenter with tip diameter of 10 μm , which is in contact with a square counterbody with 30 μm in length, 30 μm in width and 5 μm in height. (likewise the experimental tests)
- Fracture toughness was selected as 5 $\text{MPa m}^{0.5}$, based on the literature that indicates a variation from 2 to 8 $\text{MPa m}^{0.5}$



Influence of Sintering Parameters on Micro-Scale Mechanical and Tribological Behavior of Niobium Carbides

N.K. Fukumasu, A.J.O.Tertuliano, C.F. Bernardes, V. Seriacopi, R.M. Souza, I.F. Machado
Plansee Seminar - 2017

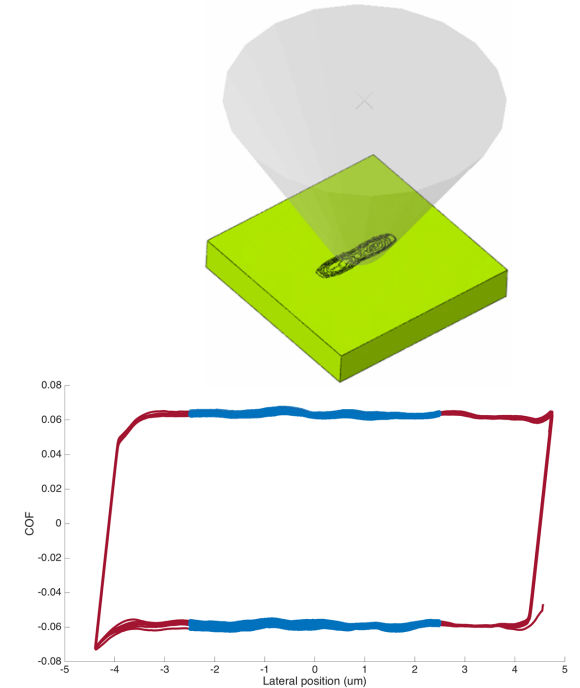
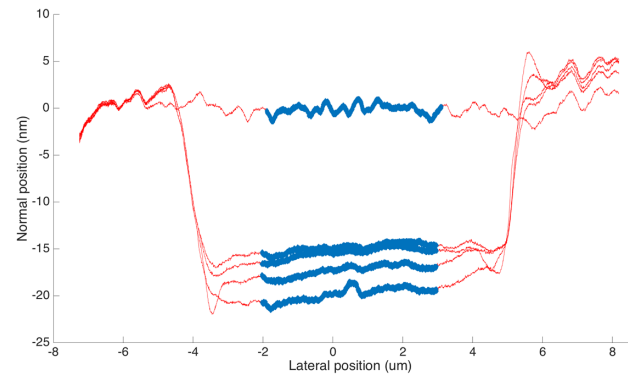
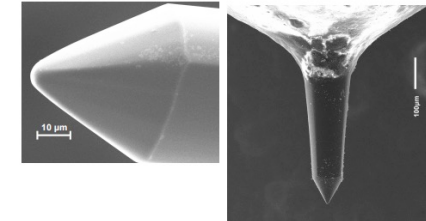
Table displays the values of hardness (H), reduced elastic modulus (E_r), elastic modulus (E), and the ratio between E and H. Different E porous NbC

Sample	H (GPa)	E_r (GPa)	E (GPa)	E/H
NbC95	21.9 ± 1.7	299.7 ± 5.4	388	17.7
NbC97	24.1 ± 1.3	362.1 ± 4.0	506	20.1
NbC99	23.7 ± 2.1	356.2 ± 2.0	494	20.8

Wear

Blue -> analyzed region

Red -> whole curve



Influence of Sintering Parameters on Micro-Scale Mechanical and Tribological Behavior of Niobium Carbides

N.K. Fukumasu, A.J.O.Tertuliano, C.F. Bernardes, V. Seriacopi, R.M. Souza, I.F. Machado
Plansee Seminar - 2017

Wear

NbC95 and NbC99 were evaluated (threshold)

Archard's wear coefficient for the samples NbC99 and NbC95 are presented during the wear cycles for the 1st cycle, 10th cycle, 20th cycle and 30th cycle.

Eq Archard $V_{loss} = kWs/H$

Number of Cycles	Average Archard's wear coefficients - K		Removed Volume - V_{loss} (μm^3)	
	NbC95	NbC99	NbC95	NbC99
1	5.8 ± 1.8	15.8 ± 7	13.2 ± 4.1	32.9 ± 15
10	-0.4 ± 0.2	0.7 ± 0.9	-0.9 ± 0.5	1.5 ± 2.0
20	-1.0 ± 0.6	0.2 ± 0.2	-2.3 ± 1.4	0.4 ± 0.4
30	-0.4 ± 0.2	0.0 ± 0.2	-0.9 ± 0.5	0.4 ± 0.4
Total	4.0	16.9	$9.1 \mu\text{m}^3$	$35.2 \mu\text{m}^3$

After the 30 th cycle		
E (GPa)	Average Archard's wear coefficients - K	Removed Volume - V_{loss} (μm^3)
300	0.4	0.8
350	1.1	2.3
400	2.3	4.8
450	5.9	12.3
500	14.4	30.1

H is similar in all samples ,
E values seem to be related to the density/porosity
The higher the E the higher the wear



Influence of Sintering Parameters on Micro-Scale Mechanical and Tribological Behavior of Niobium Carbides

N.K. Fukumasu, A.J.O.Tertuliano, C.F. Bernardes, V. Seriacopi, R.M. Souza, I.F. Machado
Plansee Seminar - 2017

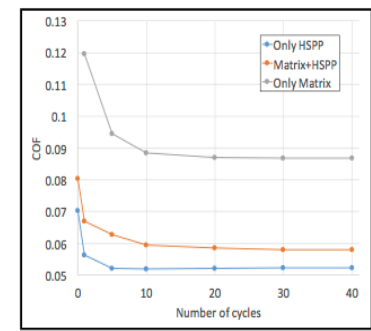
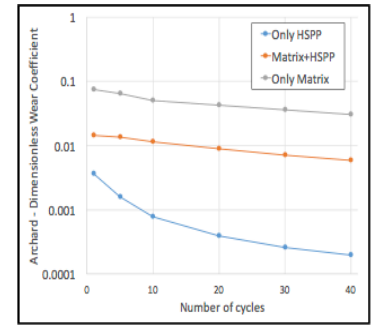
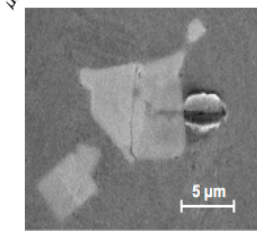
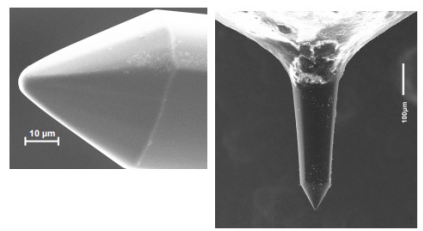
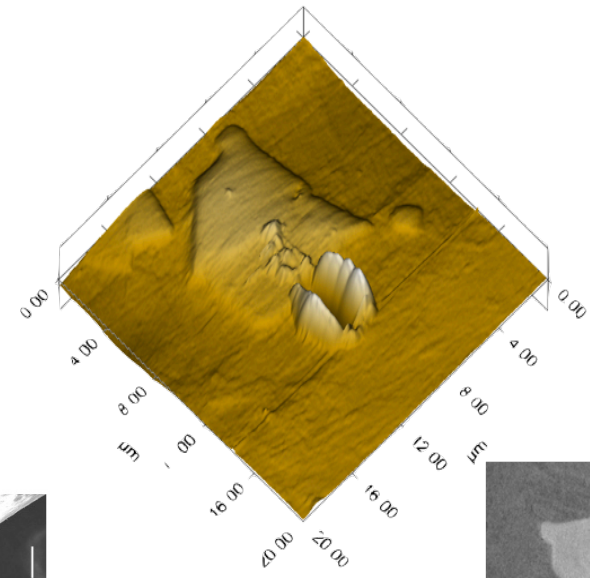
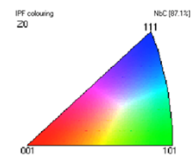
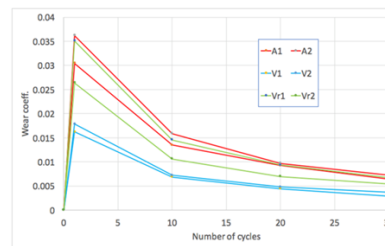
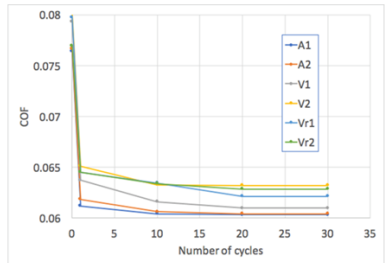
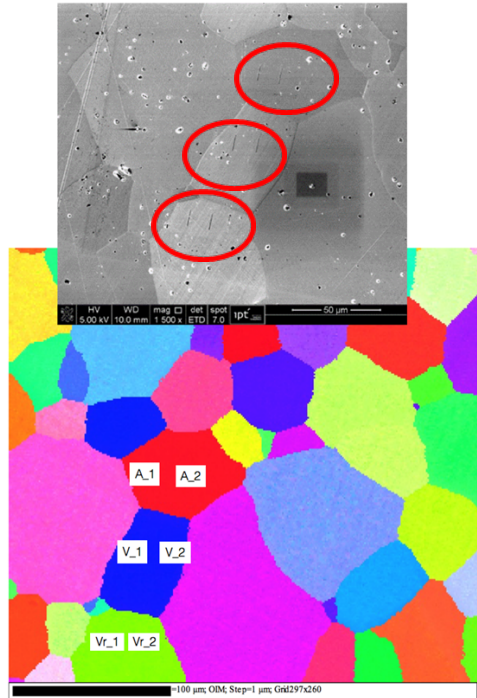
Wear



Influence of Sintering Parameters on Micro-Scale Mechanical and Tribological Behavior of Niobium Carbides

N.K. Fukumasu, A.J.O.Tertuliano, C.F. Bernardes, V. Seriacopi, R.M. Souza, I.F. Machado
Plansee Seminar - 2017

Wear



EBSD analysis was carried out in selected regions to evaluate the effect of grain orientation on wear

Matrix – precipitate Interface

Local transformation of amorphous hydrogenated carbon coating induced by high contact pressure

N.K. Fukumasu, C.F. Bernardes, M.A. Ramirez, V.J. Trava-Airoldi, R.M. Souza, I.F. Machado

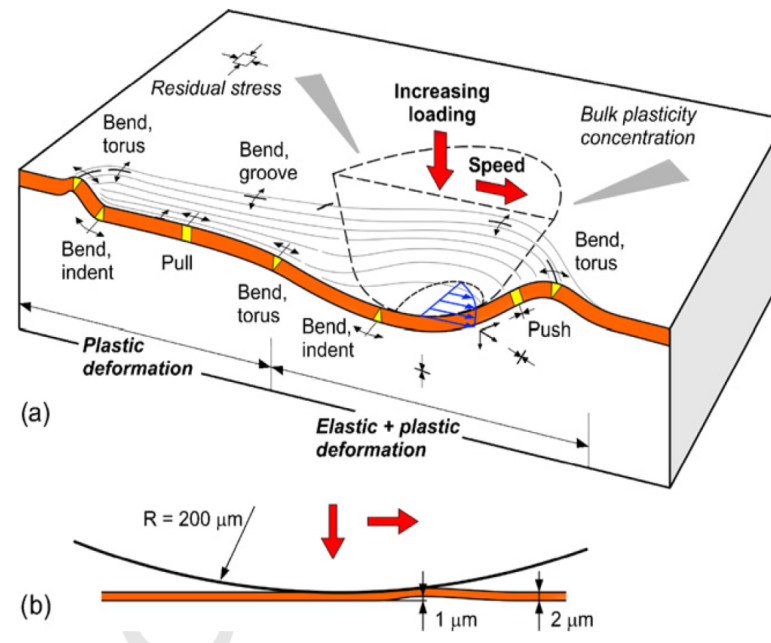
Tribology International

<https://doi.org/10.1016/j.triboint.2018.04.006>

The coating and the interlayer were deposited using a pulsed Direct Current Plasma Enhanced Chemical Vapor Deposition (DC PECVD)

Under dry sliding condition, DLC coated systems may present a reduction of friction force based on the graphitization of the contacting surfaces, as observed by Liu et al. [9]. This phenomenon is related to the re-arrangement of the sp³ and sp² carbon bonds by energy transferred from the mechanical movement to chemical bond kinetics.

Scratch test on coated systems –
sequence of stress states



[Holmberg *et al.* Wear
267 (2009) 2142–2156]

Local transformation of amorphous hydrogenated carbon coating induced by high contact pressure

N.K. Fukumasu, C.F. Bernardes, M.A. Ramirez, V.J. Trava-Airoldi, R.M. Souza, I.F. Machado

Tribology International

<https://doi.org/10.1016/j.triboint.2018.04.006>

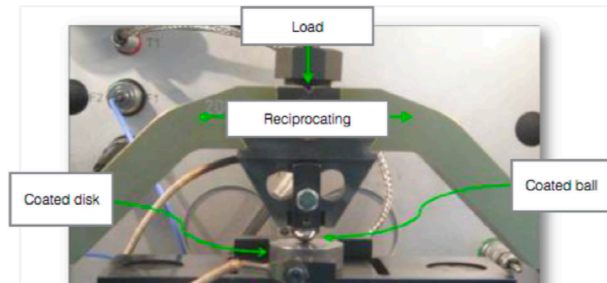


Fig. 1. Macroscale reciprocating test configuration analyzed in this work, in which both sphere and disk were coated.

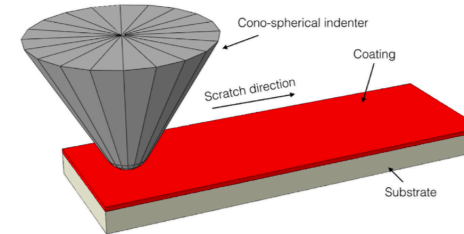


Fig. 2. Numerical model configuration consisting of a cono-spherical tip used to scratch the coated (red) substrate (light gray). (For interpretation of the references to color in this figure legend, the reader is referred to the Web version of this article.)

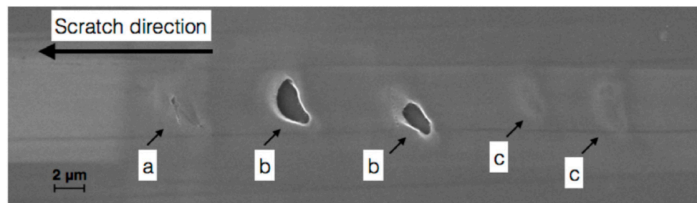


Fig. 8. Microscale scratch track presenting the local typical observed failure modes: a) adhesive and cohesive failures of the coating; b) complete spallation of coating and c) adhesive failure of the coating/substrate interface.

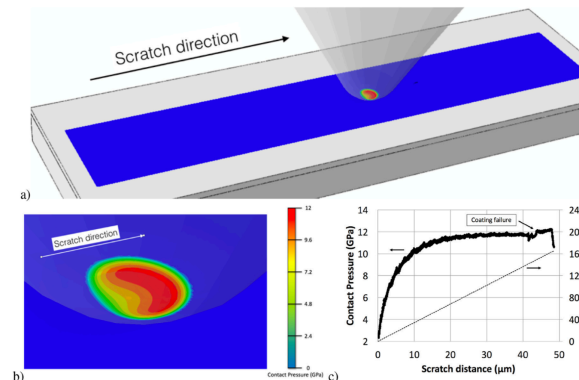


Fig. 14. Contact Pressure at the coating promoted by the indenter movement: a) Instantaneous spatial distribution of the contact pressure; b) detail of the contact region and c) evolution of the contact pressure with the ramping load during the scratch test.

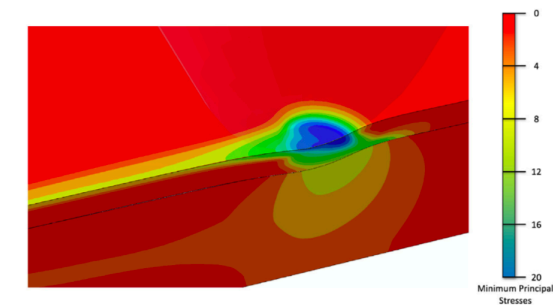


Fig. 15. Minimum Principal Stresses distribution developed inside of the material during the scratch test.

Local transformation of amorphous hydrogenated carbon coating induced by high contact pressure

N.K. Fukumasu, C.F. Bernardes, M.A. Ramirez, V.J. Trava-Airoldi, R.M. Souza, I.F. Machado, Tribology International

<https://doi.org/10.1016/j.triboint.2018.04.006>

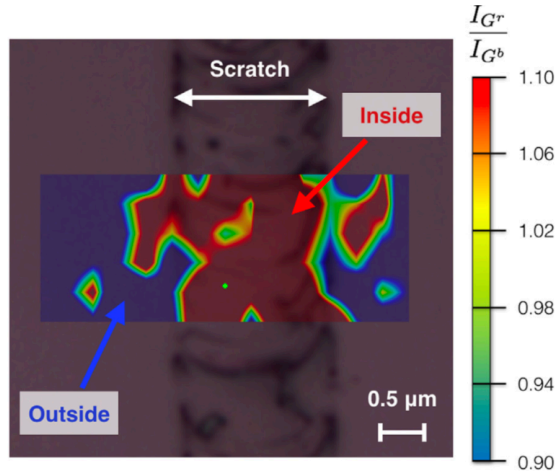


Fig. 9. Superimposed Raman spectroscopy map of I_G^r/I_G^b ratio on the scratch track of Fig. 8. Higher ratio values (red colored regions) indicate a red-shift of the G band. (For interpretation of the references to color in this figure legend, the reader is referred to the Web version of this article.)

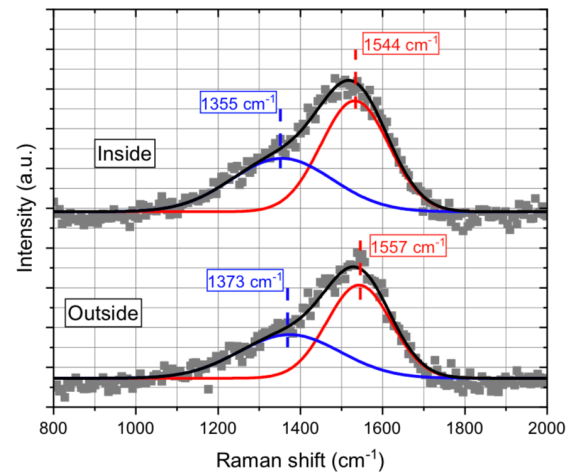


Fig. 10. Raman spectroscopy analysis of a-C:H coatings after the scratch test. Gray squares indicate typical spectra obtained for inside and outside the scratched regions, while lines indicate the deconvolution of the Raman spectra into D (blue) and G (red) bands. (For interpretation of the references to color in this figure legend, the reader is referred to the Web version of this article.)

Numerical simulation indicates high contact pressure (>12GPa) developed at the surface and high internal stresses, ranging from 20 GPa to 12 GPa, are developed along coating thickness. The increase on indentation hardness inside the scratched region are compatible with the nucleation of sp³ carbon bond sites derived from sp² bonds.

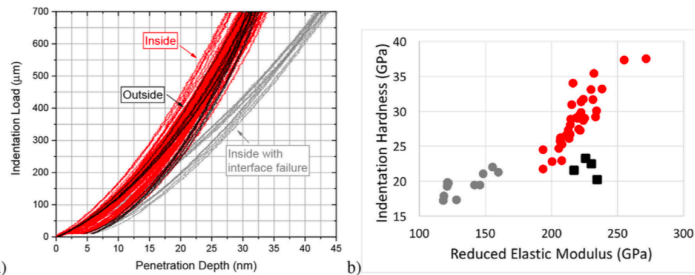


Fig. 6. Nano-indentation measurements of the coating: a) nano-indentation curves for inside (red and gray lines) and outside (black lines) of the wear track; b) results for hardness and reduced elastic modulus of the coating for inside (circles) and outside (squares) of the wear track. Red circles indicate similar reduced elastic modulus but higher hardness compared to outside measurements (black squares), while gray circles indicate a reduction on both characteristics. (For interpretation of the references to color in this figure legend, the reader is referred to the Web version of this article.)

Influence of spark plasma consolidation conditions on the superconducting properties of (Bi,Pb)-Sr-Ca-Cu-O ceramic samples

F. Rosales-Saiz, L. Pérez-Acosta, I.F. Machado, J.E. Pérez-Fernández, R.F. Jardim, E. Govea-Alcaide, Ceramics International

<http://dx.doi.org/10.1016/j.ceramint.2016.08.053>

Influence of the material die and plungers on the superconducting properties of $\text{Bi}_{1.65}\text{Pb}_{0.35}\text{Sr}_2\text{Ca}_2\text{Cu}_3\text{O}_{10-\delta}$ samples processed by the Spark Plasma Sintering method. Samples were then consolidated by using two setups comprised of different materials: **all-steel and all-graphite**. Finite element simulations (FEM) were performed to provide extra information regarding the distribution of temperature within the samples. X-ray diffraction (XRD) analysis and DC magnetization as a function of temperature, $M(T)$, have been conducted in all synthesized samples as complementary characterizations. The main motivation of this study is to evaluate the influence of the material setup of the SPS apparatus on the de-oxygenation of Bi-2223 compounds consolidated by the SPS method.

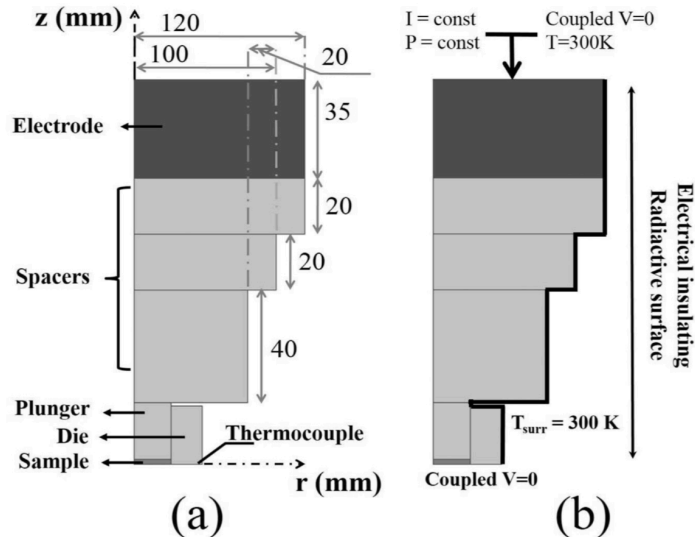


Fig. 1. (a) Schematic drawing of the consolidation system; (b) boundary conditions.

Table 1

Consolidation parameters used during the SPS process for producing Bi-2223 samples. T_D is the consolidation temperature, HR is the heating rate, t_r is the heating time, and t_D is the consolidation time. We also included values of the density of the pellets, D .

Sample	T_D (°C)	HR (°C/min)	t_r (min)	t_D (min)	D (g/cm ³)
H1	700	135	5	5	4.8
H2	750	50	15	5	5.5
G1	750	145	5	5	5.7

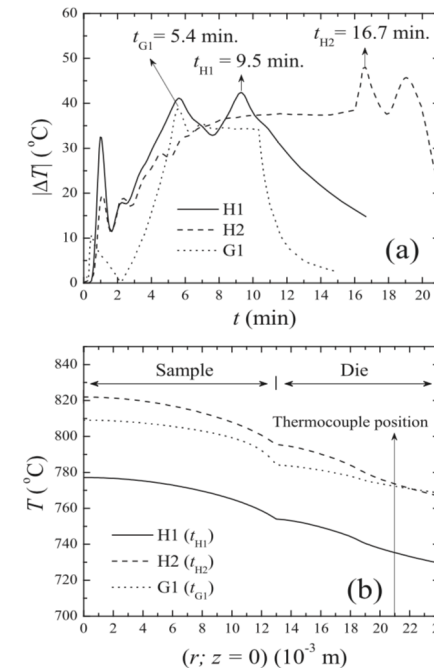
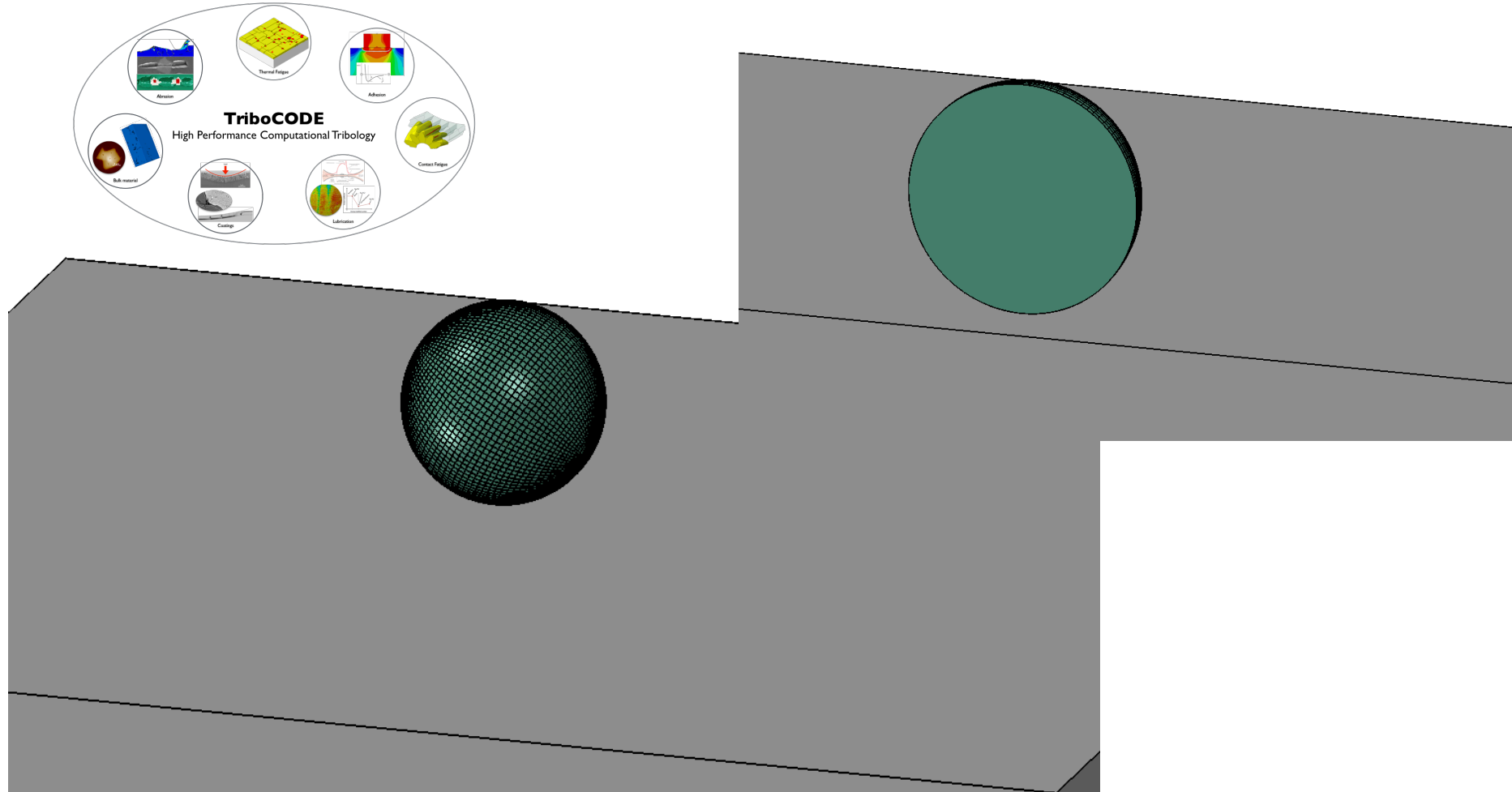
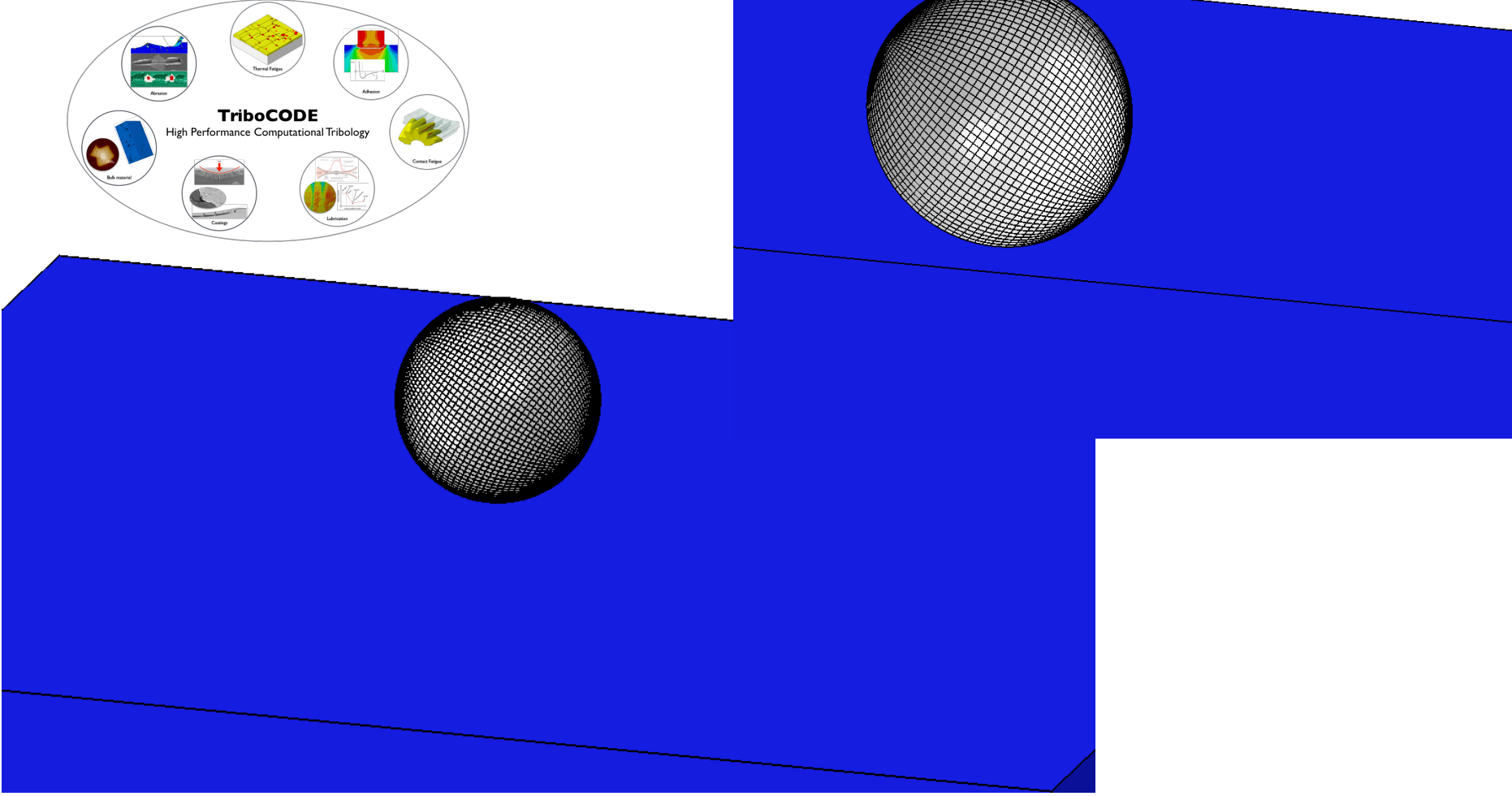
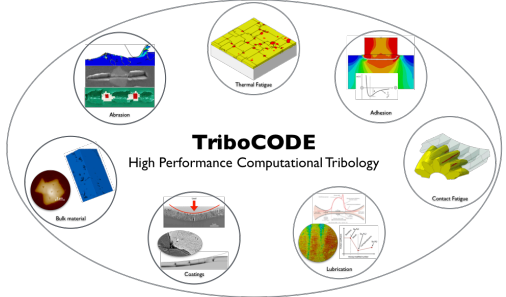


Fig. 3. (a) Estimated temperature difference during the SPS process for the studied samples; (b) the simulated radial temperature profiles for $z=0$ of samples H1, H2, and G1, respectively (see text for details).

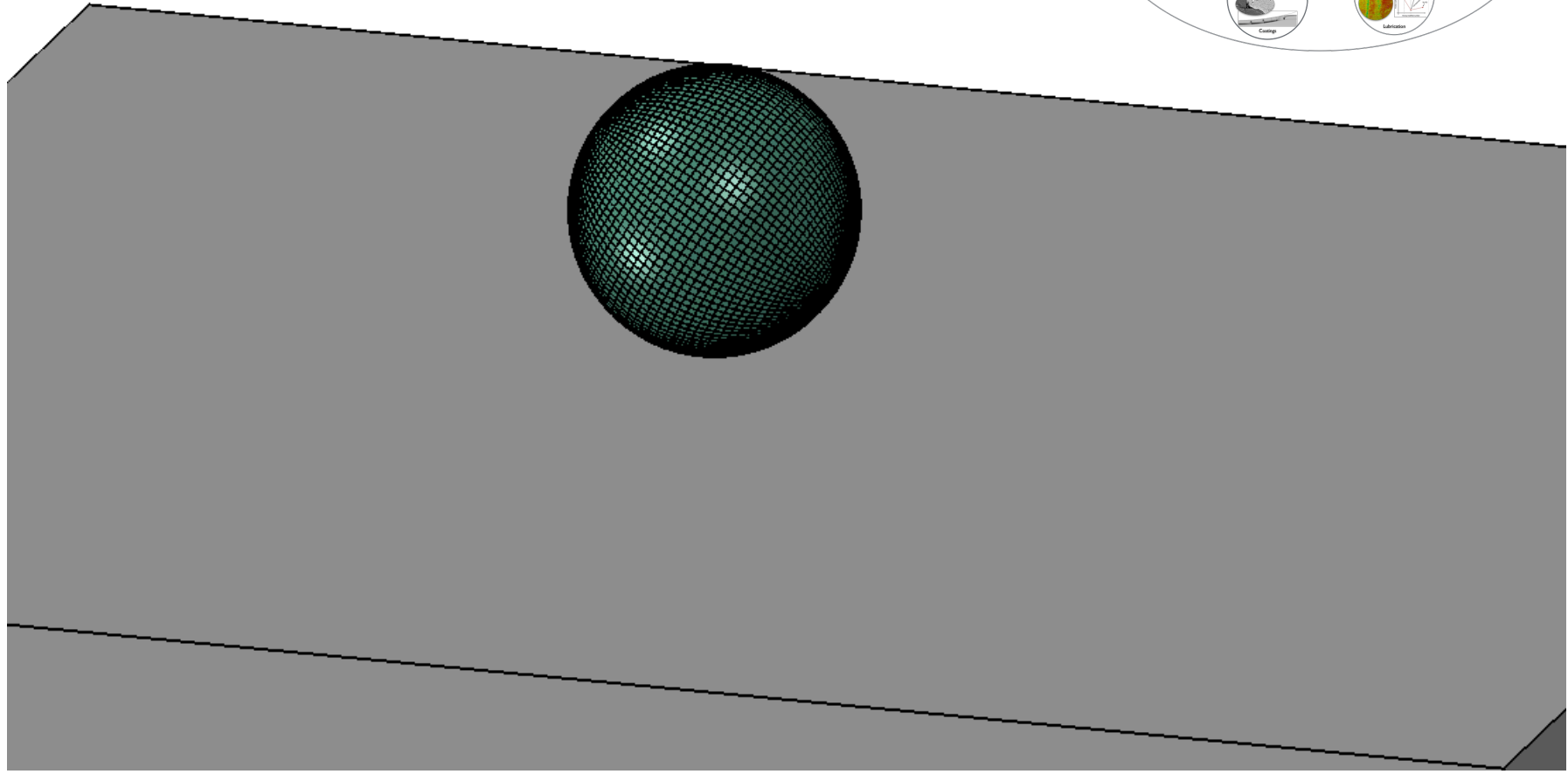
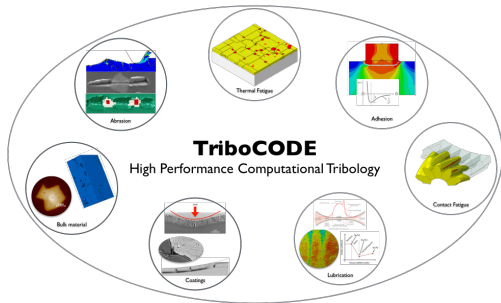
Surface damage modeling



Surface damage modeling



Surface damage modeling



Atividade

- Dê 3 exemplos do uso do CAD, FEA e CAM para simulação da fabricação de componentes mecânicos.
- Esses exemplos devem ser descritos detalhadamente, mostrando cada etapa em CAD, FEA e CAM
- Não há necessidade de programar, mas de ilustrar cada uma das etapas
- Exemplo: Uma barra engastada: Material, dimensões, solicitações (mecânicas, térmicas...), seleção de processos de manufatura (fundição, usinagem, laminação??) com justificativa.



Agradecimentos

Dr Newton Kiyoshi Fukumasu

Dra Vanessa Seriacopi

Prof. Dr. Roberto Martins de Souza

LFS - USP